PROCESSING REMOTELY SENSED DATA FOR GEOLOGICAL CONTENT OVER A PART OF THE BARBERTON GREENSTONE BELT, REPUBLIC OF SOUTH AFRICA

D Cloete (Sci.Nat.)

RESEARCH REPORT

M.Sc. (IMAGE PROCESSING)

DEPARTMENT OF COMPUTATIONAL AND APPLIED MATHEMATICS

FACULTY OF SCIENCE

UNIVERSITY OF THE WITWATERSRAND

March 1993

ABSTRACT

Various methods and techniques developed by researchers worldwide for enhancement and processing ATM, MSS and TM remotely sensed data are tested on LANDSAT 5 Thematic Mapper data from a part of the Barberton Greenstone Belt straddling the border between the Republic of South Africa and the Kingdom of Swaziland.

Various enhancement techniques employed to facilitate the extraction of structural features and lineaments, and the findings of the ensuing photogeological interpretation are compared with existing geological maps. Methods for the detection of zones of hydrothermal alteration are also considered.

The reflectance from vegetation, both natural and cultivated, and the possible reduction of the interference caused by this reflectance, are considered in detail. Partial unmixing of reflectances through the use of various methods and techniques, some of which are readily available from the literature, are performed and its effectiveness tested. Since large areas within the study area are covered by plantations, the interference from the two types of vegetation present (i.e. natural and cultivated), were initially considered separately. In an attempt to isolate the forested areas from the natural vegetation, masks derived through image classification were used to differentially enhance the various features.

Results indicate that the use of any particular method to the exclusion of all others will seriously limit the scope of conclusions possible through interpretation of the information present. Enhancement of information in one domain will inadvertently lead to the suppression of information from one or more of the co-existing domains. A series of results from a sequence of procedures interpreted in parallel will in every case produce information of a higher decision making quality.

DECLARATION

I declare that this research report is my own, unaided work. It is being submitted for the degree of Master of Science in the University of the Witwatersrand, Johannesburg. It has not been submitted for any degree or examination in any other university. It has been prepared with financial and material assistance from the Chief Director, Geological Survey of South Africa, to which I am indebted.

Derik Cloete

19 March 1993

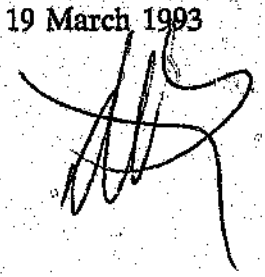

For Linette and Nadia

Table of Contents

1. Introduction ..... 1 - 1

2. Locality ..... 2 - 2

3. General Geology ..... 3 - 4
   3.1 Barberton Sequence ..... 3 - 4
      3.1.1 Onverwacht Group ..... 3 - 6
      3.1.2 Fig Tree Group ..... 3 - 6
      3.1.3 Moodies Group ..... 3 - 6
   3.2 Metamorphism ..... 3 - 7
   3.3 Diabase dykes ..... 3 - 7
   3.4 Dolerite dykes ..... 3 - 8
   3.5 Folding and faulting ..... 3 - 8
      3.5.1 Folding ..... 3 - 9
         3.5.1.1 The Eureka-Moodies syncline ..... 3 - 9
         3.5.1.2 Saddleback syncline ..... 3 - 10
         3.5.1.3 Makonjwa synclinorium ..... 3 - 11
         3.5.1.4 Emlembe synclinorium ..... 3 - 11
      3.5.2 Faulting ..... 3 - 11
         3.5.2.1 Strike faults ..... 3 - 11
            3.5.2.1.1 Sheba fault ..... 3 - 11
            3.5.2.1.2 Scotsman fault ..... 3 - 12
            3.5.2.1.3 Barbrook fault ..... 3 - 12
            3.5.2.1.4 Saddleback fault ..... 3 - 12
            3.5.2.1.5 Inyoka fault ..... 3 - 12
         3.5.2.2 Oblique faults ..... 3 - 13
   3.6 Mineralization in the Barberton Mountain Land ..... 3 - 13
      3.6.1 Sheba Hills ..... 3 - 14
         3.6.1.1 Eureka syncline ..... 3 - 14
         3.6.1.2 Ulundi syncline ..... 3 - 15
         3.6.1.3 Jamestown Schist Belt ..... 3 - 16
      3.6.2 Moodies Hills ..... 3 - 16

3.6.3 Region east of Barberton ..... 3 - 17

4. Platforms and sensor systems ..... 4 - 18

5. Image processing techniques ..... 5 - 20
5.1 Preprocessing ..... 5 - 20
5.2 Single Band Image Enhancement ..... 5 - 22
5.2.1 Contrast Stretching ..... 5 - 23
5.2.2 Spatial Filtering ..... 5 - 27
5.2.2.1 Band Independent Edge Enhancement ..... 5 - 28
5.2.2.1.1 Linear Edge Enhancement ..... 5 - 29
5.2.2.1.2 Non-linear Edge Enhancement ..... 5 - 30
5.2.2.2 Band Dependent Edge Enhancement ..... 5 - 32
5.3 Multiple Image Enhancement ..... 5 - 33
5.3.1 Ratioing ..... 5 - 33
5.3.2 Data Transformations ..... 5 - 37
5.3.2.1 Principal Components Transformation ..... 5 - 37
5.3.2.2 Canonical Analysis ..... 5 - 46
5.3.2.3 Geological Applications of PCT ..... 5 - 47
5.3.2.3.1 Spectral Feature Separation ..... 5 - 48
5.3.2.3.2 Spectral Classification ..... 5 - 48
5.3.3 Enhancement through Colour ..... 5 - 49
5.3.3.1 Colour Composite Selection ..... 5 - 49
5.3.3.2 Colour Enhanced Original Band Imagery ..... 5 - 49
5.3.3.3 Edge and Colour Enhanced Imagery ..... 5 - 50
5.3.3.4 Colour Transformations ..... 5 - 50
5.4 Classification ..... 5 - 53
5.5 Predictive techniques for identifying spectral anomalies ..... 5 - 56
5.5.1 Pair-wise Principal Components ..... 5 - 57
5.5.2 Multiple Linear Regression ..... 5 - 57
5.5.3 Polynomial regression ..... 5 - 58
5.5.4 Data-adaptive linear filter ..... 5 - 58

6. Obstacles in Geological Remote Sensing ..... 6 - 59
6.1 Deep weathering ..... 6 - 59
6.2 Fireburn ..... 6 - 59
6.3 Vegetation and Geological remote sensing ..... 6 - 61
6.3.1 Vegetation Spatial Variability ..... 6 - 63

6.3.2 Forest Classification ..... 6 - 64
6.4 Mineral Mapping and Vegetation Removal ..... 6 - 65

7. Processing for Geological Content ..... 7 - 68
7.1 Edge Enhancement ..... 7 - 75
7.2 Band Combination Selection ..... 7 - 76
7.3 Band Ratioing ..... 7 - 79
7.3.1 Band Ratios vs Difference ..... 7 - 80
7.3.2 Alternatives to Band Ratios ..... 7 - 82
7.4 Principal Components Transformation ..... 7 - 85
7.4.1 Feature Orientated Principal Component Selection ..... 7 - 89
7.4.2 A Fourth Dimension in PC Colour Composites. ..... 7 - 91
7.4.3 Directed Principal Component Analysis ..... 7 - 92
7.4.4 Further Processing ..... 7 - 99

8. Conclusions ..... 8 - 105

9. Reference List ..... 9 - 110

10. Select Bibliography ..... 9 - 113

List of Figures

Figure 5.1 Nearest Neighbour . . . . . 5 - 21
Figure 5.2 Bilinear Interpolation . . . . . 5 - 22
Figure 5.3 Cubic Convolution . . . . . 5 - 22
Figure 5.4 Linear Contrast Stretch . . . . . 5 - 23
Figure 5.5 Piece-wise Linear Stretch . . . . . 5 - 25
Figure 5.6 Histogram Equalization . . . . . 5 - 26
Figure 5.7 Logarithmic Stretch . . . . . 5 - 26
Figure 5.8 Density Slicing . . . . . 5 - 26
Figure 5.9 Isotropic Laplace . . . . . 5 - 29
Figure 5.10 Sobel Horizontal . . . . . 5 - 30
Figure 5.11 Sobel Vertical . . . . . 5 - 30
Figure 5.12 Roberts 1 . . . . . 5 - 30
Figure 5.13 Roberts 2 . . . . . 5 - 30
Figure 5.14 Low Pass Kernel . . . . . 5 - 32
Figure 5.15 PCT: Step 1 . . . . . 5 - 39
Figure 5.16 PCT: Step 2 . . . . . 5 - 41
Figure 5.17 PCT: Step 3 . . . . . 5 - 41
Figure 5.18 Munsell Colour Coordinates . . . . . 5 - 50
Figure 7.1 TM Spectral and Radiometric Characteristics . . . . . 7 - 72
Figure 7.2 Edge Enhance Kernel . . . . . 7 - 75

List of Tables

Table 3.1 Stratigraphy of the Barberton Sequence . . . . . 3 - 5
Table 4.1 Generalized Spectral Band-passes for ATM, MSS, TM and SPOT . . . . . 4 - 18
Table 5.1 Some common Classification methods . . . . . 5 - 54
Table 5.2 Means and Standard Deviations for MAX64 Classification . . . . . 5 - 56
Table 6.1 Ratios used for Vegetation Indexes . . . . . 6 - 63
Table 7.1 Principal Application of TM Spectral Bands . . . . . 7 - 69
Table 7.2 TM Ratios for Geological Applications . . . . . 7 - 79
Table 7.3 Contributions to Principal Components . . . . . 7 - 90

List of Photographs

Photo 2.1 Part of the 1:250 000 Topographical map covering the study area . . . . . 2 - 2
Photo 3.1 Part of the 1:250 000 Geological map covering the study area . . . . . 3 - 4
Photo 5.1 Natural Colour False Colour TM-123 Composite . . . . . 5 - 24
Photo 5.2 Histograms for Auto-2-Linear stretch on TM-123 . . . . . 5 - 24
Photo 5.3 Extracted edges for Barberton Mountain Land . . . . . 5 - 31
Photo 5.4 Band Ratio TM5/TM7:TM3/TM1:TM4/TM3 with Auto Gaussian stretch . 5 - 33
Photo 5.5 Band Ratio TM5/TM7 on black and white . . . . . 5 - 34
Photo 5.6 Band Ratio TM3/TM1 on black and white . . . . . 5 - 35
Photo 5.7 Band Ratio TM4/TM3 on black and white . . . . . 5 - 35
Photo 5.8 Band Ratio TM5/TM1 on black and white . . . . . 5 - 36
Photo 5.9 Scattergrams TM5 vs TM7 and TM4 vs TM3 . . . . . 5 - 37
Photo 5.10 Scattergrams TM 1-7 Unstretched . . . . . 5 - 40
Photo 5.11 Scattergrams PC 1-6 Unstretched . . . . . 5 - 40
Photo 5.12 Principal Components 123 unstretched on Blue-Green-Red . . . . . 5 - 42
Photo 5.13 Principal Components 123 viewed through Auto-2-Linear stretch . . . . . 5 - 42
Photo 5.14 Histograms for Auto-2-Linear stretch on PC-123 . . . . . 5 - 43
Photo 5.15 Principal Components 456 viewed through an Auto-2-Linear stretch . . . . 5 - 45
Photo 5.16 RGB to IHS to RGB Colour Transformation . . . . . 5 - 52
Photo 5.17 RGB to HLS Colour Transformation . . . . . 5 - 52
Photo 5.18 Classes for Maximum Likelihood Classifier . . . . . 5 - 55
Photo 5.19 Classified Image . . . . . 5 - 55
Photo 7.1 TM-234 on BGR with Auto-2-Linear stretch . . . . . 7 - 77
Photo 7.2 Histograms for Auto-2-Linear stretch on TM-234 . . . . . 7 - 77
Photo 7.3 TM-247 on BGR with Auto-2-Linear stretch . . . . . 7 - 78
Photo 7.4 Histograms for Auto-2-Linear stretch on TM-247 . . . . . 7 - 78
Photo 7.5 Ratio TM5/7, TM 5/1 and TM3/1 through an Auto Gaussian stretch . . . 7 - 81
Photo 7.6 TM(1+2), TM(3+4) and TM(5+7) with Auto-2-Linear stretch on BGR . . . 7 - 83
Photo 7.7 TM(1*2), TM(3*4) and TM(5*7) on BGR . . . . . 7 - 83
Photo 7.8 TM(1*2), TM(3*4) and TM(5*7) with Auto Gaussian stretch on BGR . . . 7 - 84
Photo 7.9 Histograms for Auto Gaussian stretched multiplied TM bands . . . . . 7 - 84
Photo 7.10 Principal Components 2, 3 and 4 on BGR . . . . . 7 - 86
Photo 7.11 Principal Components 5, 3 and 4 through an Auto-2-Linear stretch . . . . 7 - 86
Photo 7.12 Decorrelation stretch Combinations 645 with Auto Gaussian stretch . . . . 7 - 87
Photo 7.13 C-stretch Combinations 423 viewed through an Auto-2-Linear stretch . . . 7 -
Photo 7.14 Square roots of Principal Components multiplied . . . . . 7 - 92
Photo 7.15 Directed Principal Component 1 False Colour Composite . . . . . 7 - 95
Photo 7.16 Directed Principal Component 2 False Colour Composite . . . . . 7 - 95
Photo 7.17 Normalized Vegetation Index viewed through an Auto Mean stretch . . . . 7 - 98

Photo 7.18 Directed Principal Components using Normalized Vegetation Index .... 7 - 98
Photo 7.19 Multiplicative technique applied to Defoliated view ..... 7 - 99
Photo 7.20 Step 2: PC-123 from pair-wise TM bands with Auto Linear stretch .... 7 - 100
Photo 7.21 Step 3: Inverse PCT with DN128 grey as PC1 with Auto Linear stretch . 7 - 100
Photo 7.22 Step 4: HLS transformation viewed without stretch ..... 7 - 102
Photo 7.23 Step 4: HLS transformation viewed through an Auto-2-Linear stretch .. 7 - 102
Photo 7.24 Step 5: HLS to RGB transformation viewed without stretch ..... 7 - 103
Photo 7.25 Inverse PCT on IHS transformation of three PC combinations ..... 7 - 103
Photo 8.1 C-stretch Combination 145 viewed through an Auto-2-Linear stretch ... 8 - 106
Photo 8.2 Two Directed Principal Component second combination added together . 8 - 107

1. Introduction

In 1956 Dr F.C. Truter, the then Director of the Geological Survey, wrote the following about a manuscript on the Barberton Mountain Land being submitted: "..The revision of its [the Barberton area] mapping was undertaken with the purpose of obtaining more detailed information on its complicated stratigraphy and geological structure, assessing more accurately its mineral potentialities, and establishing the relation between structure and ore deposits..." [From: Visser, D.J.L. (1956) p(iii), para 2.]

Since then, and guided and inspired by the maps accompanying this special publication, quite a few studies of a more detailed nature were undertaken by geologists and researchers from various institutions. The underlying objective of all these studies were to further our knowledge of the area, and each and everyone contributed to our knowledge and understanding of the Barberton Mountain Land.

During the last decade or so, new technologies increasingly enabled us to spend less time in the veld gathering data, and more time in the office dissecting, digesting, interpreting and eventually composing that piece which could complete the puzzle.

This study is aimed at providing one of those pieces.

2. Locality

This study centres on an area just to the east of the town of Barberton in the Eastern Transvaal, Republic of South Africa. The area is covered by parts of six 1:50 000 sheets, viz. 2530 DB Kaapse Hoop & DD Nelshoogte, 2531 CA Sheba, CB Kaapmuiden, CC Barberton & CD Shiyalongybo. It lies roughly between 30°57′:25°38′ northwesterly and 31°23′:25°57′ southeasterly and includes the northwestern part of Swaziland.

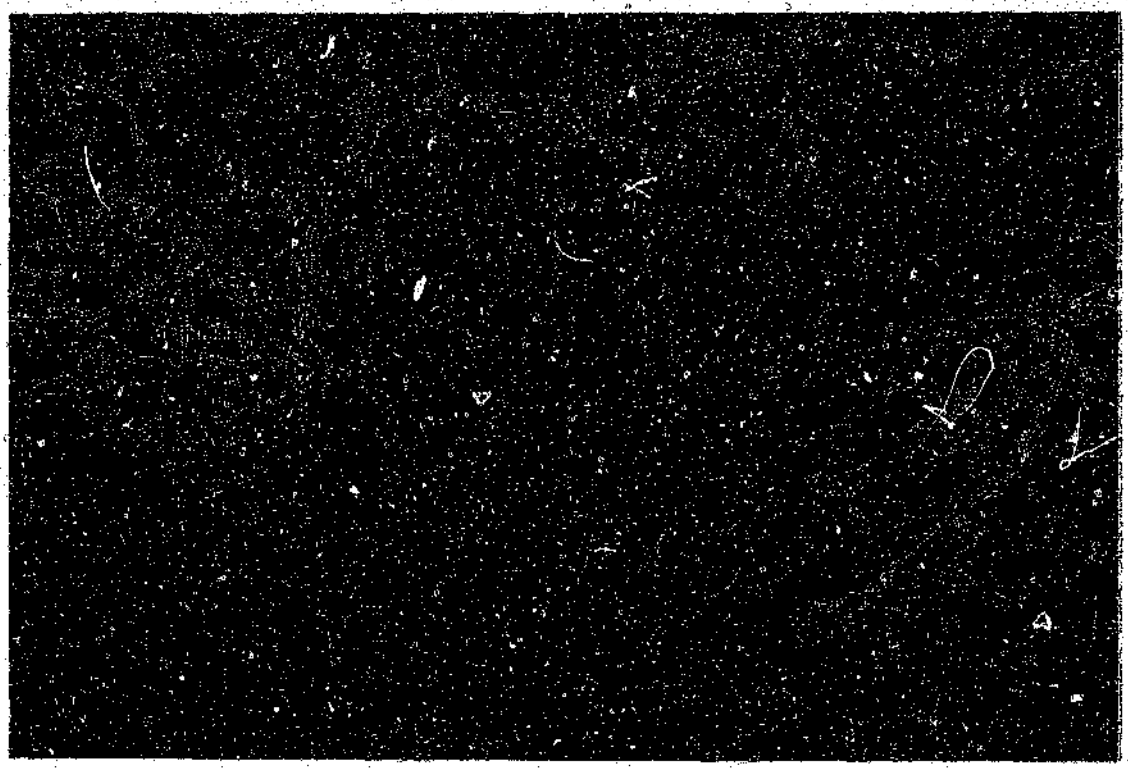

Photo 2.1 Part of the 1:250 000 Topographical map covering the study area

Topographically the Barberton Mountain Land comprises a series of nearly parallel ranges of rugged mountains separated by deeply incised v-shaped valleys.

The ranges consist mainly of quartz or chert, while the valleys were cut into softer shaly material. The northwestern path of the area consists of a basin, formed on the Kaap Valley Pluton, which lies around 700 meters lower than most the mountain land itself. Rivers in the area drain towards the northeast. The town of Barberton lies at the foot of the mountain land, with a view towards the northwest, over the basin.

A substantial part of the mountain land is covered with either Pine or Eycaluptus forests, mostly commercial plantations.

3. General Geology

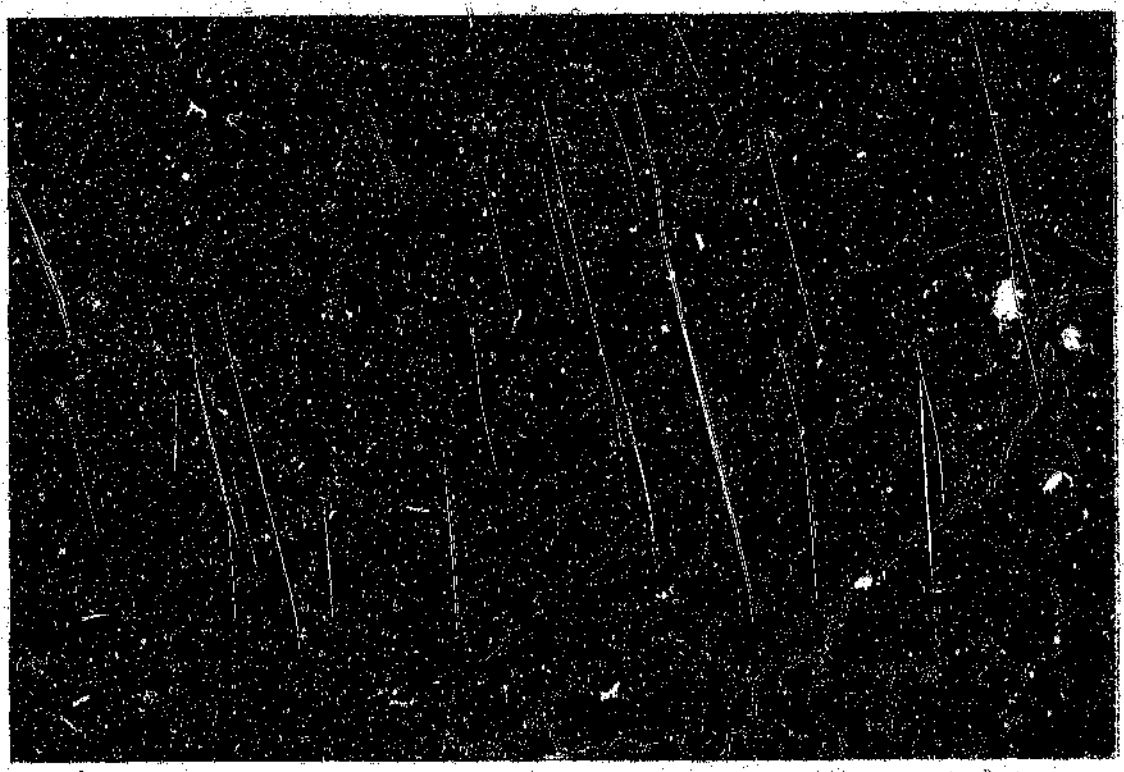

Photo 3.1 Part of the 1:250 000 Geological map covering the study area

3.1 Barberton Sequence

The Barberton Sequence constitutes the major part of the Barberton Greenstone Belt volcano-sedimentary pile. The sequence has been divided by SACS (1980) into three lithological groups: a dominantly volcanic lower assemblage, the Onverwacht Group, and a dominantly sedimentary upper assemblage displaying the largely argillaceous Fig Tree Group and the largely arenaceous Moodies Group. The base of the sequence is nowhere exposed. Although disconformable

GROUP	SUB-GROUP	FORMATION (Informal Unit)	LITHOLOGY
MOODIES (3500 m)		Baviaanskop	Sandstone, grit, conglomerate, shale, subgreywacke, phyllite.
		Joe's Luck	Shale, subgreywacke, sandstone, quartzite, phyllite, jaspilite, ferruginous shale, basaltic lava.
		Clutha	Shale, quartzite, conglomerate, jaspilite.
FIG TREE (2000 m)		Schoongezicht	Trachytic tuff, agglomerate, lava, tuffaceous greywacke, conglomerate.
		Belvue Road (Ulundi bar)	Siltstone, shale and subordinate greywacke, banded ferruginous chert, trachytic tuff.
		Sheba	Greywacke and shale with interlayers of chert and ferruginous chert.
ONVERWACHT	Geluk	Zwartkoppie (920 m)	Mafic and felsic lava, tuff, agglomerate, chert, shale, carbonate rocks, ultramafic lava.
		Kromberg (1920 m)	Mafic and felsic lava, tuff, agglomerate, pillow breccia, shale, komatiitic lava, porphyry. Mainly metamorphosed.
		Hooggenoeg (4330 m) (Middle marker)	Mafic to felsic volcanic rocks, porphyry, shale, komatiitic lava, rhyodacitic tuff and agglomerate, chert-carbonate layers. Metamorphosed at lower Greenschist Facies
	Tjakastad	Komati (3500 m)	Basaltic and peridotitic komatiite, tholeiite, chemical sediment. Metamorphosed.
		Theespruit (1980 m)	Various mafic and ultramafic schists interlayered with banded iron formation and ferruginous, black, white and grey chert, acid to intermediate volcanic rocks. Mainly metamorphosed.
		Sandspruit (3200 m)	Ultramafic and subordinate mafic lavas, mainly metamorphosed.

Table 3.1 Stratigraphy of the Barberton Sequence

and unconformable relationships exist locally, the succession as a whole is conformable (Table 3.1).

3.1.1 Onverwacht Group

Consisting of two well defined geological entities, the group is subdivided into the ultramafic and mafic magnesium-rich lavas of the lower Tjakastad Subgroup, and the mafic and intermediate to acid volcanics of the upper Geluk Subgroup. A persistent cherty band, the middle marker, at the base of the Hooggenoeg Formation separates the Subgroups. Each of the Subgroups is divided into 3 formations. The Tjakastad Subgroup is preserved around the periphery of the Barberton Belt, while the Geluk Subgroup is confined to the southern and central parts.

3.1.2 Fig Tree Group

The Fig Tree Group consists of greywackes at the bottom, shale with banded ferruginous chert in the middle and mainly volcanic rock on top, and is divided into three formations.

3.1.3 Moodies Group

Consisting of repeated cycles of arenaceous and argillaceous rocks with a well developed and persistent basal conglomerate, banded magnetite-jaspilites and poorly exposed basaltic lavas, the Moodies Groups is also divided into three formations.

The Fig Tree and Moodies Groups are preserved in the synclinal core of the belt.

3.2 Metamorphism

The Barberton Mountain Land has undergone only greenshist facies regional metamorphism. While the sedimentary core often show almost no signs of metamorphism at the contacts with the granitoids, the Onverwacht volcanics have been upgraded to the upper greenshist facies, and locally even to the amphibolite and granulite facies with a very narrow higher grade aureole. Regardless of the high grade contact aureole present around most of the individual granitoids, the rock still retain a fabric indicative of regional metamorphism.

3.3 Diabase dykes

The whole mountain range is also cris-crossed with diabase dykes, primarily striking northwest-southeast, forming conspicuous topographic features. These dykes cut across the folds and faults associated with the orogenic movements that caused the formation of the mountain land, and are older than the Godwan Formation.

The dykes show considerable variation in texture and mineralogical composition, varying from mostly typically mafic to more felsic types. The leucocratic hybrids are thought to have formed due to the assimilation of granitic or siliceous

sedimentary material, and show quartz and micropegmatite instead of olivine. A typical dyke shows an equigranular medium grained rock with a dark green to greenish grey fresh, and brown weathered colour. The mineral assemblage is typically orthopyroxene and olivine, with the orthopyroxene altering to a fine, needle-like actinolite (Visser, 1956).

3.4 Dolerite dykes

Dykes of Karoo dolerite, showing a strike of generally northeast-southwest, are distributed over the entire Barberton area. While they can display a local abundance, with their moderate width they are not nearly as topographically imposing as the diabase dykes. Rapid disintegration had, however, a marked effect on the development of the drainage pattern in the area.

Very few of the dolerite dykes show persistence for more than a few kilometres. One of the more noteworthy exceptions in the study area stretches from the Swaziland border in the south to Three Sisters in the northeast, a distance of more than 10 kilometres.

The Karoo dolerite in the area is a remarkable fresh fine grained, dark, blue grey rock that weathers to display a smooth, greyish brown surface.

3.5 Folding and faulting

Intense faulting and complicated folding of the rocks that built the mountain

land is obvious from any geological map of the Barberton area. On closer examination it is apparent that the general trend of the folding axes are roughly east-northeast and west-southwest. This is also the trend of the longer strike faults.

3.5.1 Folding

The Onverwacht Group lavas display a fairly uniform composition, making determination of the extent and nature of the folding within the group rather difficult. Because of its massive nature, the rocks yielded most to shearing, and some shear cleavage planes is visible in some of the deep valleys leading off to the east.

The thinly bedded, predominantly argillaceous sediments of the Fig Tree Group have been intensely deformed, resulting in a series of isoclinal folds. To the south of Barberton, these folds have a strike of roughly northeast-southwest and numerous crossfolds occur. To the east end northeast of the town numerous synclinal structures occur, some being separated by anticlinal structures. Extremely complex folding is characteristic of the Fig Tree beds in the Sheba and Hlambanyati Hills.

Because of the coarser, more heterogenous and more competent nature of the beds of the Moodies Group, only a series of simple folds resulted from tectonic action. The beds are largely preserved in synclinal closures within the Fig Tree Group.

3.5.1.1 The Eureka-Moodies syncline

One of the most conspicuous structural elements of the area, it stretches from roughly 31°16′ to 31°06′ east and from 25°41′ to 25°48′ south; and even beyond to the southwest. The axis of the syncline changes from approximately east-west in the east to almost north-south in the southwest. The bending is accompanied by the development of tension fractures along the northern limb and compression faults along the southern limb of the syncline. To the northeastern side of the structure shear faulting occurs.

The contact between the Moodies and Fig Tree beds to the south are characterized by massive shearing as well as overfolding of the beds from the southeast. The fault bounding the syncline in the east may very well continue beyond the main Barberton-Havelock road, possibly even as far southward as Concession Creek on the farm Brommer 28 (approximately 31°02′ E:25°49′ S).

Along the northwestern rim of the syncline the basic rocks of the Tjakastad Subgroup are intrusive into the Moodies Group, but the contact is marked by extensive shearing of both formations.

3.5.1.2 Saddleback syncline

Situated between roughly 31°14′ E:25°46′ S and 30°59′ E:25°52′ S, it also displays a change in strike direction from west-southwest to southwest from north to south. The syncline is terminated on the southwestern side by the Inyoka fault, which strike northwest. On the western side the syncline is bounded by the Saddleback fault striking northwest and cutting progressively higher across the northwestern flank of the syncline.

3.5.1.3 Makonjwa synclinorium

The synclinorium, consisting of a series of simple anticlinal and synclinal structures, can be traced in a northeasterly direction from roughly 31°03′ E:25°53′ S to past the edge of the area. It is bounded on the northwest flank by the Inyoka fault. Since no marker horizons exists here, mapping of the fold axes are difficult.

3.5.1.4 Emlembe synclinorium

Traceable along the Swaziland border from roughly 31°13′ E:25°52′ S in a southwesterly direction, the synclinorium varies in width, with a series of three synclines separated by two anticlines at the widest point (roughly 31°07′ E:25°56′ S).

3.5.2 Faulting

Parallel with the folding deformation, large scale faulting also occurred. The principal faults strike mostly parallel to the regional strike of the beds. Several smaller faults cut across the beds at angles ranging from as much as 90° to as little as a few degrees. Movement along these oblique faults seems to have been horizontal in nature. In general the mechanism of faulting is extremely complex.

3.5.2.1 Strike faults

3.5.2.1.1 Sheba fault

Running from the southern side of the Eureka syncline, it is a high angle

overthrust along which the argillaceous sediments of the Fig Tree Group have been pushed over the more arenaceous sediments of the Moodies Group.

3.5.2.1.2 Scotsman fault

Situated mostly within Fig Tree sediments and stretching roughly from 31°20′ E:25°50′ S in a northeasterly direction, its nature is difficult to determine due to the lack of marker beds.

3.5.2.1.3 Barbrook fault

Visible from about 31°04′ E:25°47′ S to the northeasterly edge of the area, it separates Fig Tree sediments (north) and the Onverwacht volcanics (south) in the south and falls entirely within the sediments of the Fig Tree Group in the middle, where mylonite is typically present along the fault plane. This zone of mylonitization characterizes the fault all the way east, also where it separates Fig Tree (north) and the Moodies (south) sediments in the northeast.

3.5.2.1.4 Saddleback fault

Running roughly parallel with the Barbrook fault, it terminates in the south against a east-west striking oblique fault. In the middle (approximately 30°07′ E:25°47′ S) it is displaced along an oblique fault striking almost north-south. South of Barberton it separates the Onverwacht volcanics (north) and the Fig Tree and Moodies sediments (south) on the northern limb of the Saddleback syncline. To the east it joins the Inyoka fault.

3.5.2.1.5 Inyoka fault

Having a persistent northeast-southwest trend, it separates Moodies quartzites (southeast) and Fig Tree sediments (northwest), except where diabase occur to

the north of the fault. To the southwest of the area a parallel fault occurs some 200 meters southeast of the Inyoka fault.

3.5.2.2 Oblique faults

Although they are not as extensive as the strike faults, they nevertheless have topographic significance. Almost none of these faults follow a straight course. Some of the oblique faults cut across and displace some of the strike faults, others seem to branch off from the strike faults.

It appears that none of the oblique faults are mineralized.

3.6 Mineralization in the Barberton Mountain Land

Gold has been mined in the Mountain Land for over a century. Since the first production in 1884, more than seventy percent of the production came from four mines in the area: Sheba, New Consort, Fairview and Agnes gold mines. The remaining thirty percent came from some 350 occurrences, often nothing more than a small working or a short lived prospect.

Distribution of the gold seems to be closely linked to structural disturbances, however, not all the structural features are gold bearing. Most of the deposits seem confined to areas to the north and northeast of Barberton, known as the Jamestown and Sheba Hills area, and southwest of the town, in the Moodies Hills.

Other occurrences are found along, and adjacent to, the major strike faults: Scotsman, Lily, Albion, Sheba, Barbrook and Moodies faults.

In Swaziland gold occurs along the granite-greenstone contacts in the Hhohho, Pigg's Peak and Forbes Reef areas. It is thought (Anhaeusser, 1986a) that the absence of mineralization in the central part of the Mountain Land south of the Barbrook fault may be due to the absence of rocks from the Onverwacht Group volcanic assemblage. These rocks are perceived to have been the primary source of gold and sulphides for mineralization. In addition, the distance from the granite-greenstone contact also seems to have a significant effect on mineralization, since suitable structural environments do exist in the area, but no mineralization have been found.

3.6.1 Sheba Hills

Two prominent structural features account for most of the gold production in the Sheba Hills area.

3.6.1.1 Eureka syncline

Most of the current production of gold are from reefs occurring on the inner arc of the syncline. All these occurrences can be traced to either the Fairview or Sheba mines.

The mineral deposits in the Eureka syncline owe their origin to structural control, the locations of the ore bodies being determined through faulting in particular.

Numerous tension fractures radiate about the arcuate structure, which consists of structurally competent Moodies quartzite interlayered with shale, sandstone and subgreywacke. Most of the gold mined came from the gold-quartz veins in these tension fractures. (Wiggett et al., 1986)

On the southern and eastern limbs of the fold, between the Fairview and Sheba mines, numerous fractures are found the orientation of which approximates that of the Sheba fault. These fractures are thought to have been caused by concentric shearing due to strike movements between fold units. Mineralization was due to the later infiltration of hydrothermal fluids.

In general, it seems that the distance from the Sheba fault have a direct bearing on the overall abundance of mineralization, with the highest production yield closest to the fault.

3.6.1.2 Ulundi syncline

Two of the biggest mines, Sheba and Fairview, are located symmetrically about the northwest orientated fold axes of the Eureka and Ulundi synclines.

Most of the mineralization in the Ulundi syncline is epigenetic in character, since the minerals are present in concordant and discordant fractures in greywacke and shale of the Sheba Formation at Fairview mine, and also in a zone of schist and associated banded chert in the Swartkoppie Formation at Sheba mine.

The fractures resulted mainly from tangential shear movements produced during folding episodes. Payable gold are usually found in discrete, shorter pay shoots,

irregularly spaced along strike of the main fracture (Wiggett et al., 1986).

3.6.1.3 Jamestown Schist Belt

Practically all the gold mineralization in the Jamestown Schist Belt is structurally controlled, being confined to fold, fault and shear zones. Except for two larger producers, Worcester and New Consort mines, all the other deposits were small producers.

The New Consort mine is situated at the contact between the mafic and ultramafic schists of the Onverwacht Group and the overlaying Fig Tree assemblage consisting of metamorphosed shale sediments at the bottom and feldspathic tuffaceous greywacke on top.

The mineralization is associated with a fine grained silicious zone which separates komatiite dominated Onverwacht rocks from the Fig Tree metasediments. This zone, known as the Consort Bar (Voges, 1986) is a roughly four metres thick, intensely folded and contorted in places, laminated and highly siliceous chert rock with interlayered sulphide rock bands.

The gold enriched sulphide bands are found above or below the Consort Bar over a distance of about two metres.

3.6.2 Moodies Hills

Southwest of Barberton the greatest cluster of gold deposits occur in the vicinity of the Agnes mine, which is one of the four large mines in the area.

As with most of the mineralization in the Mountain Land, the locations of the mineralization display distinctive evidence of structural control. The gold bearing pyritic zones generally straddle the contact between calcareous mudstone and more shaly units in a zone several hundred metres wide. The gold is normally not visible.

3.6.3 Region east of Barberton

Areas of prime importance are situated in the Three Sisters region and strung out along the Barbrook fault. Mines in the area are located in greywacke, shale, banded iron formation and chert of the Fig Tree Group. Shears are generally found close to shale-greywacke contacts, or along contacts with chert layers. Where shears join, or diverge, an increase in the degree of silicification, which usually show good gold values, is often apparent.

4. Platforms and sensor systems

Since this study was undertaken using only LANDSAT Thematic Mapper data, other sensors systems and platforms will not be dealt with in detail. However, quite a few of the procedures evaluated or used were in fact derived by the various workers using data from other instruments. The similarities and differences between these instruments will be indicated where necessary.

Band-pass (μm)		ATM Spectral Band	MSS Spectral Band	TM Spectral Band	SPOT Spectral Band	
0.42 - 0.45		1				
0.45 - 0.52		2		1		
0.52 - 0.60		3	4	2	1	
0.605 - 0.625		4	5		2	PAN
0.63 - 0.69		5		3		
0.695 - 0.75		6	6		3	
0.76 - 0.90	0.76 - 0.80	7		4		
	0.80 - 0.90		7			
0.91 - 1.05		8				
1.55 - 1.75		9		5		
2.08 - 2.35		10		7		
8.50 - 13.0		11				
	10.4 - 12.5		8	6		

Table 4.1 Generalized Spectral Band-passes for ATM, MSS, TM and SPOT

One of the instruments whose datasets feature quite prominently in the

literature, is the Daedalus AADS-1268 "Airborne Thematic Mapper" (ATM), which originated as a simulation instrument for the not-then-launched LANDSAT Thematic Mapper (TM). The ATM scanner employs 10 spectral bands in the visible to middle infrared and one broad band thermal infrared channel featuring the same spatial resolution as the reflective channels (unlike the TM). The spectral similarity is apparent from Table 4.1.

Despite the extra channels, the ATM remains a broad band multi-application instrument. It's main advantage over TM is the increased spatial resolution due to the lower flying hight. Problems common to all aircraft-based scanners, such as geometric distortion, non-uniform scene illumination and limited view often negates any perceived advantage increased spatial resolution may bring.

5. Image processing techniques

This section looks at the different techniques used to prepare and beautify remotely sensed data. The aim is of course to present the data in such a way that useful information can be gleaned from the processing product. Four descriptive categories are defined:

1. Preprocessing,
2. Image Enhancement,
3. Classification, and
4. Multi-source data correlation.

Since the current research excluded the last category, only the first three will be discussed.

5.1 Preprocessing

During data acquisition, various errors routinely occur. Preprocessing is necessary to correct these errors, which can be divided into four groups:

a) Platform effects - Attitude variations (roll, pitch, yaw), altitude variations, scan skew and spacecraft velocity changes;

b) Sensor effects - Mirror scan non-linearity, detector sampling delay, detector bias/gain, geometric perspective and panoramic distortion;

c) Scene effects - Earth rotation, curvature and elevation, and

d) Atmospheric effects - Attenuation and scattering.

Since most of the radiometric correction and preprocessing are done at the receiving station as part of the service to the customer, it was only necessary for the author to do geometric correction during the data preparation phase.

During geometric correction and image registration a new grid for the spatial distribution of the pixels is constructed. For the data to fit this new grid, it is necessary to resample the data to fit the new relative positions. This spacial interpolation is done through a geometric coordinate transformation, constructed by identifying the geometric relationship between the input pixel location and the associated map coordinate of the same point.

While the radiometric value of the displaced pixels no longer represent the value sensed in the first place, the approximation ranges from spot on to close enough for the overall difference to be negligible. The technique used for intensity interpolation will determine the difference between the original and resultant radiometric values of the pixels.

Three commonly used resampling routines are:

1. Nearest Neighbour - A zero order interpolation routine, which is computationally efficient and does not alter the pixel brightness values during resampling. The value of the

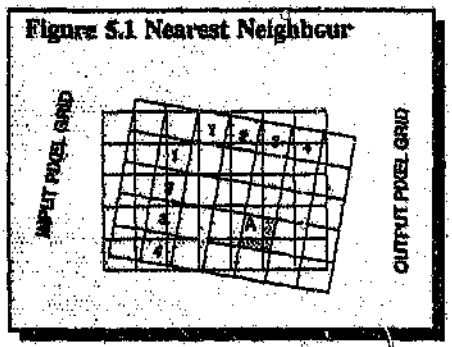

Figure 5.1 Nearest Neighbour

closest input pixel to the corresponding one in the transformed output array is accepted as equal to the new one;

2. Bilinear Interpolation - This first order routine assigns output pixel values by interpolating brightness values in two orthogonal directions in the input image. The new pixel is assigned a brightness value calculated as the distance weighted average value of the four input pixels surrounding the transformed output pixel, and

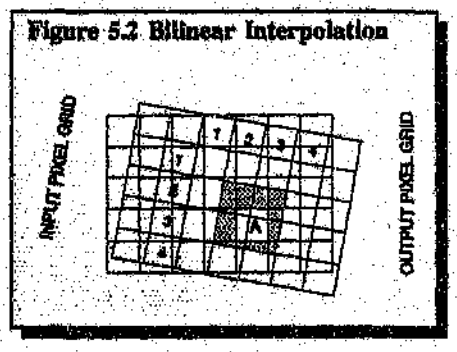

Figure 5.2 Bilinear Interpolation

3. Cubic Convolution - The distance weighted average value for the 16 closest input pixels grouped around any new pixel is adopted.

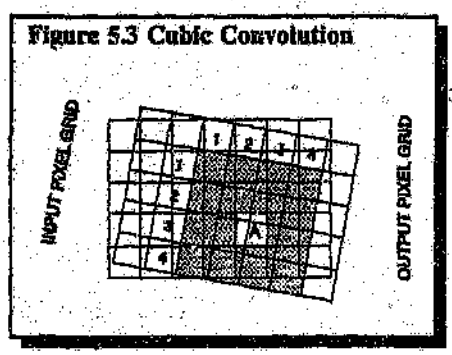

Figure 5.3 Cubic Convolution

It follows that the accuracy of the output values, statistically speaking, increases from one through three. The resampling method used for this study was cubic convolution.

5.2 Single Band Image Enhancement

Although enhancement may be looked upon by some as part of the preprocessing phase, it should be noted that some enhancement routines are powerful enough to produce stand alone results, therefore the author believe it

to rather be part of the processing than the preprocessing phase.

Single image manipulation concentrates on applying successful enhancement techniques to a single band or image. Some of these techniques are discussed below.

5.2.1 Contrast Stretching

Changing the range of grey levels within an image is often the single most revealing and informative operation performed on the scene. The technique involves the calculation of the DN range for each band, which is then displayed in a histogram. Typically the limits of the brightness values lie within a rather narrow range within the full scale.

Stretching the values to spread out over the full scale, typically 0 - 255, can be done through either linear or non-linear processes.

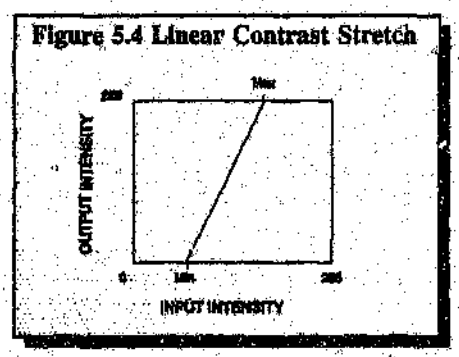

Figure 5.4 Linear Contrast Stretch

Linear stretching (Figure 5.4) is the easiest and most common. This enhancement is best applied to images with Gaussian (which is rather uncommon) or near-Gaussian histograms.

A piece-wise or multiple linear stretch, (Figure 5.5) where the analyst identifies the number of different linear enhancements to be performed, is preferred for non-Gaussian images (Photo 5.1 and Photo 5.2).

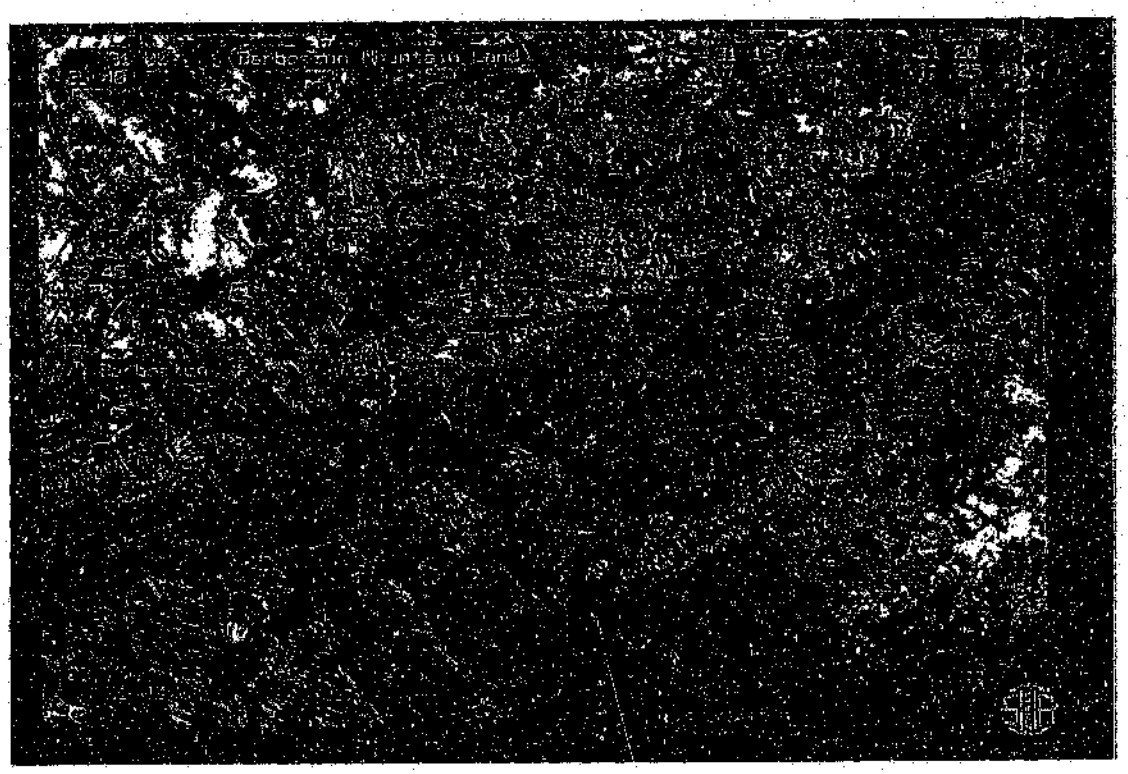

Photo 5.1 Natural Colour False Colour TM-123 Composite

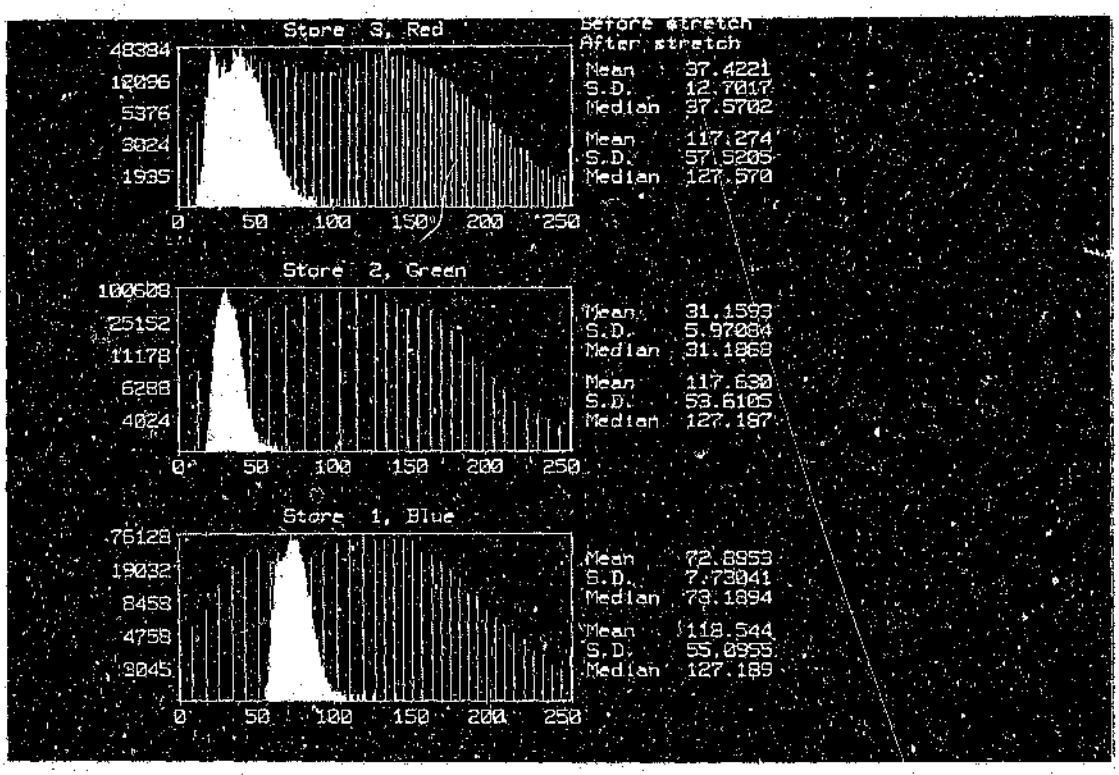

Photo 5.2 Histograms for Auto-2-Linear stretch on TM-123

Photo 5.1 displays TM Bands 1, 2 and 3 on Blue-Green-Red to simulate natural colour. The scale of the photograph is approximately 1:300 000. For visual clarity the data is viewed through a lookup table which stretches the data to fully utilize the available range of grey levels. For the equipment used in this study 255 grey levels are available. The stretch used was an Auto 2 Linear stretch, which is a piece-wise linear stretch utilizing one break in the line (Figure 5.5). This breakpoint is automatically calculated according to the spread of the data and the result usually displays a slightly higher percentage of the data in the upper 128 grey levels as opposed to the lower 128 grey levels, as can be seen on the histograms of the datasets (Photo 5.2). Since the whole input store is stretched, the stretch is based on a 128 x 128 point regular grid across the input area. Only when a mask is used is the histogram calculated from every pixel underlying the mask.

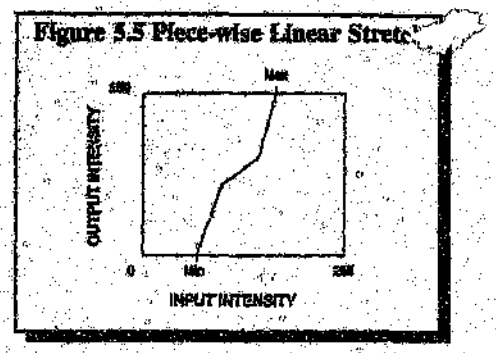

Figure 5.5 Piece-wise Linear Stretch

The histograms also quite clearly show the amount of stretch that had to be applied to the dataset to fill the available range. The Standard Deviation increased by almost 50 in all three cases, with the movement of the Median to around grey level 127. To get an idea what the unstretched scene would look like, notice the dark background underneath the text. The difference between that and the rest of the scene is some 80 grey levels, which is similar to the difference between the before and after median values for the three datasets. (TM1:90, TM2:96 and TM3:54). It should also be noted that the narrow spread of the input dataset is not unusual, therefore contrast stretching is usually applied as a matter of course before viewing the dataset. It is, however, normal

to keep the data unstretched for further processing.

Non-linear stretching functions, which tend to favourably extend some parts of the DN range at the expense of other parts, include:

1. Histogram Equalization (Figure 5.6) - where approximately equal numbers of pixels are assigned to each of the predetermined number of output grey-scale classes;

Figure 5.6 Histogram Equalization

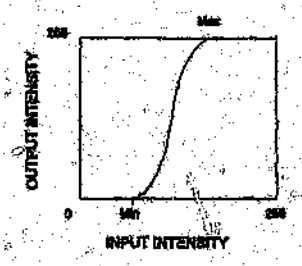

2. Logarithmic (Figure 5.7) - where the greatest impact are on the brightness values found in the darker part of the histogram, and

Figure 5.7 Logarithmic Stretch

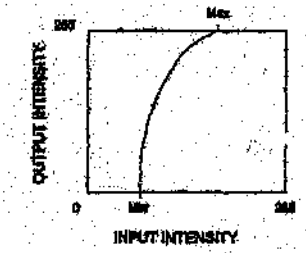

3. Gaussian - where the emphasis is placed on values found in the middle of the range.

Density slicing (Figure 5.8) is the lumping of DN's (Digital Numbers) with different values within a specified range, into a single value. This method works best if the given surface feature has a unique and narrow spread of values. Several features, each with its own separable narrow range of DN's, can be separated into several grey level slices. With different colours assigned to each grey level set, the entire range can be

Figure 5.8 Density Slicing

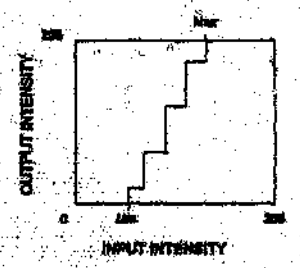

displayed at once.

5.2.2 Spatial Filtering

This technique differs from the previous techniques in that it look at the values of neighbouring pixels as well, when determining the output pixel value.

A linear spatial filter is a filter for which the brightness value at a specified location in the output image is a function of some weighted average of brightness values located in a particular spatial pattern around the specified location in the input image. By using this weighted neighbouring pixel evaluation, or two-dimensional convolution (Jensen, 1986), the spatial frequency characteristics of any image can easily be changed.

Linear spatial filters emphasizing high spatial frequencies, or high-pass filters, enhances fine detail, that is, sharpen up an image, while filters emphasizing low frequencies, or low-pass filters, are used for image smoothing, because they suppress the high frequencies by generating moving averages over, say, a 5 x 5 pixel square area or kernel. Each pixel value is replaced by the average value, hence the smoothed output. This technique can also be used to clean up noisy images. In effect, the high-pass filtered output is simply the difference between the input image and the low-pass filtered output.

Edge Enhancement is a technique applied to enhance those features that are characterized by abrupt changes in radiometric response. Structural and stratigraphic details can thus be accentuated by enhancing the linear and curved image features that represent them. The technique typically involves three steps:

1. Creation of a low-pass filtered image where the high frequency data are removed;
2. Subtraction of the averaged image from the original image, thereby separating the edge or high frequency component, and
3. Adding the edge component back to the original image to produce an image with double brightness edges.

The result is invariable enhanced linear features and drainage patterns, as the enhancement is done irrespective of the direction of the edges.

5.2.2.1 Band Independent Edge Enhancement

Although Fourier Transform methods and filtering in the frequency domain are more exact for spatial processing of image data, small window convolution methods have achieved greater popularity due to their lesser computing power requirements, versatility, and proven effectiveness.

One of the more basic, but very popular edge enhancement techniques is using the "moving average" derivation from an image. This averaged image contains only the lower spatial frequencies of the original image. Subtracting the averaged image from the original would result in an image containing the higher spatial frequencies of the original image. Combining this higher frequencies with the original results in the enhanced image. As explained before, the enhanced image is simply the combination of the input image and the high-pass filtered output.

It should be noted that although the structure and stratigraphy is enhanced, some loss of colour contrast will occur as a result of the edge enhancement.

5.2.2.1.1 Linear Edge Enhancement

One simple method of extracting edges is the application of the running difference operation. The original image is shifted by one pixel, and then tested for a difference in corresponding pixels in the two images. A DN value of 127 is substituted for the pixel if there is no difference, a darker value, of say DN = 30, is substituted for the pixel if the difference is a negative, and a lighter value, of say DN = 200, is substituted for the pixel if there is a positive difference. Therefore transitions from dark to light produce black lines and from light to dark produce white lines.

It is also possible to perform edge enhancements by convolving the original data with a weighted mask or kernel. The optimum kernel size (i.e. 3 x 3, 5 x 5, 7 x 7, or 9 x 9) is a function of the surface roughness and sun angle characteristics at the time the data were collected. The values used in the chosen kernel depends on the direction the enhancement is required for. This compass gradient method is generally preferred for finding lines.

Edge enhancement without regard to edge direction may be obtained by applying a Laplacian convolution mask (Figure 5.9) to the imagery. The Laplacian is more useful in edge and boundary detection, but it is a second derivative (as opposed to the gradient, a first derivative) and therefore more troubled by image noise. The Laplacian edge enhancement emphasizes maximum values, or peaks, within the image.

Figure 5.9 Isotropic Laplace

$$\begin{vmatrix} 0 & -1 & 0 \\ -1 & 4 & -1 \\ 0 & -1 & 0 \end{vmatrix} + 128$$

5.2.2.1.2 Non-linear Edge Enhancement

Non-linear edge enhancements are performed using non-linear combinations of pixels, mostly using 2 x 2 or 3 x 3 kernels. The Sobel edge detector is based on a 3 x 3 window and is computed according to the relationship:

Figure 5.10 Sobel Horizontal

1	2	1
0	0	0
-1	-2	-1

$$Sobel_{3,out}=\sqrt{x^2+y^2}$$

where

$$x=[DN_3+(2(DN_6))+DN_9]-[DN_1+(2(DN_4))+DN_7]$$

and

$$y=[DN_1+(2(DN_2))+DN_3]-[DN_7+(2(DN_8))+DN_9]$$

Figure 5.11 Sobel Vertical

1	0	-1
2	0	-2
1	0	-1

The Robert's edge detector is based on the following 2 x 2 pixel window:

$$DN_1 \quad DN_2$$
$$DN_3 \quad DN_4$$

Figure 5.12 Roberts 1

0	2
-2	0

The new pixel value at pixel location DN_1 is computed according to the equation:

$$DN_{1,out}=Abs[DN_1-DN_4]+Abs[DN_2-DN_3]$$

where Abs refers to absolute values.

Figure 5.13 Roberts 2

-2	0
0	2

Utilizing these different filters, it was possible to extract virtually all the edges for the study area, as can be seen on Photo 5.3. Starting with a single input band, (in this case a TM5/TM1 ratio), the output from Sobel

Horizontal (Figure 5.10) and Sobel Vertical (Figure 5.11) was added together and displayed on blue. Similarly the sum of Roberts 1 and 2 (Figure 5.12 and Figure 5.13) was displayed on green while the red is the high-pass filtered output from the input image using an isotropic Laplace filter (Figure 5.9).

Enhancing features that trend in a specific direction will need a directional filtering technique. This may be necessary if one orientation is of particular significance.

Applying weighted digital filters, through Fourier analysis or convolution techniques to the data will result in extracted edge components having a selected, dominant orientation, rather that the non-directional result of a standard edge enhancement technique. Interpretation must, however, be done with caution, as artifacts of processing may be included in the result.

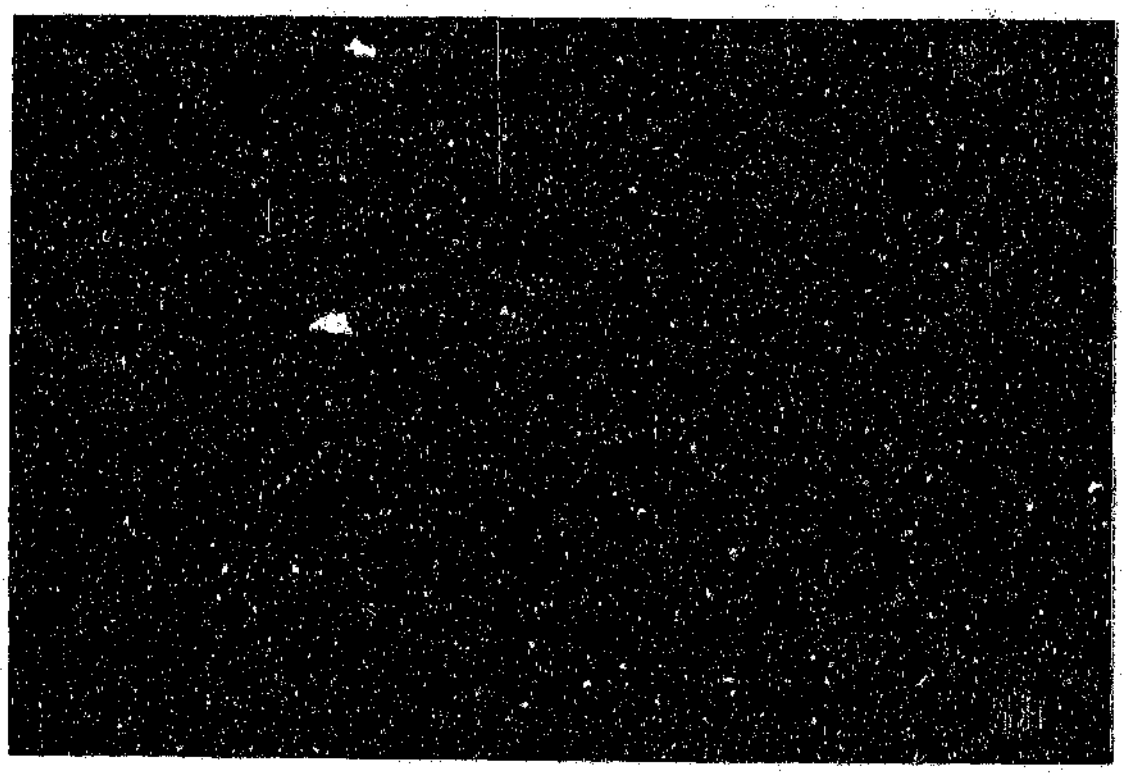

Photo 5.3 Extracted edges for Barberton Mountain Land

5.2.2.2 Band Dependent Edge Enhancement

Principal components produce an effective tonal and colour separation as the first two components, which represent the commonality and differences between spatial bands, respectively. By definition, the PC1 vector is along the major axis of the elliptical distribution, and the PC2 vector along the next widest minor axis of the ellipsoid (See 5.3.2.1).

Preserving the colour contrast is possible because of the separability of the PC1 & PC2 components. By performing the moving average process on PC1, using a 3 x 3 low-pass kernel (Figure 5.14), and subtracting the result from the spectral bands, the spectral differences between the bands are preserved. This process results in a 25% improvement over normal edge enhancement.

Figure 5.14 Low Pass Kernel

1/9	1/9	1/9
1/9	1/9	1/9
1/9	1/9	1/9

This method produces better results if the image variance accounted for by PC2 is less than 25%. If the image variance accounted is more than 25%, edge enhancing bands independently from one another produces better results (Longshaw, 1983).

Separation of the convolution window method into two processes, enables one to directionally bias the edge enhancement. This can be done by separating a directional convolution kernel into two components. The first component will operate on the original pixel as a 3 x 1 weighted average function and the second component will operate on the supervised PC1, (derived through the analysis of training areas on the image), as a 3 x 3 non-directional averaging window:

$$(\frac{P_{n-1}}{4})+(\frac{3P_n}{8})+(\frac{P_{n+1}}{4}) - \begin{vmatrix} 1 & 2 & 1 \\ 2 & 2 & 2 \\ 1 & 2 & 1 \end{vmatrix} = \begin{vmatrix} -1 & -2 & -1 \\ 2 & 4 & 2 \\ -1 & -2 & -1 \end{vmatrix}$$

A mixture of the two resultant components will have the properties of the directional kernel, but retain the colour enhancement attributes.

5.3 Multiple Image Enhancement

5.3.1 Ratioing

Somewhat favoured by geologists, this technique enables one to look at the spectral aspects of certain types of ground features. The DN of any one pixel in

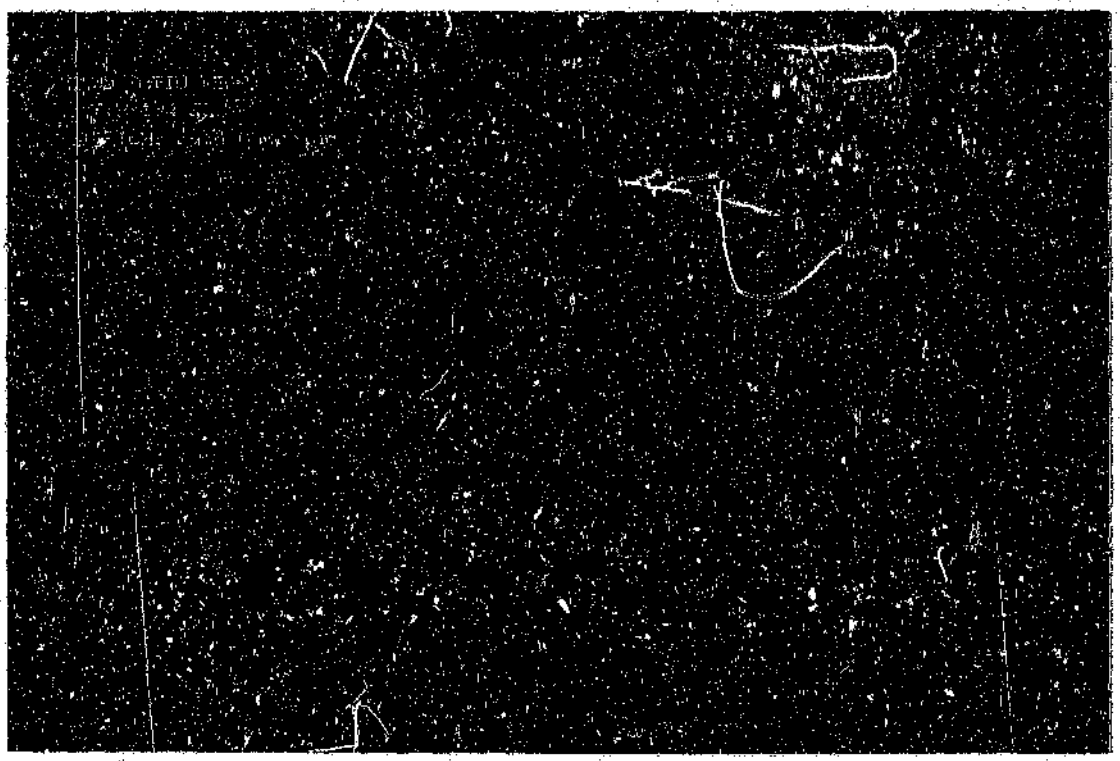

Photo 5.4 Band Ratio TM5/TM7:TM3/TM1:TM4/TM3 with Auto Gaussian stretch

any band is simply divided by the DN of the equivalent pixel in another band. The resulting quotient is a number that can theoretically lie between zero and infinity, but in practice lies somewhere between 0.3 and 3 (Short, 1982. p 438) These values are normally expanded to fit the range 0 - 255 for visual clarity.

Ratio images tend to smooth out intrinsic tonal contrasts related to topography by removing differences in reflectances from surfaces composed from the same features caused by topography. This is clear when Photo 5.4 is compared to Photo 5.1. It should be noted that Photo 5.4 was stretched using a Auto-2-Linear stretch while Photo 5.1 is displayed through a Auto Gaussian stretch.

Ratioing different bands will produce, enhance or suppress different features. This is evident when comparing the different band ratios used to create the false colour composite Photo 5.4. Ratios TM5/TM7 (Photo 5.5), TM3/TM1

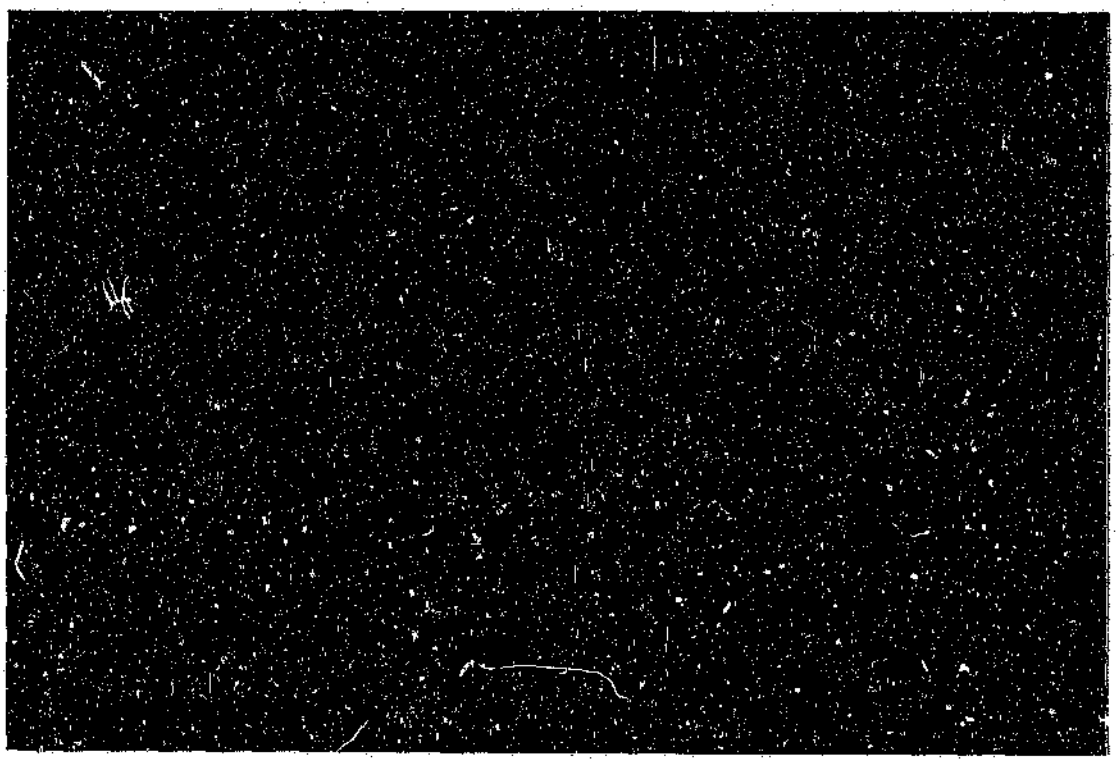

Photo 5.5 Band Ratio TM5/TM7 on black and white

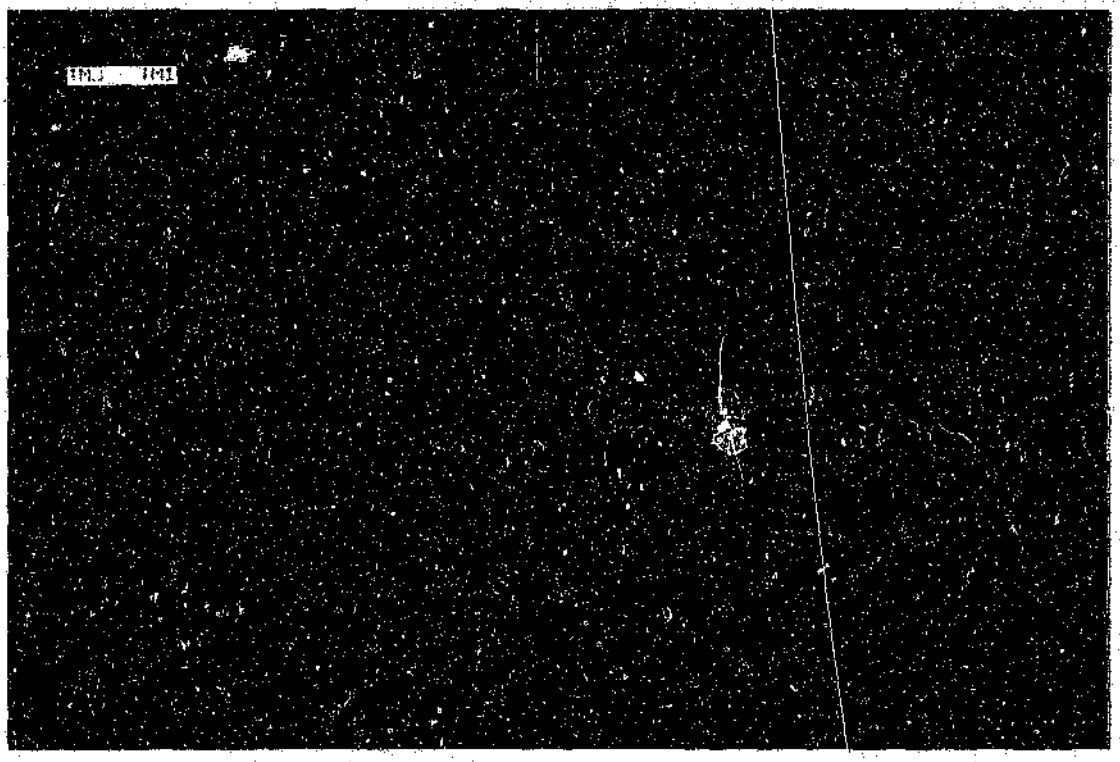

Photo 5.6 Band Ratio TM3/TM1 on black and white

Photo 5.7 Band Ratio TM4/TM3 on black and white

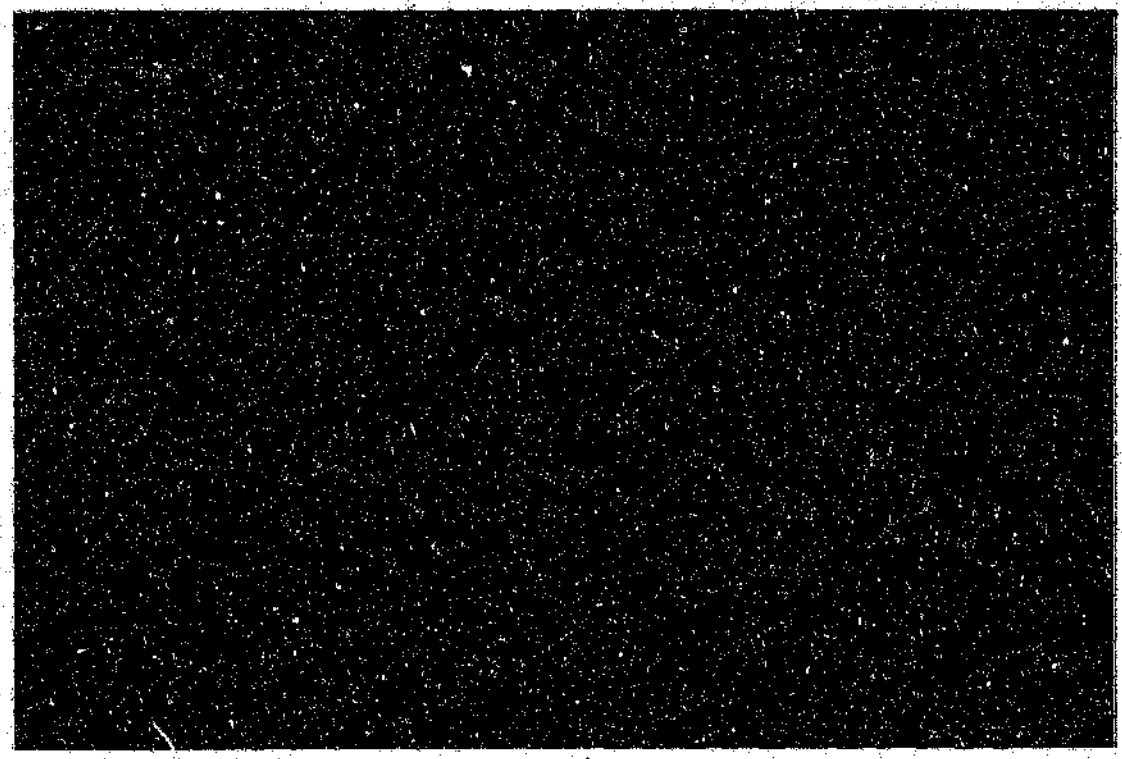

Photo 5.8 Band Ratio TM5/TM1 on black and white

(Photo 5.6) and TM4/TM3 (Photo 5.7) was displayed on blue, green and red, respectively.

Generally, the lower the correlation between the bands, the greater the information content of the band ratioed image. Note the difference between the TM4/TM3 ratio and the TM5/TM1 ratio (Photo 5.8) with regards to the vegetation. Scattergrams of TM5/TM7 and TM4/TM3 ratios (Photo 5.9) clearly display the correlation between the bands. From these scattergrams is should be clear that ratio TM4/3 will display 2 distinct trends. Photo 5.7 confirms this. Similarly Photo 5.5 confirms the expected rather trendless dull image.

Band ratios become rather inadequate with higher spectral resolution data, where the aim is to extract and characterize the shape of the spectral reflectance curve. Here the approach is to partition the image into spectral classes based on

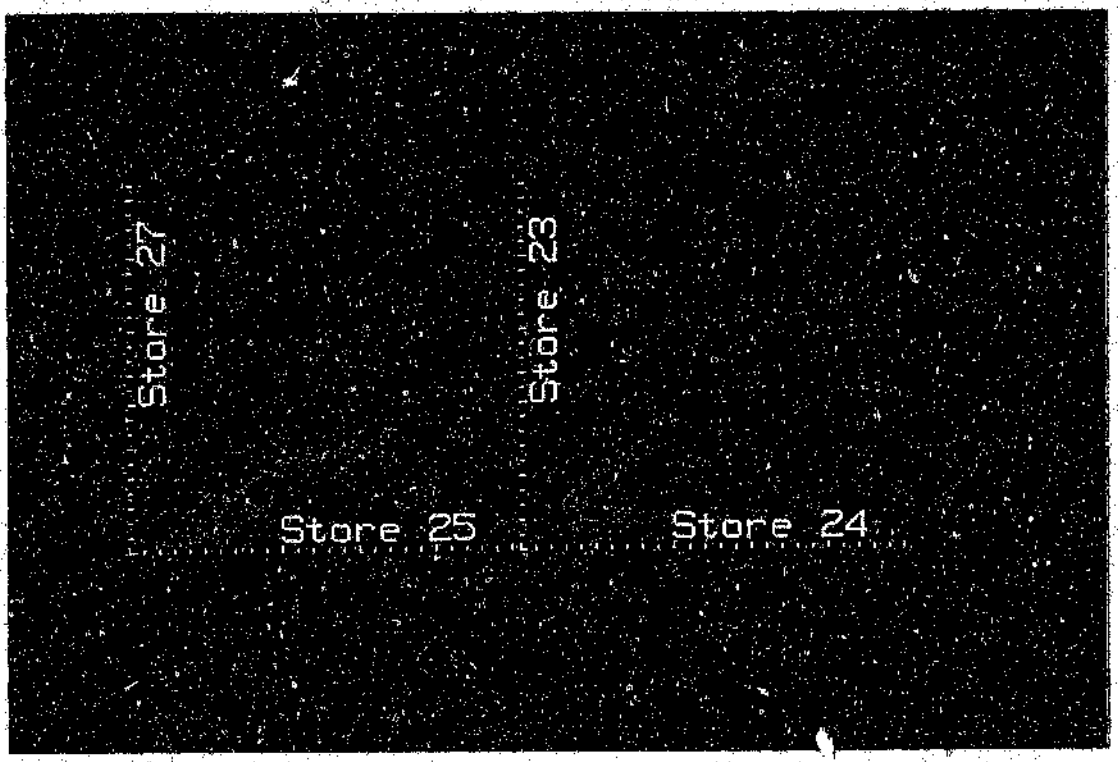

Photo 5.9 Scattergrams TM5 vs TM7 and TM4 vs TM3

similarity of shape.

5.3.2 Data Transformations

Rather than choosing three "best" bands from n-bands, one can use data compression techniques to extract most of the n-dimensional information into typically a three dimensional space. This also minimizes data redundancy characteristic of highly correlated datasets and enhances subtle spectral differences. Favoured methods are the important mathematical transformation Principal Components Analysis. The results are typically colourful, but often difficult to interpret, imagery. Canonical Analysis also belongs to this group.

5.3.2.1 Principal Components Transformation

Principal Components Transformation (PCT) is a multivariate statistical technique which is often used to determine the underlying statistical dimensionality of the image data set for image enhancement, for digital change detection and for characterization of seasonal changes in cover types, to mention but a few avenues reported on in the literature.

The technique basically consists of choosing uncorrelated linear combinations of variables in such a way that each linear combination (the principal components) extracted successively, show less variance. The result is to redefine the axes on which the data plot so that all the DN values are redistributed with respect to a new set of axes. Basically an axis rotation and translation procedure resulting in a linear combination of the original data, where each new axis defines a new dimension of information. The correlation that exists between the individual bands of the image is therefore removed.

A covariance matrix, derived from a random sample of the original data, is used to calculate a set of eigenvectors and eigenvalues which represent new or transformed axes. The new axes are uncorrelated, and contain a percentage of the total variance from the original dataset. If the linear intercorrelations of the variables are significant, the first few components will account for a large part of the total variance. The first order component contains the largest percentage of variance, typically 80% or more, with each successive component containing less. The first component can be thought of as an albedo or brightness image produced by data from all the bands. Random uncorrelated DN values (noise) from the input bands are normally relegated to the lower order components, where useful information is minimal. The information contained in these lower components are, however, often significant from a geological point of view.

Correlation between the bands arise from:

1. Natural spectral correlation - a bright object will tend to appear bright in a wavelength range, with a value distribution approaching a gaussian distribution;
2. Topographic slope and effect - for all practical purposes topographic shading is the same in all solar reflectance bands and can even be the dominant image contrast component in mountainous areas like the Barberton Mountain Land, and also at low sun angles, and
3. Overlap of spectral sensitivities between adjacent spectral bands. This factor is minimized through design, but cannot be eliminated.

Looking at the scattergrams of the TM bands (Photo 5.10), the high degree of correlation between the bands are clear. Most of the bands display a definite linear correlation between bands. The exception is band 4, which has a distinct bimodal relationship with the other bands. This is due to the large percentage uniform canopy cover (Pine and Eucalyptus plantations) which reflects strongly in the NIR (Near InfraRed).

To simplify, creating a scattergram of say band 1 against band 2, with means μ_1 and μ_2, the plot would look like Figure 5.15. It is clear that by shifting the axes to $X'(\mu 1, \mu 2)$, a new coordinate system is defined.

Figure 5.15 PCT: Step 1

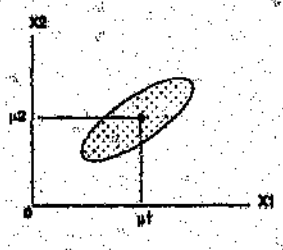

Values for the new data points are found by the transform relations $X'_1 = X_1 - \mu_1$ and $X'_2 = X_2 - \mu_2$ (Figure 5.16).

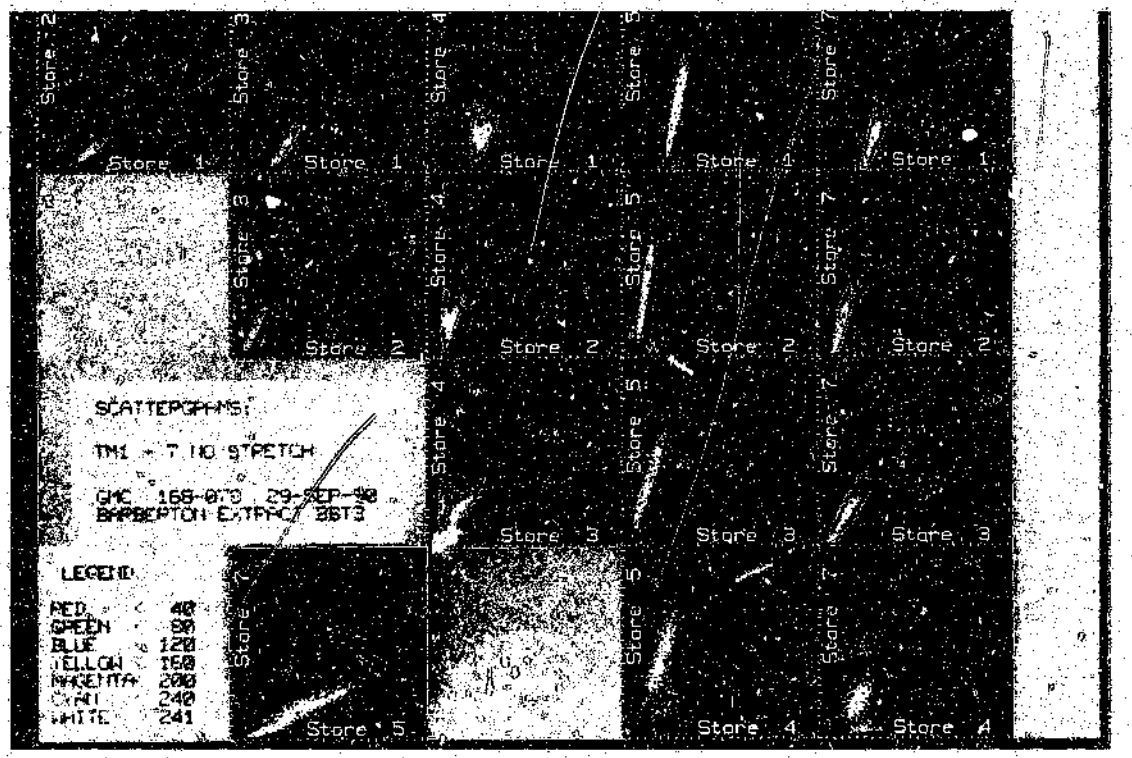

Photo 5.10 Scattergrams TM 1-7 Unstretched

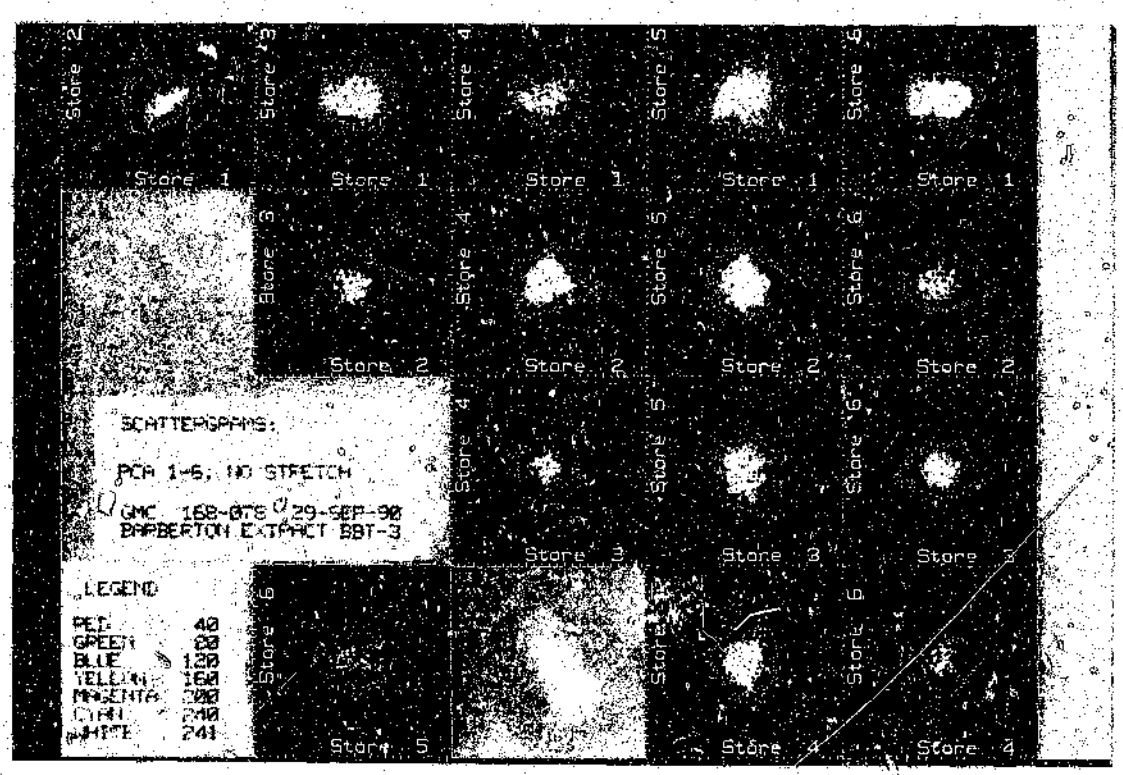

Photo 5.11 Scattergrams PC 1-6 Unstretched

The X axis system is rotated about its origin (μ_1,μ_2 in the original system) so that the variance σ^2_{PC1} is a maximum (Figure 5.17). Since PC2 must be perpendicular to PC1, and there are only two dimensions, PC2 is fixed. The PC axes are the Principal Components of this 2-dimensional space, with PC1 essentially a weighted average albedo image containing most of the scene brightness information.

Figure 5.16 PCT: Step 2

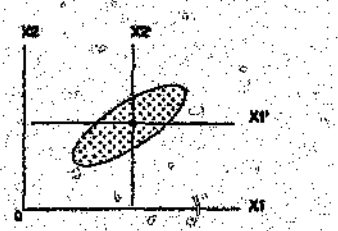

Figure 5.17 PCT: Step 3

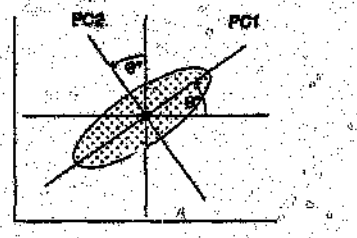

Related to an N-dimensional feature space, correlation between bands will tend to result in a strongly elliptical pixel distribution. The principal components of this N-band image data set are thus the orthogonal axes of the N-dimensional ellipsoid constituting the image feature space. The longest axis of the ellipsoid accounts for most of the reflectance variance in the multiband image, the First Principal Component. By definition the second longest axis of the ellipsoid is the Second Principal Component. Subsequent higher axes contain successively smaller portions of the remaining scene variance with a decrease in signal to noise ratio.

Setting the mathematics aside, the following characteristics of the principal components transformations are of special interest to remote sensing:

1. The total variance is preserved in the transformation, i.e.:

$$\sum_{i=1}^{N} \sigma_i^2 = \sum_{i=1}^{N} \lambda_i$$

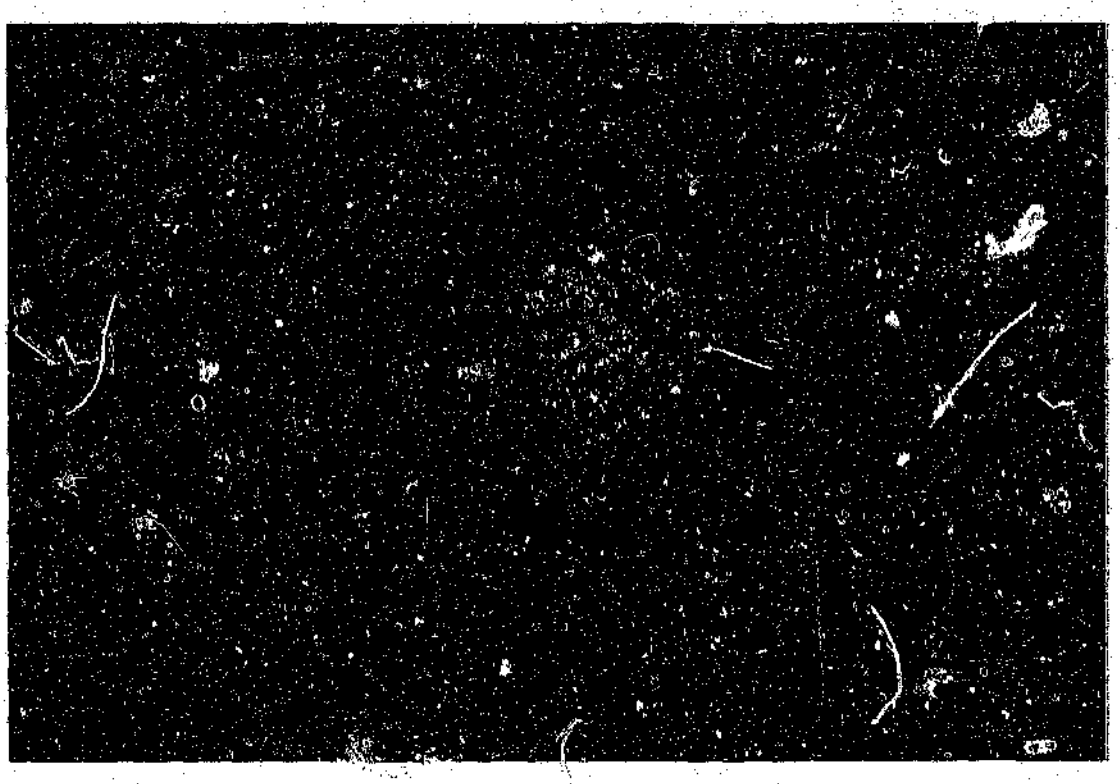

Photo 5.12 Principal Com **re hed on Blue-Green-Red**

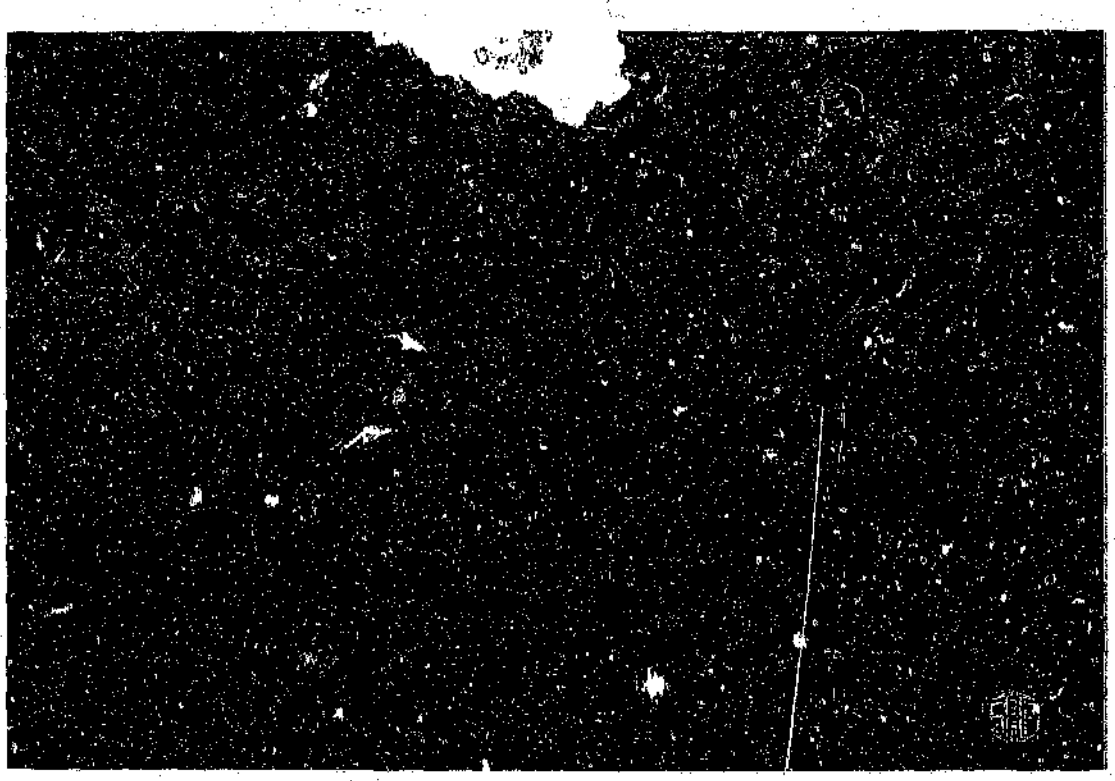

Photo 5.13 Principal Components 123 viewed through Auto-2-Linear stretch

where σ_i^2 are the variances of the original variables.

2. It minimizes the mean square approximation errors.

3. This is the only transformation that generates uncorrelated coefficients (Moik, 1980). In a geometrical sense, it rotates the highly correlated features in N-dimensions to a more favourable orientation in the feature space, orthogonal to each other, such that the maximum amount of variance is accounted for in decreasing magnitude along the ord ·ed components. The process has been viewed as an information compression into a smaller number of components from the large number of features by discarding redundant information into higher order components.

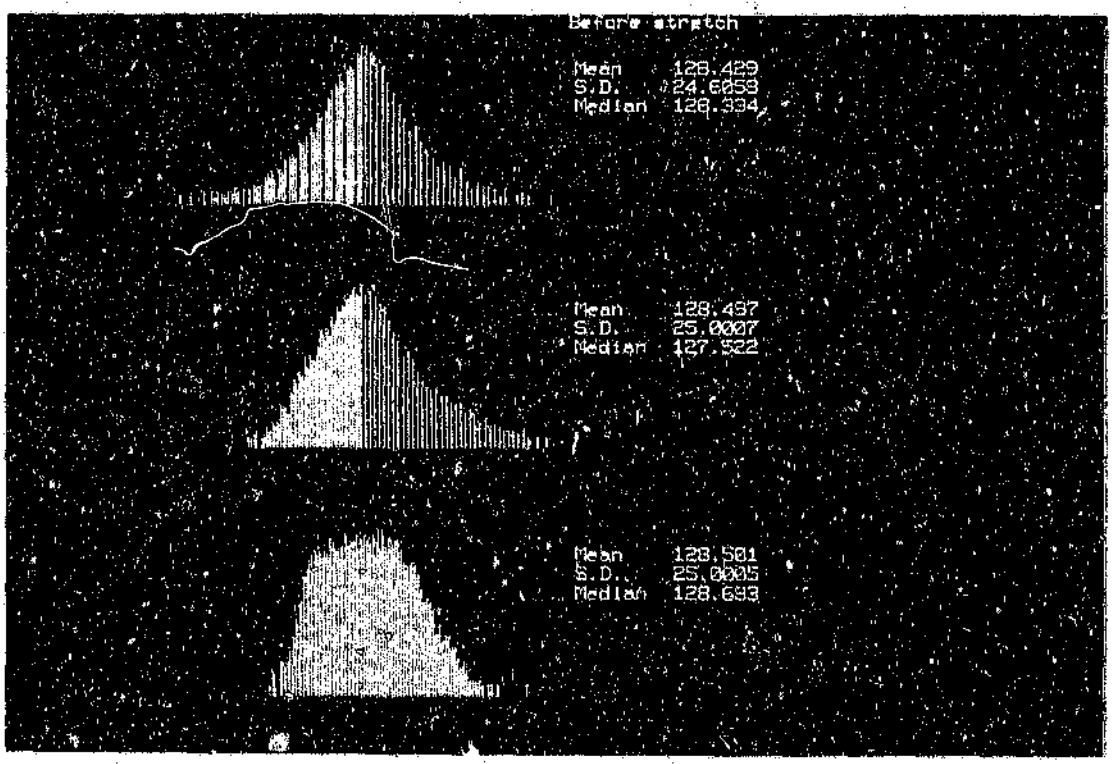

Photo 5.14 Histograms for Auto-2-Linear stretch on PC-123

Photo 5.12 displays principal components PC-123 on BGR. Although the change in colour from the natural false colour composite (Photo 5.1) is most striking, it is the increase in the volume of visual information that is remarkable. The north-northwest striking dykes are much more prominent on the principal components image. As this image seemed not to make use of the full digital number range available, a stretch was applied. The stretch chosen was the Auto-2-Linear stretch, which was also applied to the natural colour composite (Photo 5.2). The resultant enhancement to the visual quality of the image is quite drastic, considering that the principal components transformation should have utilized more of the available DN range. The histograms for the three components confirms this apparent shortcoming.

As indicated before (Section 5.2.1) the statistics for any of the operations are calculated using a 128 x 128 grid, which explains why the transformation output occupies a narrower than expected range. Calculating the eigenvectors and eigenvalues under a mask covering the complete input store should eliminate this problem, but it is computationally very expensive and the results are not perceptibly better than the results from the two stage procedure used here.

The higher order components from principal components transformation usually contains very little useful information, however with regards to geology, one often finds that some feature which is drowned out in the lower order components, becomes quite noticeable when the surrounding features are less prominent (Photo 5.15).

In remote sensing applications the principal components are usually calculated from a variance-covariance matrix. Another approach is that of using the

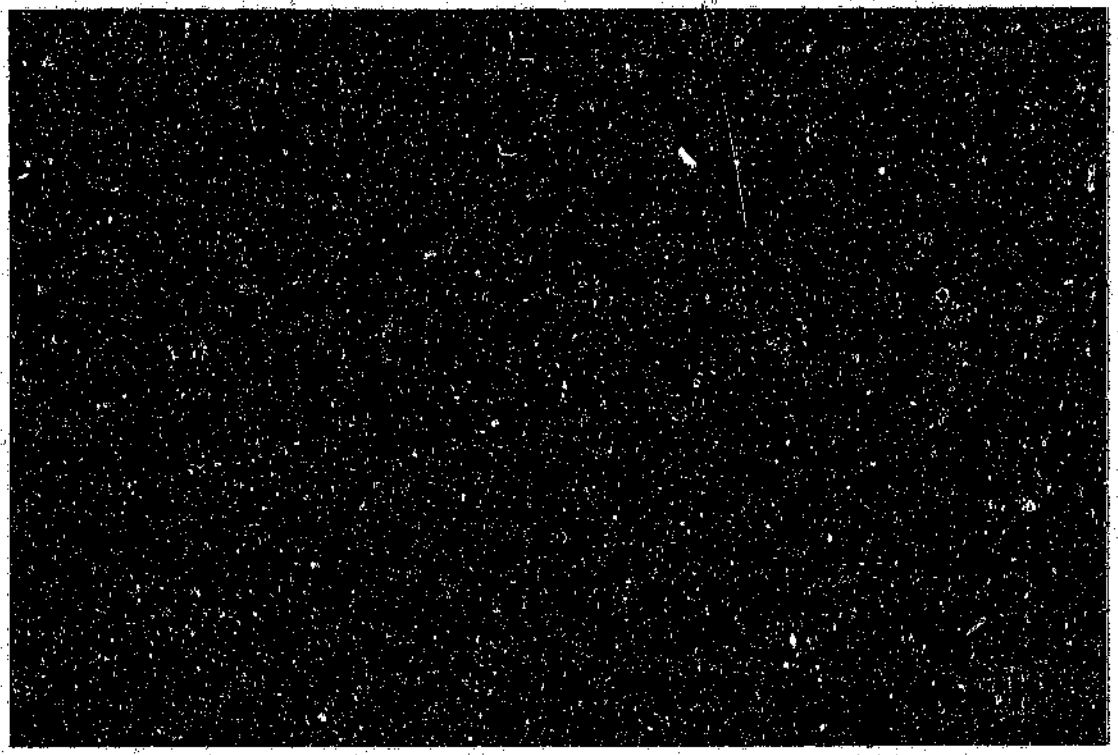

Photo 5.15 Principal Components 456 viewed through an Auto-2-Linear stretch

correlation matrix, derived from the division of the covariance matrix by the appropriate standard deviations. This reduces all the variables to equal importance as measured by scale. Since principal components are not invariant under the linear transformation where separate scaling of the original variables exists, it is clear that the principal components of the covariance matrix and that of the correlation matrix are not the same, since principal components of the correlation matrix are invariant under separate scaling of the original variables.

External variances can be minimized through standardization of all the data from different bands to a standard deviation of one. Then each band would contribute equal variance.

A significant difference is evident when comparing the results from using variance-covariance and correlation matrices for two LANDSAT subscenes

(Singh & Harrison, 1985). Regarding these variables, standardized to unit variance, as a better basis for carrying out principal components analysis seems reasonable. Visual inspection of the first principal component images reveals that the images obtained from the correlation matrix has better contrast. The significant improvement in image enhancement, however, occurs in the second principal component image using the correlation matrix.

It should also be noted that a significant improvement in Signal-to-Noise ratio is effected when using the correlation matrix method of calculating principal components.

Although principal components transformation is used in data compression, it should be noted that for land cover discriminations, the higher order components contain valuable information in comparison with some of the lower order components, which have no obvious information content.

As the interband covariance for a particular scene is always unique, the outcome of principal component analysis transformation will be highly scene-dependant and difficult to apply predictively (Lamb, 1984)

5.3.2.2 Canonical Analysis

This transformation is based on the spectral characteristics of categories defined within the data. These categories are represented by training areas selected from the original data. The spectral characteristics of the training areas are statistically described in terms of the mean, standard deviation and covariance.

The objective is to maximize the covariance between categories and minimize the covariance within categories, which increases the separability of classes while minimizing the differences within each class. As with PCT, the first component contains most of the variance, and the lower order components contains the noise. Information falling outside the spectral characteristics of the training areas are looked at as being noise, therefore the lower order components will display more noise than the corresponding components of a PCT.

Canonical Analysis differs from principal component analysis in that training areas are defined from which the statistics necessary for the transformations are calculated. This is similar to PCT statistics calculated only under a masked area of the image.

5.3.2.3 Geological Applications of PCT

Enhancing edges to emphasize geological structure and colour to emphasize lithological differences are particularly relevant in a geological sense.

Subtle colour differences will feature as information poorly correlated from band to band, and are therefore more apparent in higher order components. Geological edges, representing lithological boundaries, joint and fracture patterns and fault traces, etc., are mostly visible as a result of topography and shadow. Since these boundaries occur in all the bands, the bands are strongly correlated. Therefore a PC1 image can be expected to highlight geological structure expressed through topographical features. The edges defined by colour changes will tend to be poorly correlated, and therefore only show up in higher order component images.

5.3.2.3.1 Spectral Feature Separation

In areas with minimal vegetation cover PCT can be expected to enhance spectral contrasts between rocks in a non-predictive way.

Using the first three PC's, more than 90% of the information can be displayed simultaneously. While the colour variations in the false colour composite may enhance less noticeable variations, it should be noted that colour per sé cannot be used quantitatively, only as an indicator of change. Since PC1 represents most of the topography related brightness information, composites from higher order components will be less topographic in appearance, leading to the possible detection of subtle geological contrasts enhanced in the higher order components.

5.3.2.3.2 Spectral Classification

Spectral feature separation leads to classification, a procedure that has been most successfully applied to agriculture. Classification routines have not been particularly successful when applied to geology. This is largely due to natural inhomogeneity of geological materials, gradational boundaries and the influence of vegetation, as well as the small spectral response range for geological materials in general.

While PCT may optimally separate geological features, the output component imagery will only be suitable for qualitative visual interpretation. The re-alignment of the image feature space in a different and more efficient way is only a method of assisting the analyst in the selection of features and training

areas, but it will not contribute much to an improved classification.

5.3.3 Enhancement through Colour

5.3.3.1 Colour Composite Selection

Band selection for colour composition should be based on spectral logic, rather than some statistically based approach that often confuses data variance with informati One of the more meaningful approaches is to use the correlation matrix, because we are basically attempting to maximize colour information by selec r, the three least correlated bands.

5.3.3.2 Colour Enhanced Original Band Imagery

Correlation between three spectral bands combined as a colour triplet results in a 3-D ogram in the shape of an thin ellipsoid near the achromatic brightness axis. Contrast stretching of the three input images does not remove this correlation, it merely enlarges the ellipsoid, with the result that the available colour space remains under utilized.

To maximize the utilization of the available colour space, the correlation between the individual input bands need to be removed, or at least significantly reduced. This is done by enhancing colour differences between the components by stretching, followed by a inverse principal components transformation, which will not reintroduce the original correlation. This decorrelation stretch (Photo 7.12, Section 7.4) produces a colour enhanced output with an improved signal to noise ratio and a spherical symmetrical histogram, indicating a much

better utilization of the available colour space.

5.3.3.3 Edge and Colour Enhanced Imagery

A result similar to the decorrelation stretch can be obtained by transforming the colour triplet to the Munsell Colour Space coordinates of Brightness, Hue and Saturation (Figure 5.18). As PC1 is strongly related to the scene brightness, high-pass filtering of the brightness image together with any desired stretches to the Munsell coordinates will produce a result similar to decorrelation stretch through inverse principal component transformation (Lamb, 1984).

Figure 5.18 Munsell Colour Coordinates

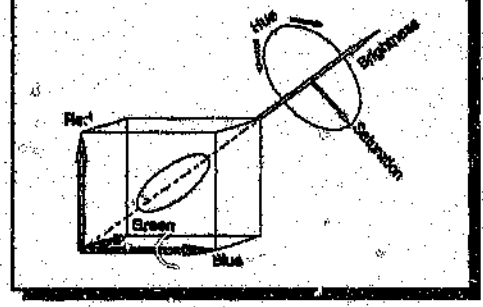

This method can be modified to produce a less noisy colour image by substituting the brightness image in the IHS transformation with the PC1 component, saturated and edge enhanced, before transforming the colour co-ordinates back to the original cartesian band coordinates. This technique has the advantage in permitting total predictive control of colour, unlike an inverse PCT transformation.

5.3.3.4 Colour Transformations

For this study the remotely sensed data are displayed using the BGR (Blue-Green-Red) colour space. A different coding technique displays data according to intensity or brightness, saturation or colour value (on grey scale) and hue or

colour tone (in the range blue-green-red-violet-blue). This is known as Intensity-Hue-Saturation (IHS) coding and displays the information pertaining to the intensity on red, to hue on green and to saturation on blue.

The processing system used calculated IHS as follows:

$$Intensity = \left(\frac{Red+Green+Blue}{3}\right)$$

$$Hue = \tan^{-1}\left(\frac{V_1}{V_2}\right)$$

$$Saturation = \sqrt{V_1^2+V_2^2}$$

where

$$V_1 = \frac{(2*Blue-Green-Red)}{\sqrt{6}} \quad \text{and} \quad V_2 = \frac{(Red-Green)}{\sqrt{2}}$$

Photo 5.16 displays the RGB colour space after a two stage IHS colour transformation. This was accomplished by transforming the RGB colour space into the IHS colour space, and inverting the transformation back to the RGB colour space, replacing the intensity component with a monotone image with DN 128. An Auto-2-Linear stretch was applied.

Another colour transformation used during the research were the transformation to Hue-Lightness-Saturation (HLS) colour space, which is a perceptual colour space recommended for computer graphics by the Graphics Standards Committee, Siggraph, ACM (Gemstone Interactive User Manual, 1990).

Hue is a circular measure of the colour (blue-green-red-violet-blue) in the range

Photo 5.16 RGB to IHS to RGB Colour Transformation

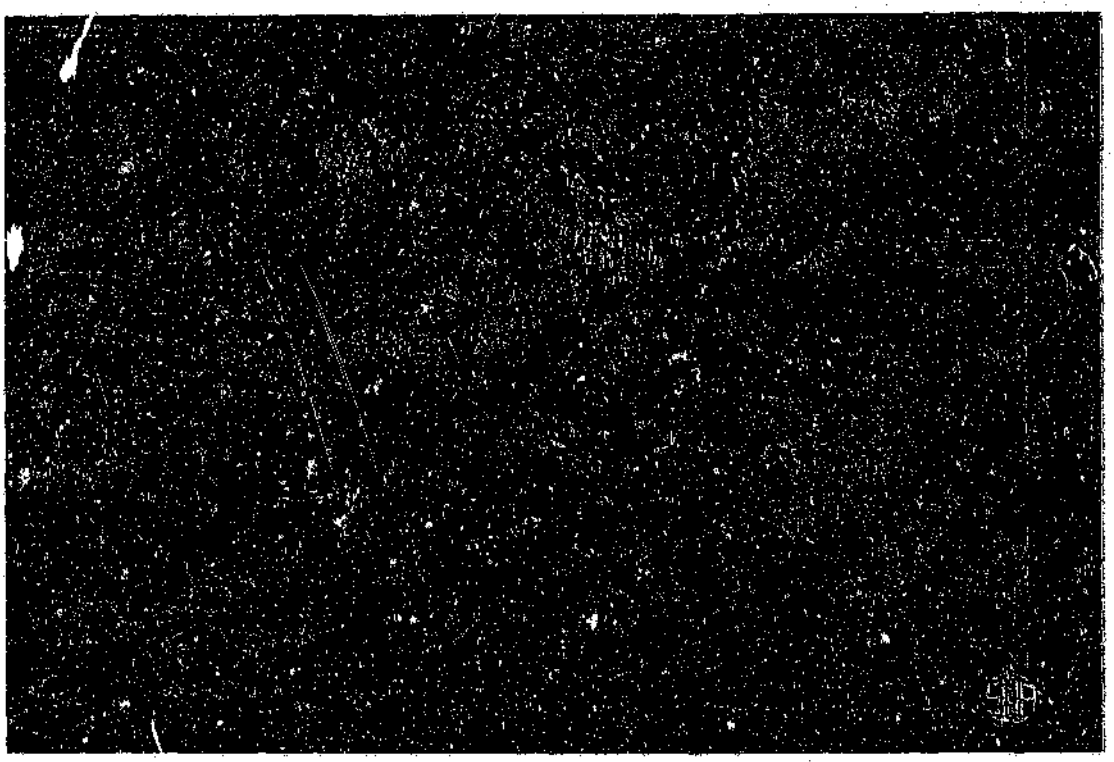

Photo 5.17 RGB to HLS Colour Transformation

0 to 360 with 0 representing blue. Lightness is a measure of the intensity or luminosity of the colour. Saturation is a measure of the purity with 0 representing no colour (monochrome) and 1 representing pure colour.

Transforming the RGB colour space into the HLS colour space results in a rather bright, but not very informative image (Photo 5.17).

5.4 Classification

The basis for classification is the correlation of different categories of interest with statistically separable groups of data as defined by their spectral properties in multidimensional space. Multivariate classification may be performed by either of two methods: supervised and unsupervised (See Table 5.1).

In an unsupervised classification, the computer is asked to group pixels into different spectral classes or clusters on the basis of mutual differences in multispectral data space. The identities of these groups are not known beforehand and a name is assigned if the classes prove to be meaningful.

In a supervised classification, the classes are known for small training areas. The computer uses these training sets to classify the rest of the scene.

The classification types available for this study were:

1. Box - The upper and lower limits for each image band are defined from training sets. Only one class results;

Type	Classification Method	Comments
Supervised	Maximum Likelihood	Based on the principle that a given pixel should be assigned to a class to which it belongs with the highest probability. A common stratagy, the Bayes-optimal, minimizes the error of misclassification when the probabilities of occurrence of each class are equal.
	Linear	A general term to mean all techniques which use linear surfaces (hyperplanes) to separate classes. Several iterative methods for deriving these classes can be used.
	Piecewise Linear	Generaliza on for linear classifiers. Useful when the classes cannot be separated by linear surfaces. The parallelepiped or 'box' classifier is an example.
Unsupervised	Distance Based Clustering	Unsupervised classification is an attempt to determine the location and limits of significant clusters in feature space with no prior knowledge of what is contained with the image. Several methods use distance measures to group data into clusters. These are iterative methods, varying slightly in detail of handling, initiation and updating clusters.
Both	Table Lookup	Can be used to implement any decision rule obtained from any classification method.

Table 5.1 Some common Classification methods

2. Discrete - The discrete or histogram classifier operates by generating a list of pixel value combinations which appear within the training set. Only one class results, and
3. Maximum Likelihood - Either 16 or 64 classes resulted from this statistical approach.

Attempts to classify the image of the study area through a maximum likelihood classifier into 64 classes failed due to hardware limitations. In order to perform a classification over the study area, an area of 300 by 400 pixel were selected and the maximum likelihood classifier initiated. Some nine classes resulted from the

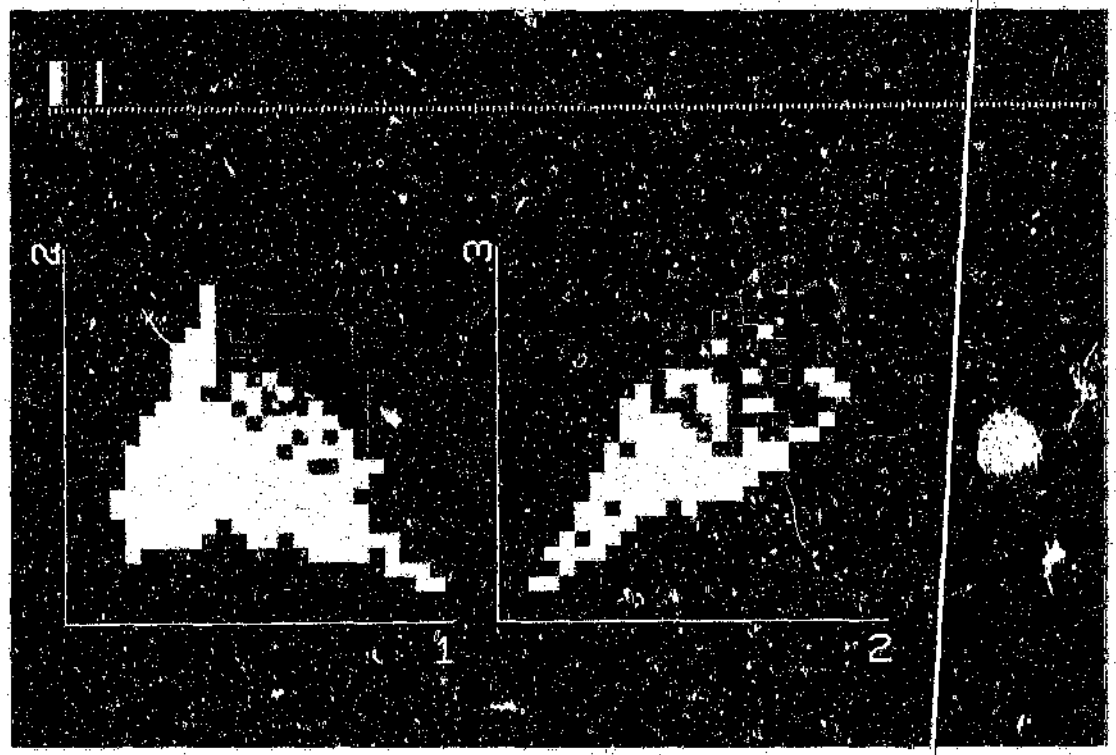

Photo 5.18 Classes for Maximum Likelihood Classifier

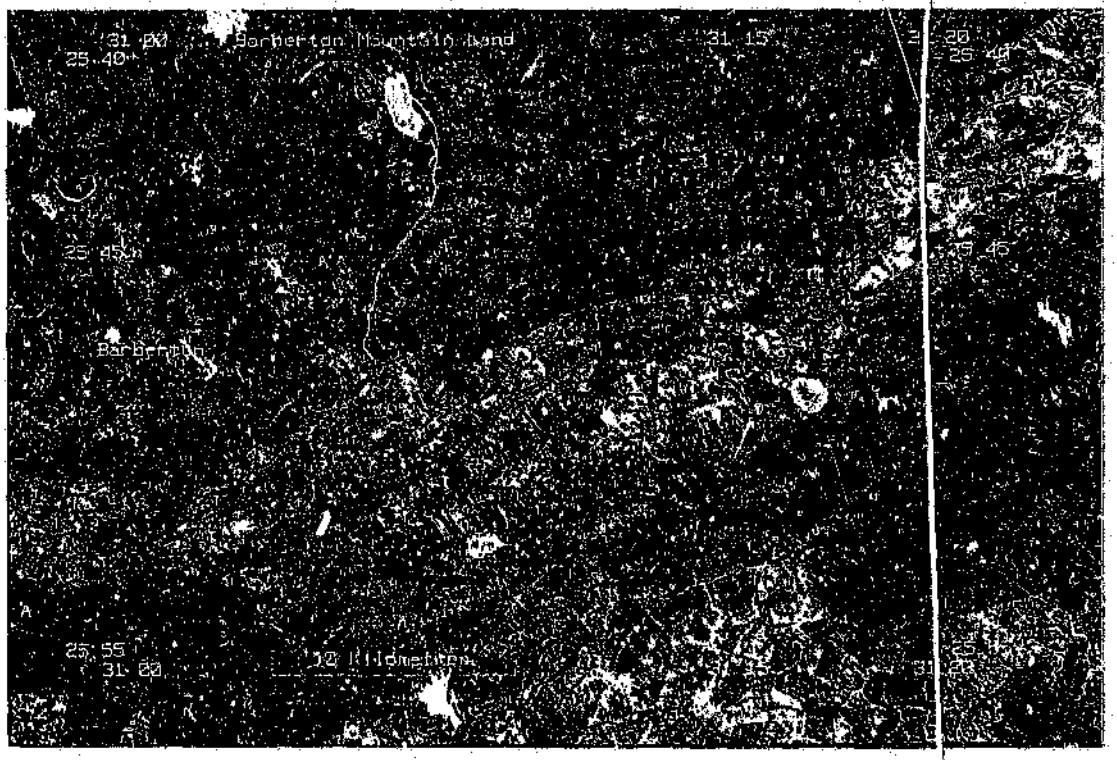

Photo 5.19 Classified Image

classification of three bands, and these were manually combined into five classes.

Class	Means			Standard Deviations		
	Band 1	Band 2	Band 3	Band 1	Band 2	Band 3
1	82.32	115.6	111.2	32.8	14.8	10.9
2	131.3	104.0	104.0	31.7	17.7	12.3
3	151.0	151.6	156.8	23.5	18.7	15.9
4	121.9	196.9	143.9	6.9	5.7	5.0
5	220.8	31.19	29.52	15.5	5.1	3.3

Table 5.2 Means and Standard Deviations for MAX64 Classification

Table 5.2 lists the means and standard deviations for the five classes displayed on Photo 5.18. When studying the scattergrams in Photo 5.18, classes four and five could conceivably be lumped together. (This is the light and darker reddish coloured classes on the photo.) As far as the band 3/2 scattergram is concerned, class two, the whitish area, does not have a definable outline. (Please note that due to photographic reproduction, there are two whitish classes. The distinction is visible only on the scattergram of band 2/1.)

Using these five classes to classify the image resulted in a rather messy and singularly uninformative view, Photo 5.19.

5.5 Predictive techniques for identifying spectral anomalies

Band ratios, spectral indices and pair-wise principal components all operate on two bands of data only, while quite a number of other bands are also available.

5.5.1 Pair-wise Principal Components

This technique compensates for atmospheric conditions automatically. The second principal component is considered in each case, since the spectral reflection and absorption contained in the second component represent the "less correlated" component of each of the two bands. In the case of TM bands 5 and 7, the resultant PC2 should give an estimate of the clay plus vegetation absorption as a more effective alternative to a ratio. Similarly, if the second component from input bands 3 and 4 is used together with the second component from bands 5 and 7, the resultant second component should give an indication of only the clay. This type of approach was used by Fraser and Green (1987) to formulate their "Directed Principal Components" method of reducing the influence of vegetation (Section 7.4.3).

5.5.2 Multiple Linear Regression

Multiple linear regression estimates the expected value of an image band as the linear combination of the other or all bands, using a single set of partial regression coefficients. The predicted value is then subtracted from the actual value to give a residual or error image. This approach assumes linear mixing of the radiance from all surface materials contributing towards the pixel of interest, and is able to separate vegetation from "clay" effects in the 2.2μm region as well as offering a good overall solution for atmospheric path radiance.

The main drawback of this technique is that a single transformation is used to predict the band of interest, which may not describe the optimal coefficients for smaller subsets of the image.

5.5.3 Polynomial regression

Polynomial regression fits a polynomial of a specified degree to each pixel spectrum. It also allows us to examine the error between the predicted and observed data values. A polynomial of degree five will uniquely describe a spectrum of six values. Choosing a lower order polynomial should result in some error between the calculated and observed values, which should increase with the decrease of the order of the interpolating polynomial.

5.5.4 Data-adaptive linear filter

Considering image spatial data in band prediction are the basis of the data-adaptive linear filter. In this instance the predictions made from neighbouring pixels influences the prediction for the current pixel. This helps in avoiding spurious anomalies. The computational expense of this technique would normally be prohibitive.

6. Obstacles in Geological Remote Sensing

Environmental conditions such as deep weathering, fireburn and vegetation are significant obstacles to geoscience remote sensing.

6.1 Deep weathering.

Extensive chemical weathering and alteration of surface rocks, sometimes to depths of hundreds of meters, like the arid environments of the Australian continent, will result in the development of surficial crusts or layers of chemically enriched material, mostly laterites, silcrete, calcrete and bauxite. Breakdown and leaching of the surface rocks also leads to the formation of clays with the mobilization of iron and silica. These deeply weathered regions are thus characterised by the extensive development of clay minerals and the various concentrations of iron oxides, carbonates and silica minerals, totally obscuring the underlying geological environment.

It can be seen that the ability of remote sensing techniques to map clay alteration directly associated with mineralization, as in the semi-arid conditions of Arizona, is unlikely to be successful in Australia's deeply weathered environment (Simpson, 1990).

6.2 Fireburn

From a remote sensing viewpoint, the effect of fire is more important that the

fire itself. The resultant drastic reduction in vegetation density and very prominent and lasting scar patterns are probably the most serious obstacle to thematic remote sensing of any kind in any arid and tropical environment worldwide.

The time necessary for regenerated vegetation to reach a density which would render it indistinguishable from the surrounding unburnt vegetation is largely determined by the climate of the area. However, as fuel from regenerated vegetation becomes available, older burns can be partially or totally overprinted by subsequent burns, leaving a patchwork of fireburn scars which appear on visible and near-infrared imagery as a dark-bright mosaic, the darkest being the oldest and the bright the newest burnt areas.

It may be extremely difficult, even impossible, to determine whether a boundary change observed in imagery is due to changes in rock type, or to vegetation density differences across a fire boundary.

Photo 5.13 shows what can only be the result of a not so recent fireburn. Towards the top half of the study area, in the region of the Copper Creek (refer to Photo 2.1), the principal components transformation, as viewed through the Auto-2-Linear stretch, displays an area which is distinctly different to the adjacent areas on both sides. Since this area seems to be enclosed by streams on all sides, the conclusion is that this represents a firescar. Note that within the forested area quite a number of these blueish patches is evident, which would be consistent with the practice of burning the newly logged areas to get rid of the undergrowth before replanting.

To enhance the underlying geological features, it is firstly necessary to enhance, detect or nullify as far as possible the overlying fireburn features. In grassland recent firescars are generally obvious, while the speed of regeneration of grassland, coupled with the frequency of burns, normally lessens the impact of older burns. Problems occur in identifying recent low intensity fires in woodland areas, particularly those in which only the ground cover vegetation and grasses are removed, since the ash darkened areas may be indistinguishable from the darker canopy vegetation.

One technique useful in detecting recent burn areas through principal component analysis, is to apply PCT to TM bands 1 to 4 and study the second principal component which gives an excellent display of vegetation density. Firescars can be easily detected visually. This will then give an indication of the likelihood of the detected edge being the termination of a lithology or rock type.

6.3 Vegetation and Geological remote sensing

In conditions where roots penetrate to the subsurface geological environment, analysis of the vegetation pattern may provide the only indirect indicator of that environment. From a geological viewpoint, vegetation spectral signatures are considered to be a noise contaminant. In the short wavelength infrared region (1.1-2.5μm) the interference of both dry and green vegetation are significant in realizing the spectral characteristics of various clays, carbonates and sulphates important to a geologist.

Another problem is lichen, which can completely cover both rock and soil

surface, even in areas where other vegetation species are sparse. The absence of a distinctive chlorophyll absorption feature at 0.65-0.70 μm or a infrared plateau between 0.7 and 1.0 μm means that processing techniques normally used to detect vegetation will not necessarily show lichen. Lichen, as small submillimetre colonies, will at any significant density completely obscure the signature from the rock below.

A typical vegetation reflectance spectrum shows a region of strong absorption in the visible due to plant pigments, including chlorophyll, adjacent to a region of much higher reflectance in the near-infrared dominated by reflectance from the cell structure. Laboratory studies have shown that anomalously high concentrations of many different metals in plant nutrients will cause a stress response. This response is displayed spectroscopically by reduced absorption in chlorophyll bands in the visible and an accompanying shift of the abrupt rise in reflectance between the visible and the near-infrared, or 'red edge' toward shorter wavelengths (Chang and Collins, 1983).

Either of the reduced chlorophyll absorption in the visible, or the shift of the red edge, can be used to detect plant stress response caused directly or indirectly by minerals derived from underlying ore bodies, by using the spectroscopic anomaly to infer a geochemical anomaly.

Scattering for vegetation is generally assumed to be Lambertian (isotropic) throughout the visible and near-infrared. It was found, however, that the reflectance properties of leaves tend to be more specular in the visible, and Lambertian in the near-infrared (Salisbury, et al., 1987).

Considering the fact that a large part of the vegetation in the Barberton Mountain Land study area are regularly spaced forests, either Pine or Eucalyptus, with very little undergrowth and a ground-covering carpet of pine needles or leaves, the absorption in both the visible and the near-infrared will be higher than for the surrounding areas where natural vegetation occurs. The shape of the pine needles also lend it to a greater amount of isotropic scattering than would leaves of other indigenous forests.

It should therefore be easier to identify a geobotanical or biogeophysical anomaly within the area covered by the plantations than in the area covered by natural vegetation, because of the uniformity of the signature returned.

6.3.1 Vegetation Spatial Variability

The NOAA AVHRR collects data in the spectrum ranging from the visible to the thermal infrared. The resolution at nadir is about 1.1 kilometre. Looking at the various ratios one can deduce quite a lot of information about the canopies being studied. Ratios developed through the use of this data include those in Table 6.1.

Ratio Name	Construction
Simple ratio -	NIR/Visible (0.9μm/0.58μm)
Normalized difference (NDVI)	(NIR - Visible)/(NIR + Visible)
Vegetative Index -	(NIR - Visible)

Table 6.1 Ratios used for Vegetation Indexes

NDVI is a bound ratio with values between -1.0 and +1.0. The usefulness of vegetation indices are dependant on the degree to which the spectral contribution of non-vegetation components (soil in this case) can de isolated from measured response data. At higher vegetation densities the Simple Ratio seems more useful.

6.3.2 Forest Classification

Spectral variations caused by topographical effects leads to difficulties in discriminating between many individual species. Using band ratioing result in an increase in classification inaccuracy because of the accumulated spectral variance between the bands.

It is generally accepted that the configuration of LANDSAT TM data is well described in a three-dimensional Euclidean space, with a loss of less than 10 percent of the total variance and that the first principal component (PC1) can be related to scene brightness.

Late summer proved to be a good period for forest discrimination through remote sensing. (Heller and Ulliman, 1983)

To overcome the high spectral variability of the TM scenes, it is accepted that subjecting all the scenes to smoothing filters with a neighbourhood function of 5 x 5 pixels (3 x 3 in band 6) without threshold, will tend to smooth the heterogenicy of the images, which can improve the final classification accuracy. In this study the images were not smoothed.

6.4 Mineral Mapping and Vegetation Removal

Techniques for mapping surface components attempt to relate the known spectral signatures of surface types to the detected band responses of the data. Two commonly used techniques are:

1) Ratio methods which compare two channels highlighting spectral absorption of particular surfaces (Podwysocki et al., 1983), and
2) Classification methods which use ground reference information to identify spectral grouping within the data (Curren, 1985).

This does not solve the problem of pixel spectra being a mixture of component spectra, i.e. the influence of one surface type will be confused by the influences of all the other contributing surface types within range.

A method is required which uses all the information to determine the composition of each pixel given some prior knowledge of component reflectances. Such a method would enable specific mapping of individual materials and, as a by-product, obscuring materials, like vegetation, could be removed.

By assuming that pixel reflectance is a linear mix of component reflectances, i.e.

$$R_i = a_i A + b_i B + \ldots n_i N$$

where

$a_i \ldots n_i$ are the reflectances of substances in the wavelength i,

$A \ldots N$ are the proportional amounts of substances which

compose the pixel, and

R_i is the pixel reflectance value in the wavelength interval i.

one is faced with the problem of non-reflective influences:

1) sensor peculiarities;
2) atmospheric interaction with radiation, and
3) variations in illumination between bands and between pixels.

The raw data consists of pixel count values, which must be converted to reflectance to facilitate the removal of the non-reflectance influences. The method consists of four stages:

1) Minimum value subtraction;
2) Band-mean division;
3) Reflectance-mean multiplication, and
4) Pixel unmixing.

Although the results from this technique is reported to agree well with field observations and mapped geology (Bierwirth, 1990), and accurate mapping of the spacial distribution of individual surface types is almost a certainty, the system is very sensitive and end-member spectral separability, very accurate reflectance calibrations and realistic modelling of the dominant scene are prerequisites for successful modelling.

Removing vegetation has particular application for mineral exploration, since

vegetation cover invariably complicates the issue enormously. Having unmixed vegetation and geological end-members it is possible to recalculate brightness values in the original bands with both green and dry vegetation removed.

By scaling mineral solutions to sum the original pixel total and recalculating the linear mix of component reflectances for each band, de-vegetated geological reflectance images can be produced with the topography retained. If vegetation totally covers the pixel, the removal thereof fails, leaving the pixel black in output images.

However, with careful modelling only a small signature from geological materials may be necessary to obtain meaningful geological information in heavily vegetated areas. Further enhancements and processing can realize even more information.

7. Processing for Geological Content

Geological remote sensing is pursued on the basis of two distinct approaches, viz.:

a) Photogeological - the classic process of visual assessment of shape, size pattern and texture of an area's weathering and erosional characteristics, i.e. the topographical expression or spatial aspect, and

b) Spectral - the spectral approach uses the known spectral characteristics of materials to enable deduction of their composition from multispectral data.

Due to the rather small scale of satellite images, features covering a larger area are more readily discernable, while the smaller regionally insignificant features are suppressed. The most common features, linear and circular are also the most easy to pick out, sometimes too easy, as there are a fine distinction between deducing correctly a feature from minimal data and supposing a feature from too little data.

The spectral basis for geological remote sensing relies on phenomena such as the FeO charge transfer absorption in the range 0.4 - 0.6 μm and the Fe^{3+} electronic transition absorption in the range 0.8 - 1.0 μm, the position of the minima varying with the particular mineral (Goetz and Rowan, 1981). Chlorophyll absorbs strongly at 0.45 and 0.68 μm. The 1.6 μm region represents the highest reflectance for most rocks, whilst the 2.08 - 2.35 μm region records absorption

TM Band	Spectral Range (μm)	Characteristics and Principal Applications of TM Spectral Bands
1	0.45-0.52 (blue)	Shorter wavelength cutoff is just below the peak transmittance of clear water, the upper cutoff is the limit of blue chlorophyll absorption for healthy green vegetation. Wavelengths below 0.45μm are influenced by atmospheric scattering and absorption. Coastal water mapping, Soil-Vegetation differentiation. Deciduous-coniferous differentiation.
2	0.52-0.60 (green)	Covers the region between the blue and red chlorophyll absorption bands. Corresponds to the green reflectance of healthy vegetation.
3	0.63-0.69 (red)	The red chlorophyll absorption band for plant species differentiation. Less affected by atmospheric attenuation. The 0.69μm cutoff is below the region where vegetation reflectance crossover take place, which can reduce the accuracy of vegetation investigations. Ferruginous minerals can be separated from vegetation due to the high reflectance of iron minerals.
4	0.76-0.90 (reflective-infrared)	The lower cutoff is above the vegetation reflectance crossover region from 0.68μm to 0.75μm. The red edge feature of vegetation with its unique high response compared to other terrain cover. Biomass surveys. Water body delineation.
5	1.55-1.75 (mid-infrared)	Sensitive to amount of water in plants. Used for vegetation moisture measurement. Snow-cloud-ice differentiation.
6	10.4-12.5 (thermal-infrared)	Measures amount of infrared flux emitted from surfaces. Plant heat stress measurement. Local geothermal activity mapping, Thermal inertia mapping, Other thermal mapping.
7	2.08-2.35 (mid-infrared)	Discrimination of geological rock formations. Effective for hydrothermal mapping.

Table 7.1 Principal Application of TM Spectral Bands

in rocks and soils of hydrous clay and micaceous minerals, where the absorption minima vary for different minerals. Moist vegetation has a similar 1.6μm/2.2μm contrast to "clay-bearing" rocks and soils.

Radiometric resolution, or signal-to-noise ratio, is vital for mineral species mapping, i.e. variability introduced by atmosphere and vegetation often hide

weak mineral signatures, making extraction in the presence of noise virtually impossible.

In spectral terms there is no pixel size that can cope with with-in pixel mixtures of minerals.

Since the geological world is inhomogeneous, quantitative conclusions through remote sensing are not aimed for. Geological image processing usually comprises optimization of the imagery to support an essentially qualitative, photo-interpretive approach. With remote sensing techniques it is possible to obtain certain structural and lithological information more efficiently than can be achieved on the ground. Geological mapping with the aid of satellite data entails the description of structure, lithological units and geobotanical relationships.

Lithological information obtained from LANDSAT images are typically derived through:

a) Textural information, as defined from landform and drainage analysis, and
b) Spectral information, as displayed by the reflectance signatures of the various mineral assemblages present in the lithologies.

The data are generally obtained from the upper micrometres or millimetres of the surface because of the high opacity and scattering characteristics of natural materials. Some information concerning body properties, as opposed to surface properties can be obtained if one analyzes the changes in surface temperature that are induced by diurnal solar heating. This property, the measure of the resistance of an material to change its temperature in response to a change in the temperature of its surroundings, is called the Thermal Inertia (P), and is

defined as:

$$P=\sqrt{kpc}$$

where k = thermal conductivity,

p = density, and

c = specific heat.

Even this method allows measurements to a depth of less than 10 cm (Goetz and Rowan, 1981).

The spectrum can be divided into several distinct segments: ultraviolet, visible and near-infrared, short wavelength infrared, mid-infrared, far-infrared and microwave. The ultraviolet region, below 0.4μm, and the far-infrared and microwave regions, above 15.0μm, are not considered here, since the data acquired came from reflectances in the region between 0.45 and 12.5μm (Figure 7.1).

The short wavelength infrared region, 1 to 3μm, provides more diagnostic spectral information about the composition of minerals and rocks than the visible and near-infrared regions. The region around 1.6μm exhibits the highest reflectance for most rocks as it is near the middle between the ultraviolet-visible iron absorption bands and a strong fundamental OH^- vibration at 2.74μm (Goetz and Rowan, 1981). Altered rocks containing clay with or without a short wavelength Fe^{3+} absorption, displays a strong peak reflectance at 1.6μm. The region 2 to 2.5μm is also of interest because it contains sharp, diagnostic spectral absorption bands which can identify various clays, micas and carbonates.

The emissive portion of the spectrum, between 3 and 15μm, are of particular

Figure 7.1 TM Spectral and Radiometric Characteristics

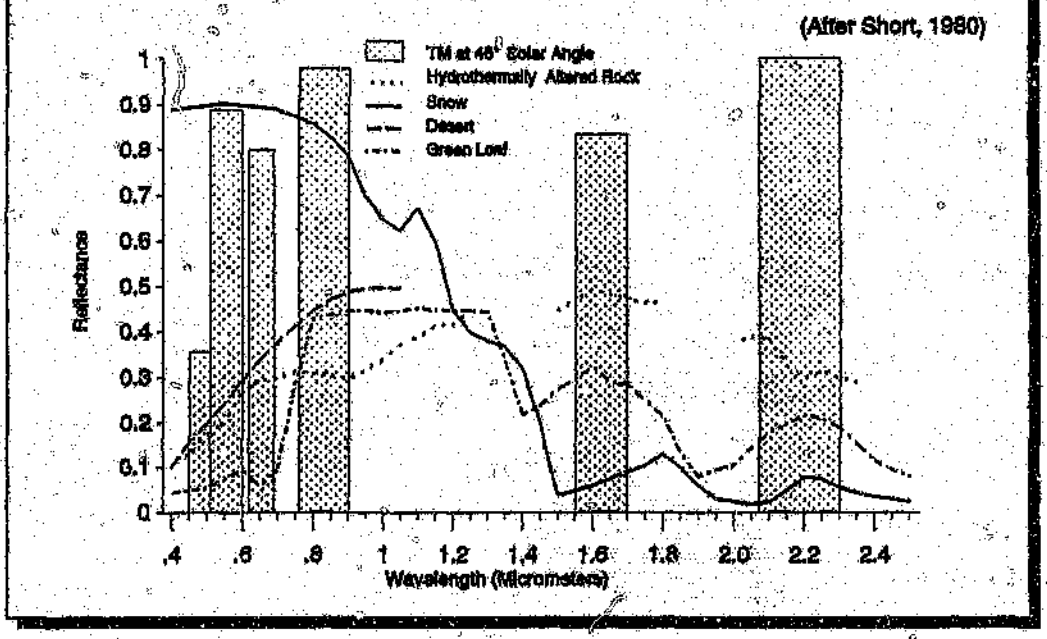

interest for terrestrial observation. Between 3 and 8μm spectra for various minerals such as nitrates and sulphates can be found. The region beyond 8μm is of prime importance for geological applications, as spectral emittance variations provide a basis for distinguishing between silicate and non-silicate rocks, and for discrimination among silicate rocks.

Because of the synoptic view of the data acquired through satollite, regional morphological features are characteristically visible in any or all the data, irrespective of the window through which the data were acquired. Quite a number of these alignments of features or lineaments, are normally found to be previously unmapped, irrespective of the depth of detail to which a particular area was mapped. The reason for this is that the larger the scale, typically 1:50 000 or 1:30 000 with a synoptic view covering less than 7 km^2 (aerial photographs), the less the likelihood of recognizing a subtle regional feature stretching for perhaps tens of kilometres, or even further.

Lineaments are particularly important in mineral resource studies, since quite a number of ore deposits are localized along fracture zones. The Barberton Mountain Land is a good example of this.

Several factors influence the detection of lineaments. Features that trend parallel to the illumination source are normally not so easy to detect as those orientated perpendicularly, therefore the angular relationship between the linear feature and the illumination source is rather important.

A lower illumination angle is also preferred for the detection of subtle topographical features, however, as LANDSAT is in a sun-synchronous polar orbit, the only variation available is through seasonal change, since data acquisition time is locally a constant throughout the year.

In the visible and near-infrared regions, the most diagnostic properties of rocks are brightness (the average reflectance in visible and near-infrared regions), spectral radiance, and the spatial distribution of landforms. Colour ratio composites are used to display spectral reflectance differences in colour while subduing brightness variations due to topographic slope.

Acid soil conditions, which characterizes many hydrothermally altered areas, tend to limit the vegetation cover. Some geobotanical associations are related to regional lithological variations, whereas others, such as barren areas or certain types of vegetation, are specifically related to anomalous concentrations of metals (Brooks, 1972; Raines and Canney, 1980).

The detectability of normal and transcurrent faults with respect to thrust faults

differ considerably. While the first two are generally characterized by high angle slip planes, resulting in rectilinear surface trend, the thrust faults correspond to low angle planes with sinuous traces, the detection of which is generally more difficult. Using band 7 (0.8-1.1 μm) yielded the best results.

Drainage systems (past and present) and their tectonic control are more clearly observable on the enhanced images. Strike slip motion along a lineament will result in drag effects on the drainage pattern. More densely vegetated areas, consisting of natural vegetation almost exclusively, indicate depressions where water may be available in greater abundance. The potential for groundwater in such areas are higher.

The images produced by band ratioing, principal components transformation, and canonical analysis provided little additional information useful in deriving the final geological interpretation, according to Bailey et al. (1982), in their study of the Qaidam basin in China.

Most of the information which contributed to the final geological interpretation of the area was derived from the standard, contrast enhanced and edge enhanced false colour images. The landform and drainage characteristics interpreted from these images were the criteria most important in both lithological and structural interpretation. Colour (tonal) variations expressed in images produced from canonical analysis, principal components analysis and band ratioing, proved useful in deriving the final geological interpretation. Some of these variations were particularly useful in resolving questions on lithological unit identity in some areas.

During processing the TM data for the study area, it was found that virtually all the procedures used yielded information. Arguably the results from computationally more expensive procedures were not necessarily significantly better or different to results possible through less expensive procedures.

7.1 Edge Enhancement

Edge Enhancement accentuates abrupt changes in DN from one pixel to the next, thereby producing an image with sharpened edges between contrasting areas. Such features are often topographically related and include lineaments and drainage.

For this study edge enhancement was done irrespective of direction trough the use of a filter with values equal to *-1/(T)* where *T = Total number of weights*, except for the centre value, which equals *(T-1)/T*.

T=25

$-1/T$=-0.04

$(T-1)/T$=0.96

Figure 7.2 Edge Enhance Kernel

-.04	-.04	-.04	-.04	-.04
-.04	-.04	-.04	-.04	-.04
-.04	-.04	.96	-.04	-.04
-.04	-.04	-.04	-.04	-.04
-.04	-.04	-.04	-.04	-.04

The sum of all the weights is equal to zero. This means that if the filter is convolved with a uniform area of the image, the result is zero, and if the area is non-uniform, the filter produces a non-zero result. The result of the filter is added to the original image to produce the image with enhanced edges. The size of the filter used for this study was 5 x 5 (Figure 7.2).

All the photographs of images contained in this report is of edge enhanced data.

7.2 Band Combination Selection

Experimentation revealed that band 5 or 7 in a three band colour combination, together with bands 4 and 3, does not show good discrimination between iron oxide and vegetation. Using TM1, which alone does not discriminate between iron oxide and vegetation, in combination with TM4 and TM3 the best original bands false colour composite image is produced for detection areas of iron minerals related to red soils (Crosta and Moore,1989a).

Correlation analysis of Landsat TM data for arid areas and laboratory spectral data for various combinations of minerals indicate that from the possible 20 band combinations, combination TM-147 maximally differentiates lithological materials in most scenes, but that band combination TM-157 is preferable for scenes in which hydroxyl rich minerals are prominent or of specific interest. Among the possible 455 band ratio combinations, 3/1 - 5/4 - 5/7 ranks high for optimal information display (Crippen, 1989) (Refer Table 7.2).

During this study it was found that using TM2 in preference to TM1 in both combinations as described above yielded a slightly better product. Photo 7.1 displays the reddish hue typical of peak chlorophyll reflectance quite clearly over the plantations in the area. Riverine vegetation is also clearly visible. As with Photo 5.2 (Section 5.2.1), the histograms also show that only a small part of the available DN range was utilized by the sensor. This is also the same for the histograms for TM-247 (Photo 7.4). Note the bimodal character of bands TM3

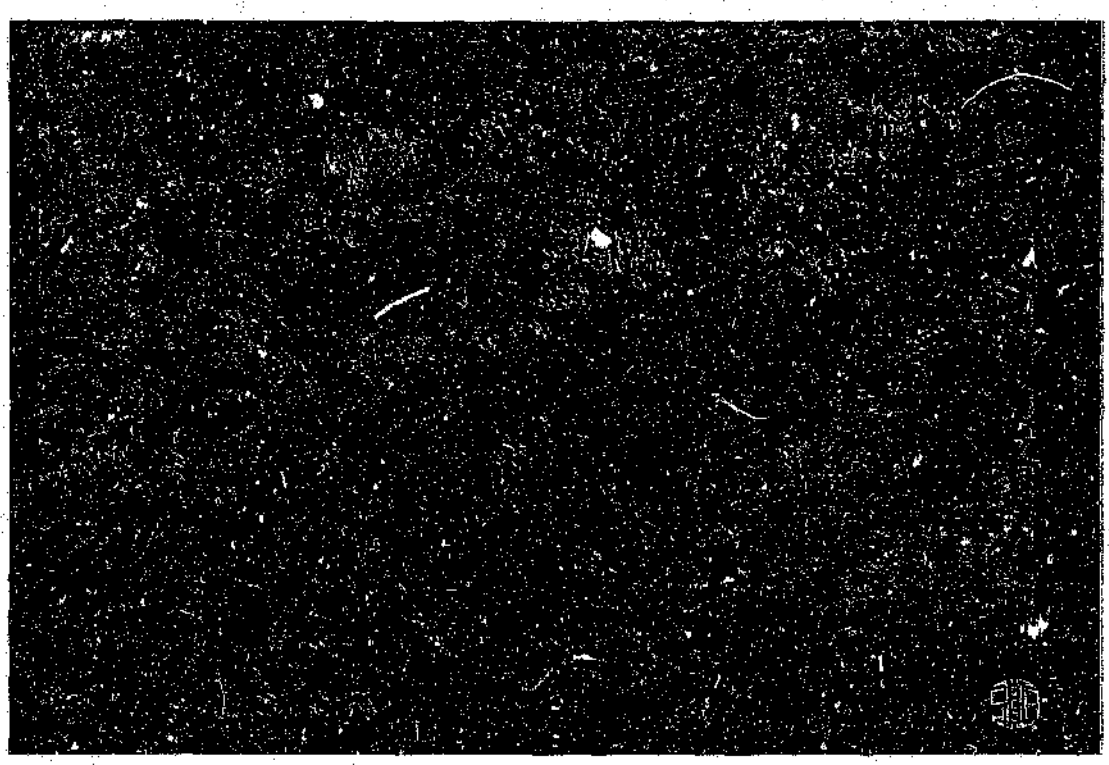

Photo 7.1 TM-234 on BGR with Auto-2-Linear stretch

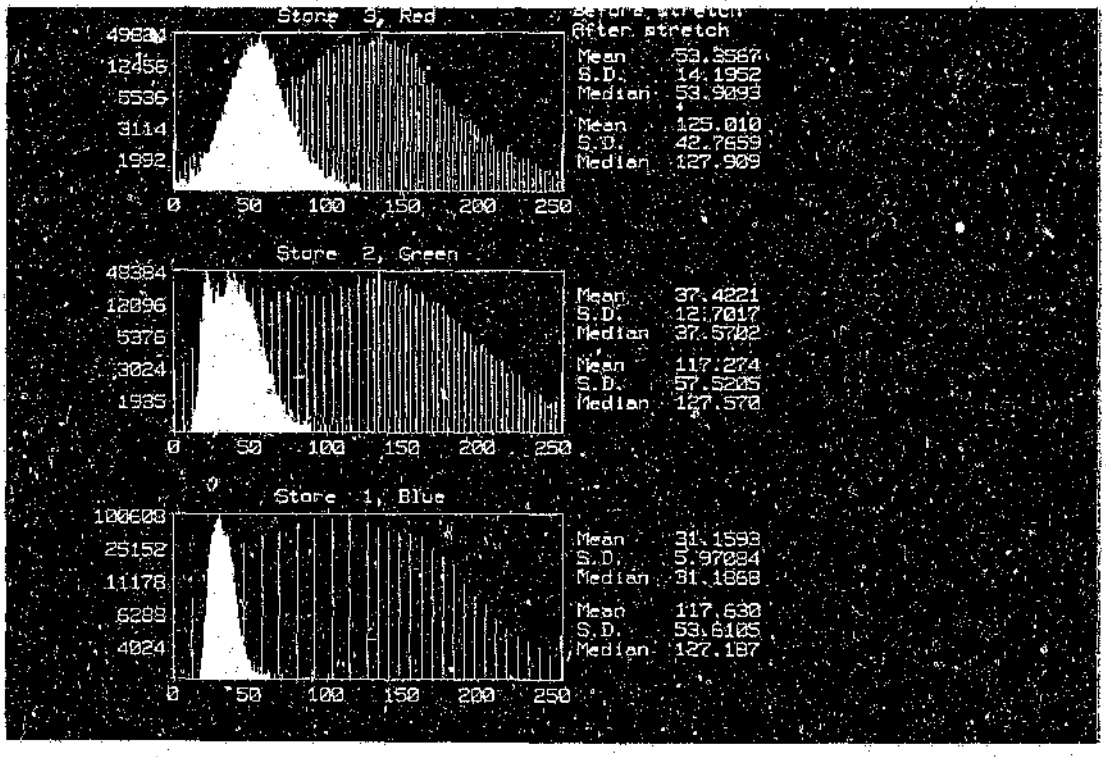

Photo 7.2 Histograms for Auto-2-Linear stretch on TM-234

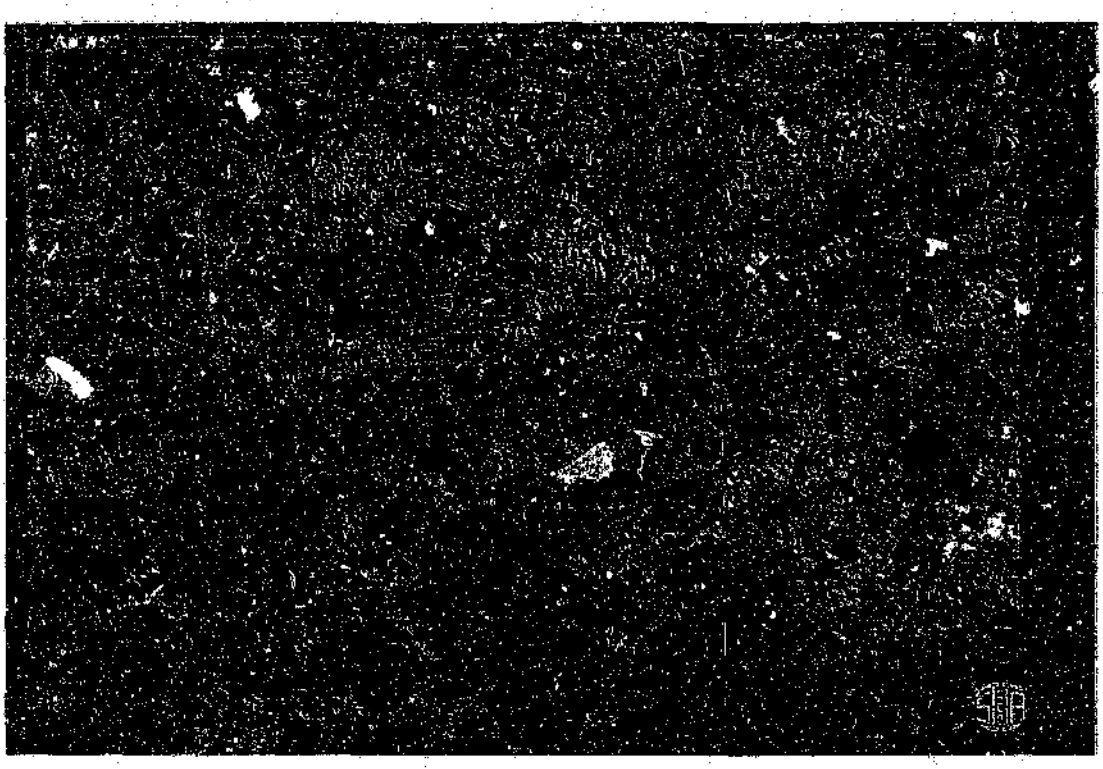

Photo 7.3 TM-247 on BGR with Auto-2-Linear stretch

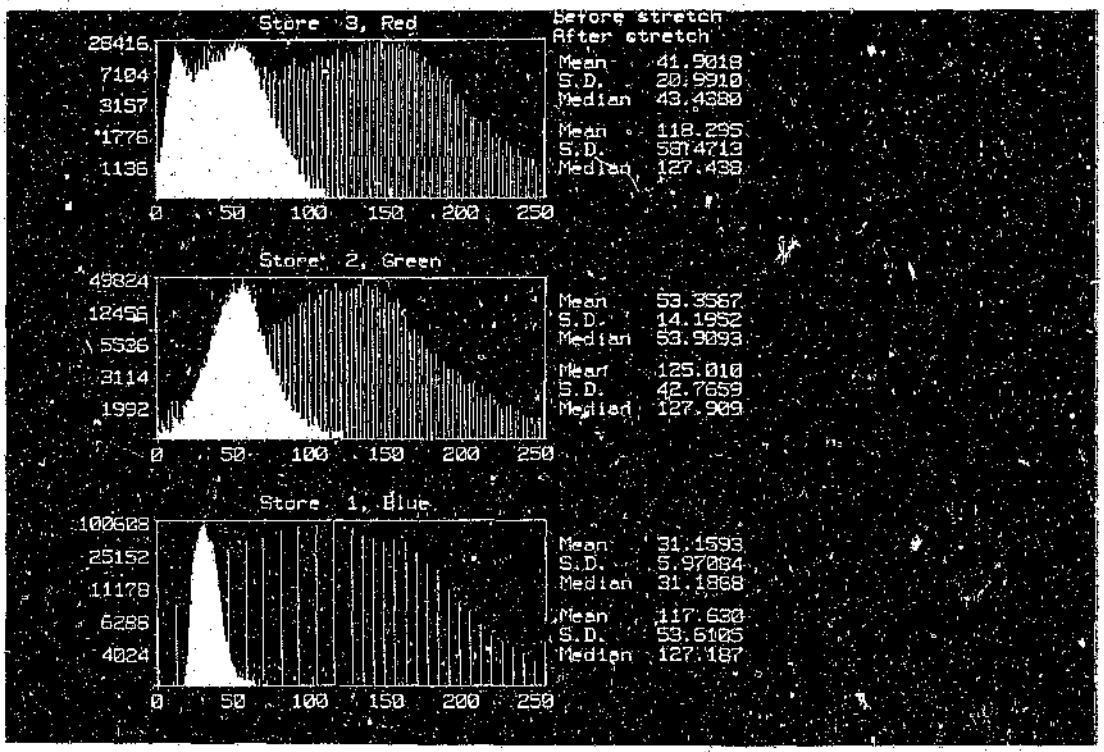

Photo 7.4 Histograms for Auto-2-Linear stretch on TM-247

and TM7 on these histograms.

Photo 7.3 displays the vegetation in the more familiar green tones, while the information from the near-infrared TM4 and mid-infrared TM7 is represented by the magenta tones. A comparison between the two photographs clearly shows that for vegetation studies Photo 7.1 is superior, while for the structural and lithological content one would choose Photo 7.3.

7.3 Band Ratioing

TM Ratio	Application
7/5	Argillic versus non-argillic
3/4	Rocks versus vegetation
5/1	Fe^{3+} + Fe^{2+} versus iron-free
5/4	Argillic versus Fe^{2+}
4/7	Argillic versus Fe^{3+}
4/2	Fe^{2+} versus non-Fe^{2+}

Table 7.2 TM Ratios for Geological Applications

The result of ratioing is to minimize the effects on scene brightness that are caused by variations in topographic slope and aspect. Thus reflectance differences between rocks, soils and other surface materials which may be the result of compositional differences, are enhanced.

The 1.55-1.75 μm wavelength region represents a reflectance peak for most geological materials, while the 2.08-2.35 μm region represents the famous clay

band where hydrous clay and micaceous minerals absorb, therefore clay-rich areas can be enhanced with a 1.6/2.2 μm (TM5/TM7) ratio (Photo 5.5, Section 5.3.1). Carbonates and sulphates also exhibit some absorption in this region.

Shortcomings of the band ratio approach are that a haze correction may be necessary for especially the shorter wavelengths before ratioing is done. It should be noted that the influence of albedo on the formulation of the ratio is normally ignored. If the desired results are of a qualitative nature only, the albedo component becomes much less critical.

It should also be noted that vegetation will also appear bright in the ratio as the spectral slope for vegetation, due to leaf moisture effects, is similar between the two bands. Separations of the vegetation can be achieved by introducing a vegetation ratio, i.e. 0.83/0.66 μm (Photo 5.7) with the 1.6/2.2 μm ratio.

It should be noted that the effectiveness of band ratioing decreases with increased correlation between the bands being ratioed.

Photo 7.5 displays the ratio TM5/TM7, TM5/TM1 and TM3/TM1 on BGR. An Auto Gaussian stretch was applied to the data. Note the orange patches indicating some on-surface disturbance, mostly due to mining activities in the area.

7.3.1 Band Ratios vs Difference

Since ratios such as TM3/TM1, TM4/TM3, TM5/TM1 and TM4/TM1 tends to show only the widespread occurrence of lateritic minerals, these ratios yield

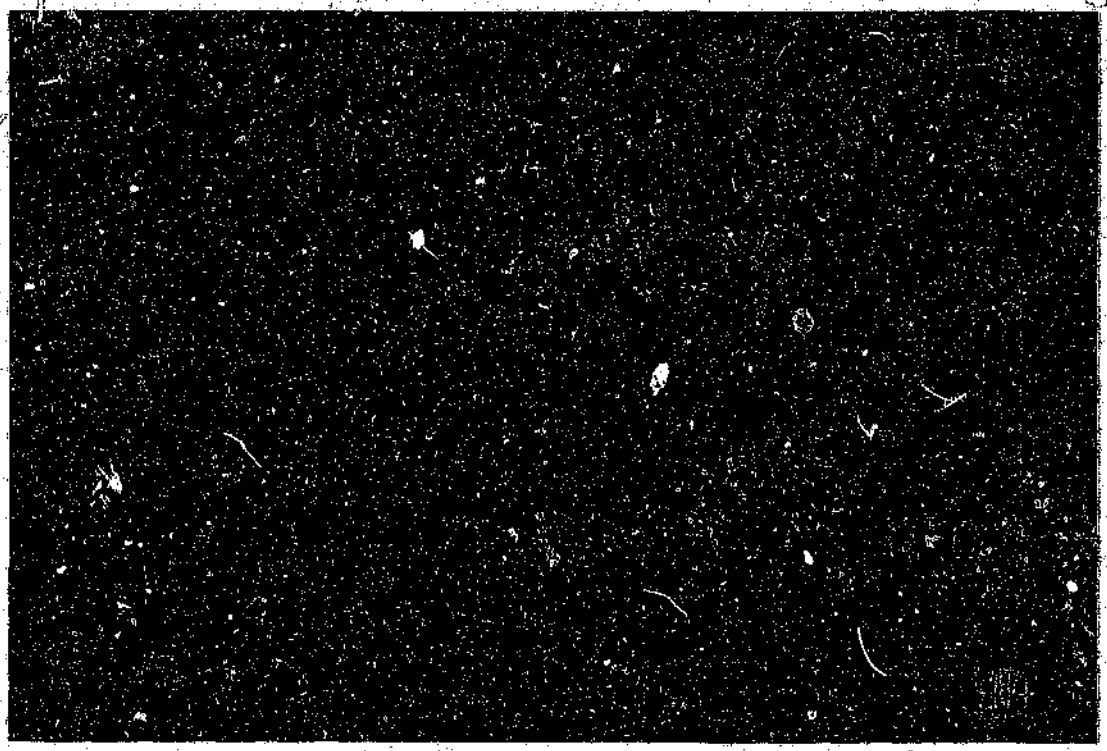

Photo 7.5 Ratio TM5/7, TM 5/1 and TM3/1 through an Auto Gaussian stretch

limited results. Lateritic minerals are common in tropical environments, where small amounts of lateritic products can be found even in soils derived from iron-poor rocks.

A more suitable result can be obtained by using differencing instead of ratioing. Similarly to ratioing, band differencing extracts spectral contrast between two bands, but does it in a linear fashion. The resulting image can therefore be linearly stretched without loss of information.

According to Crosta and Moore (1989a) TM3 minus TM1 is a good indicator of iron oxide content. As these two bands have different average intensities and contrast, the result of arithmetic subtraction of TM1 from TM3 is dominated by the brighter image, in this case TM3, with a mean DN of 11.88 and a standard deviation of 6.15, against 8.36 and 3.76 respectively for TM1. Since the common

spectral information are not totally eliminated from the resultant image, another procedure must be used to obtain better results. This can be achieved though the performance of a balanced contrast stretch (Lui and Moore, 1989) of the two bands, prior to the differencing operation. This will allow a compensation for the bias introduced by TM3, producing two almost linearly stretched images with the same mean and value range.

7.3.2 Alternatives to Band Ratios

Using the clay ratio, vegetation will be highlighted with the genuine soil and rock clay features. Separating the two is difficult.

A spectral indices approach has been proposed by Elvidge and Lyon (1984), where a regression of the 1.6 and 2.2 µm bands predicts an expected value in the 2.2 µm band. This is subtracted from the actual 2.2 µm band pixel value to give a residual representing total clay and vegetation absorption. The vegetation component is then removed by regressing total absorption against the Perpendicular Vegetation Index, where predicted PVI is subtracted from total 2.2 µm absorption to leave a residual attribute to geology. The PVI image is the perpendicular distance to a bare rock-soil baseline in red against NIR, which is determined beforehand.

During the course of this study various other simple and computationally cheap procedures were tested. Photo 7.6 displays the result of an addition operation on BGR. TM1 was added to TM2, TM3 to TM4, and TM5 to TM7. An Auto-2-Linear stretch was applied. Comparing this photo to Photo 5.1 and Photo 7.3, the increased amount of information available is clear. Moving to

Photo 7.6 TM(1+2), TM(3+4) and TM(5+7) with Auto-2-Linear stretch on BGR

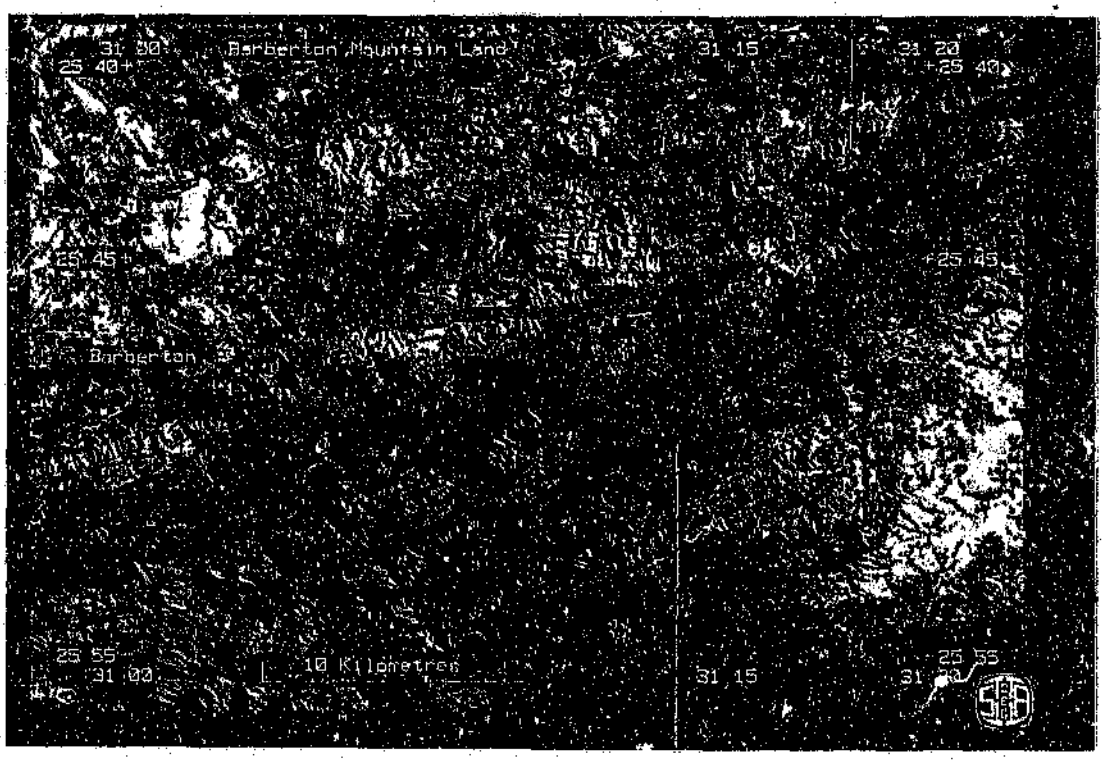

Photo 7.7 TM(1*2), TM(3*4) and TM(5*7) on BGR

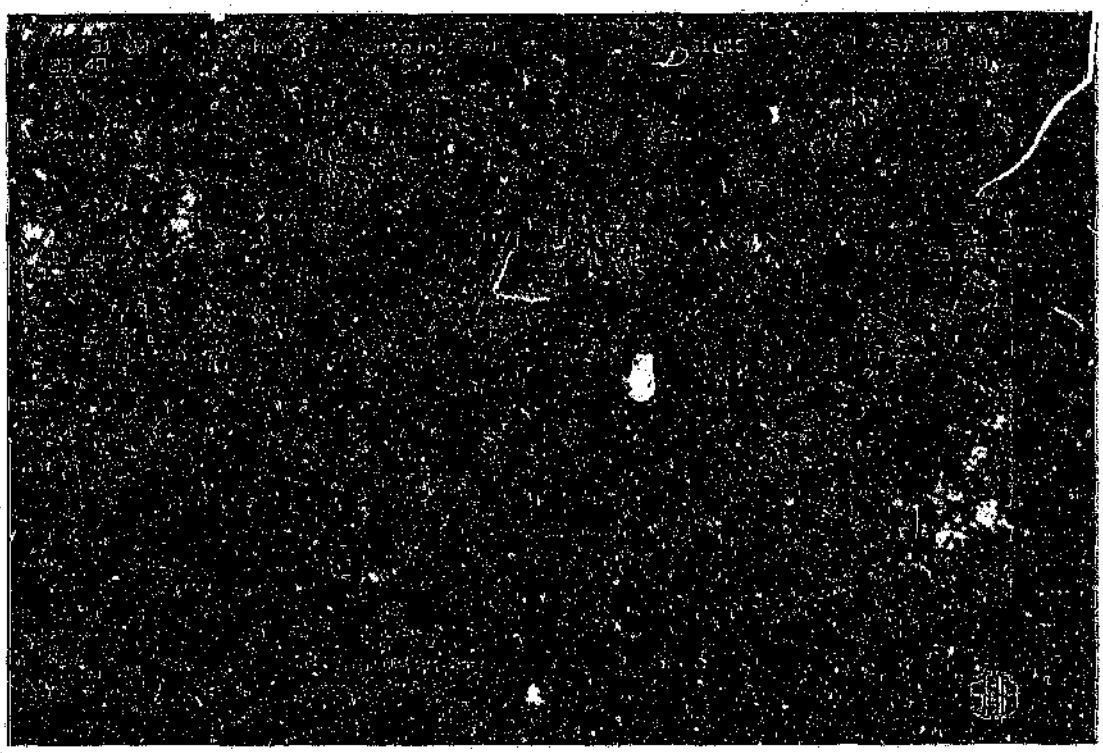

Photo 7.8 TM(1*2), TM(3*4) and TM(5*7) with Auto Gaussian stretch on BGR

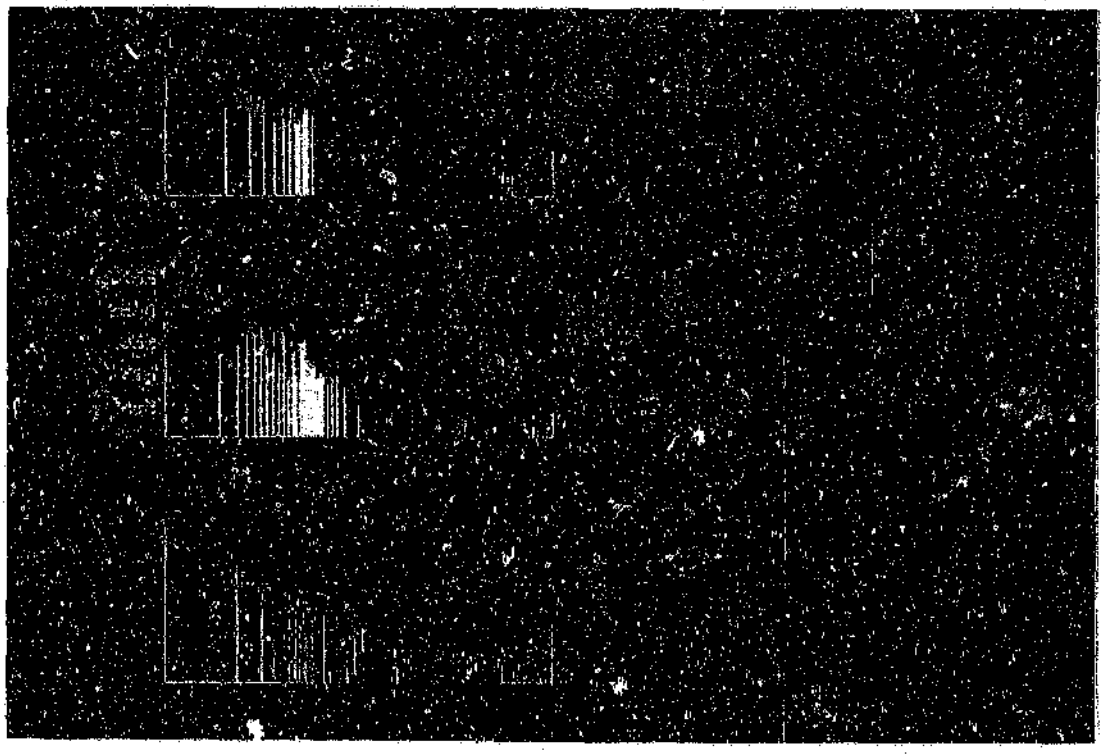

Photo 7.9 Histograms for Auto Gaussian stretched multiplied TM bands

Photo 7.7, there is a noticeable decrease in amount of information visible in the forested areas, while the non-forested areas display an increase in contrast and therefor an increase in visible information. This view was derived through the multiplication of consecutive pairs of Auto Linear stretched TM bands.

When a second stretch (Auto Gaussian) was applied to this view, Photo 7.8 resulted. The gain in information over the forested areas is quite drastic, but the price is the loss of definition over the non-forested areas. The amount of shift due to the stretch is clear from the histograms pertaining to these two photographs (Photo 7.9).

7.4 Principal Components Transformation

Principal components transformation optimizes the use of remotely sensed imagery by removing the correlation which is inherent to many sensors. Major drawbacks of this technique include the fact that colours in the PCT colour composites have no simple relationship to spectral features from the original bands.

The lower order components (PC1-3) often represent nothing more than a topographic enhancement of the original data (Photo 5.13). Photo 7.10 is an unstretched principal components combination 234 on BGR, while Photo 7.11 is an Auto-2-Linear stretched combination 534 on BGR. The sharper appearance of Photo 7.11 is the result of the applied stretch.

Note the yellowish colour or halo around the Barbrook fault (refer to Photo 3.1)

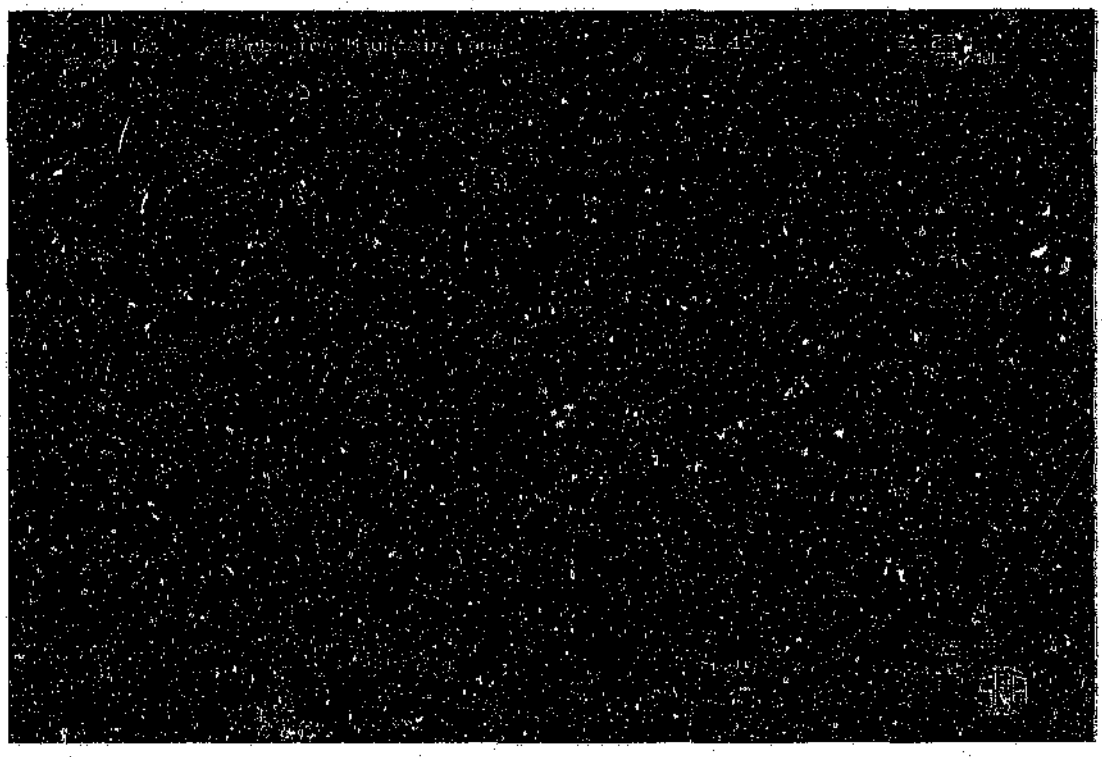

Photo 7.10 Principal Components 2, 3 and 4 on BGR

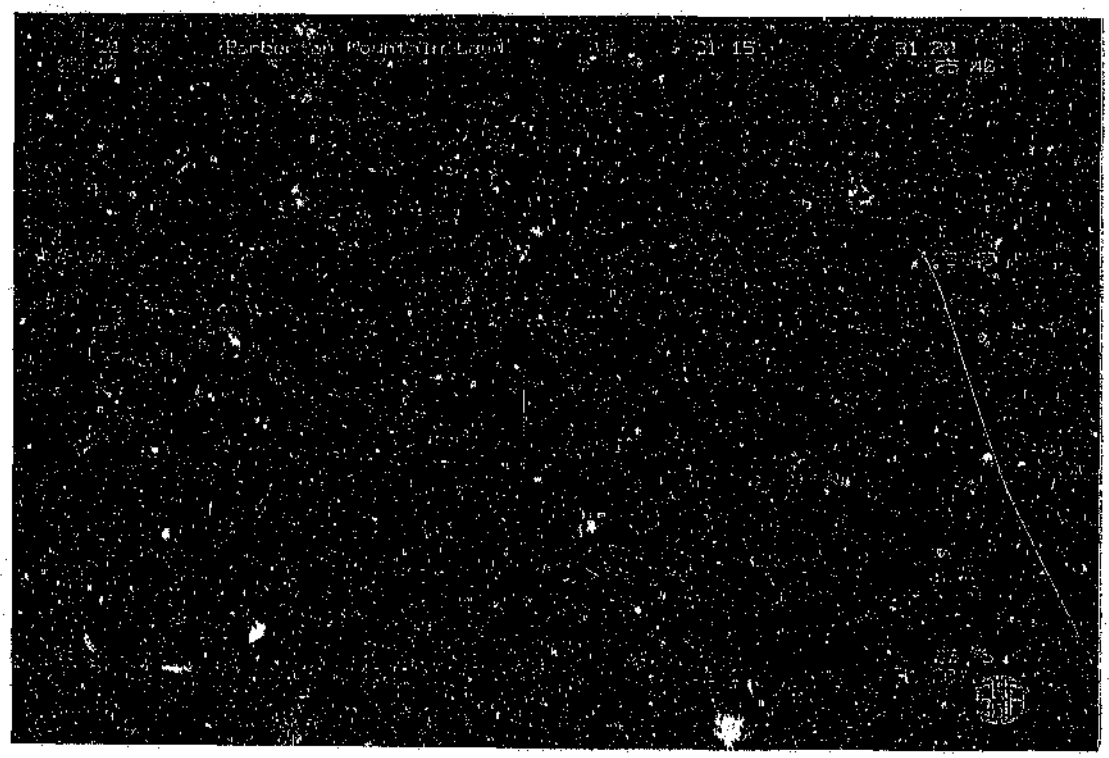

Photo 7.11 Principal Components 5, 3 and 4 through an Auto-2-Linear stretch

and Joe's Luck Formation, which is related to the ironstone and ferruginous shale associated with these features. Other surficial disturbances are also noticeable, for example both Fairview and Clutha mine slime dams appear very prominently on these views. The same with Sheba and Agnes mines.

Since the least correlated features are mapped to the higher order components, the features of most interest for mineral exploration are normally lost between the noise which, being totally uncorrelated, are also mapped to the higher order components. This causes the standard PCT to be disregarded for mineral exploration applications.

Applying a decorrelation stretch (Rothery, 1987) is one way of minimizing the problem of colour distribution. This technique makes effective use of stretching the principal components to give it a spherical distribution in PC feature space,

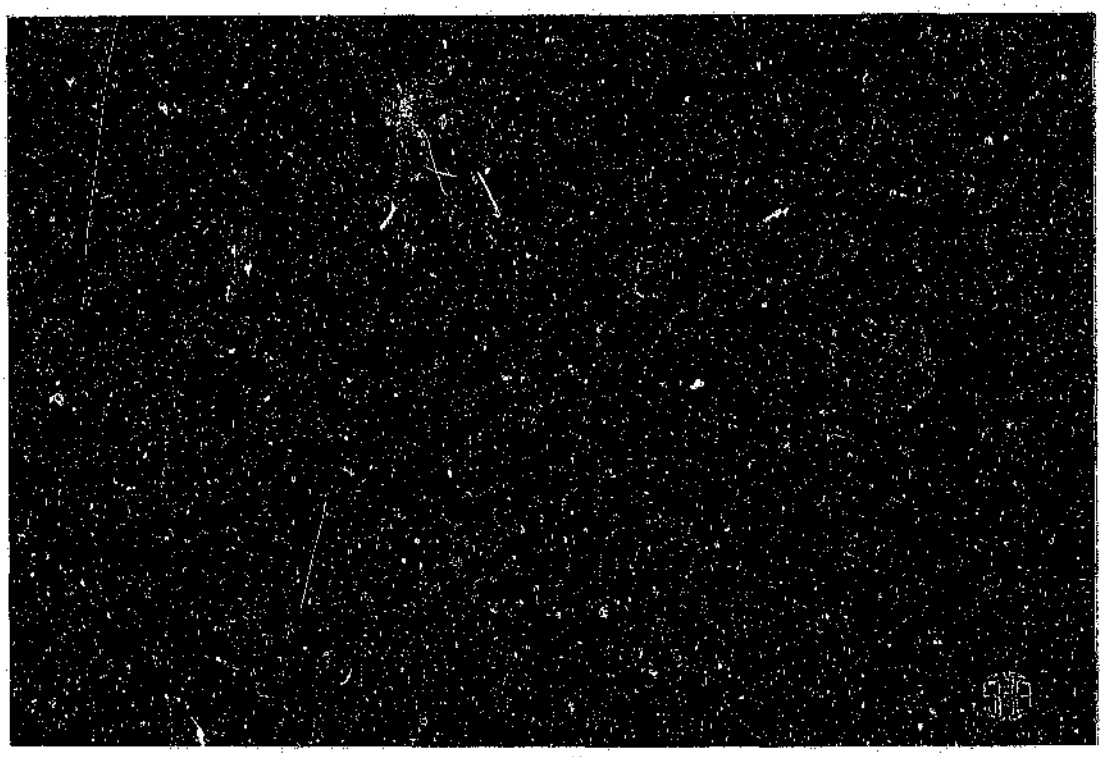

Photo 7.12 Decorrelation stretch Combinations 645 with Auto Gaussian stretch

followed by the inverse of the rotation used in the PCT, in order to produce a three band colour composite with a complete range of colour variations on the original axes. The main advantage of decorrelation lies in retaining the same colour relationships as the composite using the three original bands. The disadvantage is that it also uses information from only three spectral bands.

Crosta and Moore (1989a) found that using bands 1, 3 and 4 as input for decorrelation stretching resulted in the clear enhancement of iron rich soils in relation to vegetation.

In another approach, followed by Rothery and Francis (1987), the first principal component is replaced by an uniform DN image, before applying the inverse transformation. This method removes most of the additive atmospheric effects, since PC1, which is analogous to intensity and luminosity, is parallel to the

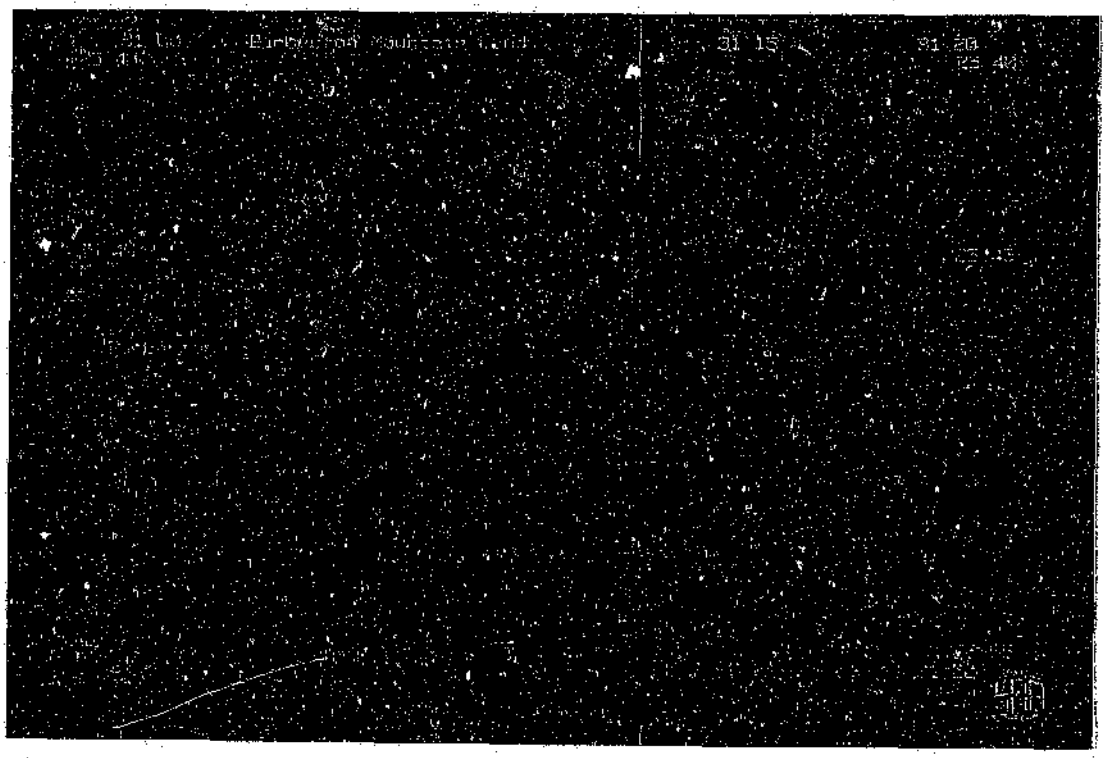

Photo 7.13 C-stretch Combinations 423 viewed through an Auto-2-Linear stretch

principal axis of the probability density function of the image. The resultant Colour stretched displays areas of identical composition but different slope aspect more consistent in colour than is possible through other methods if an atmospheric correction is not carried out on each band.

For both Photo 7.12 and Photo 7.13 all 6 TM bands were utilized in the principal components transformation. Photo 7.12 displays combinations 654 as viewed through an Auto Gaussian stretch on BGR. For the C-stretch, Photo 7.13, PC1 was replaced with a DN 128 grey image before the inverse transformation was effected. The C-stretch is viewed through an Auto-2-Linear stretch. Note that this view also enhances the ferruginous shale and ironstone, similar to Photo 7.11, while the D-stretch (Photo 7.12) does not.

7.4.1 Feature Orientated Principal Component Selection

Crosta and Moore (1989a) described an alternative approach to principal components, which is used for targets from which the theoretical spectral response is known. This technique of "*Feature Orientated Principal Component Selection*" allows for the identification of components which concentrate spectral information due to specific superficial targets. The eigenvectors used to calculate the principal components are examined, and each PC image is related to the two or three original bands which contributed the most data to it. Specific PC's can then be selected to display the desired features, based on the major contributions, both negative and positive, from the original bands most likely to display the desired target.

As expected, PC1 does not reveal any significant spectral feature, since it is

composed of a positive mixture of all the bands, in this case with a greater proportion of TM5, showing topographic shadowing and albedo information. PC2 is dominated by the contribution of TM4, showing spectral response due to vegetation, while PC3 is similar to PC1, in that several original bands contribute in balanced proportions. Detailed analysis of how the PC's are formed reveals spectral information due to iron oxides.

	PC1	PC2	PC3	PC4	PC5	PC6
TM1	7.6%	4.4%	13.0%	20.0%	50.0%	(-)19.0%
TM2	6.1%	1.0%	11.0%	12.5%	4.8%	59.3%
TM3	13.5%	(-)5.6%	19.3%	24.2%	(-)39.6%	(-)17.7%
TM4	6.0%	61.2%	12.7%	(-)7.8%	1.2%	(-)2.5%
TM5	44.0%	5.7%	(-)22.6%	4.5%	1.1%	1.1%
TM7	22.8%	(-)22.1%	21.4%	(-)31.0%	3.3%	(-)1.0%
% Variance of Total	87.99%	8.21%	2.07%	1.34%	0.31%	0.08%

Table 7.3 Contributions to Principal Components

As iron oxides have a high response in TM7 and TM5, and low in TM1, the component with the biggest contribution from TM5 and TM7 and the lowest from TM1, would reflect the most information about the presence of goethite/hematite in high digital numbers. For this area and data set, PC1 seems to fit the bill best. Similarly iron oxides will be represented by low digital numbers in PC2 and PC4. This result is in sharp contrast to that of Crosta and Moore (1989a), which reflected high DN's in PC4 and low DN's in PC5 and PC6.

The application of feature orientated principal component selection to the test area seems to be a good way to display spectral features due to the goethite and

hematite in soils derived from the greenstone volcanics. However, due to a technical problem, it was not possible to include the photograph in this report.

7.4.2 A Fourth Dimension in PC Colour Composites.

Since the highest order PC's concentrate most of the noise from the data set, a colour composite of the 3 higher order PC's usually turns out to be inappropriate for visual interpretation. The complete lack of terrain information representing topographic shadowing and albedo, which is selectively concentrated in the first PC, does not allow interpretation of geologic structures and precise location of areas containing anomalies. Crippen (1988) developed a technique whereby four statistically independent images generated through principal component transformation are combined to form a single colour composite image. The technique consists of selecting three components other than PC1, multiplying each of these by PC1, rescaling to fit the display range 0-255, and assigning each result to an additive primary colour.

Using this technique to combine the three higher order components with PC1, results in the spectral information from the high order PC's being retained as hue and saturation (chromaticity) and the terrain information from PC1 controlling the intensity. This combination represents almost 90% of the total scene variance from the 6 bands.

Taking the process one step further, the square roots of the principal components were taken before multiplication. Photo 7.14 is the result after the square root of PC1 was multiplied with the square roots of PC2-4.

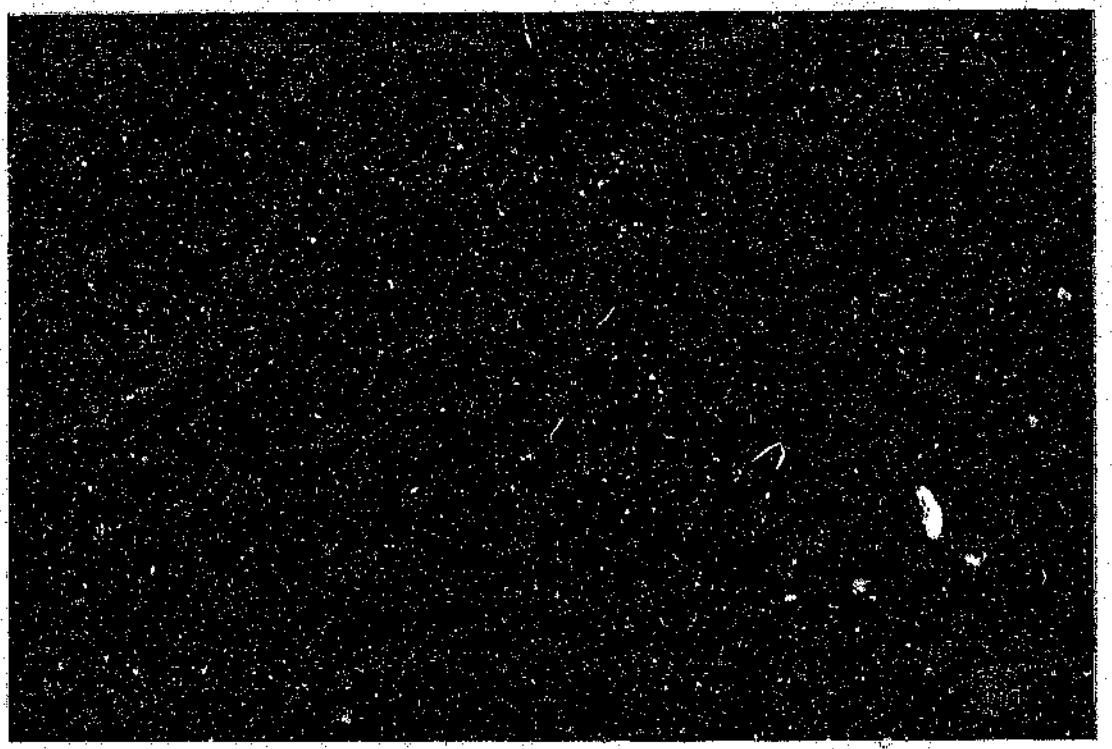

Photo 7.14 Square roots of Principal Components multiplied

$$\sqrt{PC_1} \times \begin{vmatrix} \sqrt{PC_2} \\ \sqrt{PC_3} \\ \sqrt{PC_4} \end{vmatrix} \Rightarrow \begin{vmatrix} BLUE \\ GREEN \\ RED \end{vmatrix}$$

An Auto-2-Linear stretch was applied too the dataset before display. Again, another way of viewing the same image.

7.4.3 Directed Principal Component Analysis

While vegetation can be used to indicate both geological and biogeochemical anomalies, for most geological studies its effects are a distraction. The method of "*Directed Principal Components Analysis or DPCA*" (Fraser and Green, 1987) was tested on Airborne Thematic Mapper data, and found to be successful for substantially reducing the effects of vegetation due to tropical savannah woodland with 50 to 70 per cent vegetation cover. For areas with more cover,

the results may be less definitive.

Ferric oxides and vegetation exhibit strong absorption features in the visible and near-infrared spectral region (0.35-1.1 μm), while various phyllosilicates, carbonates and sulphates, together with both dry and green vegetation, are characteristically responsive in the short wavelength infrared region (1.1-2.5 μm).

Band ratio analysis is a traditional and effective method for detecting spectral differences between bands of image data. The pixel brightness values of two spatially co-registered bands are expressed as a ratio, and the resulting values re-scaled for display purposes. Band ratios are particularly suited to those data sets where the numerator band is chosen to monitor a little-varying standard, whereas the dominator band maps the variability of a specific spectral feature. Overall brightness differences are effectively removed by ratioing. It is however difficult to decide whether changes in the denominator, numerator or both are responsible for the remaining variability.

The 0.83/0.66 μm serves as an excellent vegetation index. The strong characteristic chlorophyll absorption of green vegetation at 0.66 μm and the high infrared plateau at 0.83 μm mean that few other materials give as high a ratio.

For geological applications images of 1.65/2.22 μm (TM7/TM5) and 0.66/0.45 μm (TM3/TM1) band ratios are commonly used to enhance clays and iron oxides, respectively.

Since pixels represent mixtures of reflectances, considerable confusion exist as

to which contributing reflectance is responsible for which component characterization. The smaller the pixel, the less the likelihood of a variety of cover types being present.

However, except for cases where the sensors are flooded by very strong reflectance emanating from a single source, pixels will almost always represent a mixture of reflectances. Thus a method is needed to reduce the effect of vegetation.

The aim is to direct a PCT at two specific band ratio images. Band ratio images are used because they are theoretically easier to interpret and are already decorrelated for albedo.

Input ratios are selected on the basis that one ratio contains information regarding the component of interest (i.e. a geological discriminant); however, its effectiveness is lessened by the similar responses of another component (i.e. vegetation). The second ratio contains information about this spectrally interfering component (i.e. a vegetation index).

As long as there are no additive path radiance effects, the ratios calculated from the raw digital number (DN) values will be consistent with each image and proportional to true radiance ratios. As the DPCA uses scene statistics, and re-scales using the standardized PCT method, the results will be independent of whether raw DN or corrected radiances are used. Unless path radiance effects are very large, they should not have a marked effect on this procedure. This is because it is the correlation structure that is important, not the absolute values of the ratios. As the correlation is determined from the data themselves, the

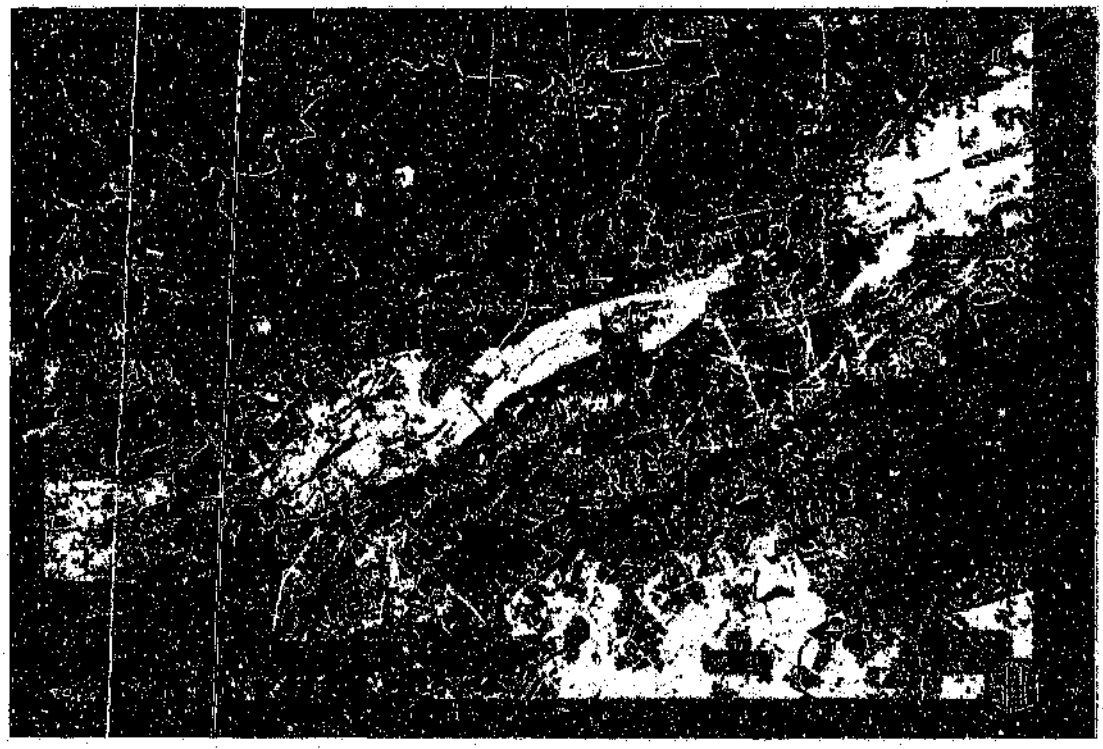

Photo 7.15 Directed Principal Component 1 False Colour Composite

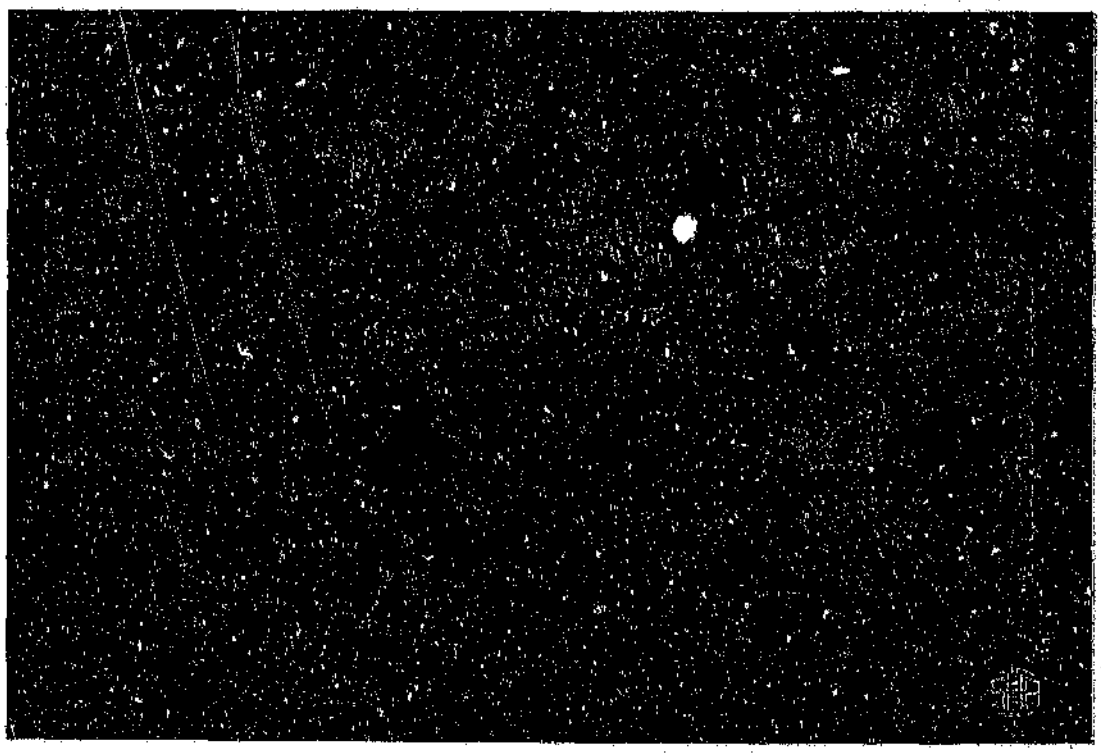

Photo 7.16 Directed Principal Component 2 False Colour Composite

procedure is in a sense self-calibrating.

The problem being addressed is one of spectral mixtures: mixtures of substrate and vegetation from which we would like to separate substrates that are absorbing from those that are non-absorbing in the 2.22μm band. The DPCA method assumes that the axis of major variability (i.e. DPC1) in the space defined by the two input band ratios is dominated by mixtures of vegetation and unaltered substrate. The high degree of correlation between the 0.83/0.66 μm and the 1.65/2.22 μm band ratios, present because of vegetation, results in the vegetation and non-vegetation (i.e. clay) components of the 1.65/2.22 μm band ratio being separated into DPC1 and DPC2, respectively.

Photo 7.15 is the view of combination 1 of the directed principal components transformation, after an Auto-2-Linear stretch was applied. The flooded pixels in the areas covered by forests and other dense vegetation are strongly contrasting with the darker pixels in the rest of the image. Photo 7.15 represents the vegetation "stripped-off" from Photo 7.16, which is the component 2, as viewed through an Auto Gaussian stretch.

Note how structural and even lithological information were "lifted out" from underneath the plantations. During the research an attempt was made to separate the plantations from the rest of the image through the use of various masks. The results were very similar, except for two things:

1) a definite edge formed between the area covered by plantations and the rest of the image, and
2) the process involved a similar number of steps but which took at least three

times the disk space and time to perform.

Photo 7.17 is a normalized vegetation index, viewed through a Auto Mean stretch:

$$NVI = \frac{[TM7 - TM5 + 127]}{[TM7 + TM5]} \times 20$$

Utilizing this vegetation index as the common denominator for the 1 to 1 principal components transformation, produces a rather different result - Photo 7.18.

Comparing this to Photo 7.16, the difference is startling. This is a typical result of overprocessing; rather a mess, with very little information decernable.

Using the square root and multiplicative technique similar to the one described earlier (Photo 7.14) on the defoliated dataset, the resultant view (Photo 7.19) show a slight decrease of information visible over the forested areas. Since the mathematical function utilizes PC1 from a normal 6 band principal components transformation as the common denominator

$$\sqrt{PC_1} \times \begin{vmatrix} \sqrt{DPC_{2_{(1)}}} \\ \sqrt{DPC_{2_{(2)}}} \\ \sqrt{DPC_{2_{(3)}}} \end{vmatrix} \Rightarrow \begin{vmatrix} BLUE \\ GREEN \\ RED \end{vmatrix}$$

the thicker vegetation is to be expected. The resultant view, as seen through an Auto Gaussian stretch, is computationally not justifiable.

Photo 7.17 Normalized Vegetation Index viewed through an Auto Mean stretch

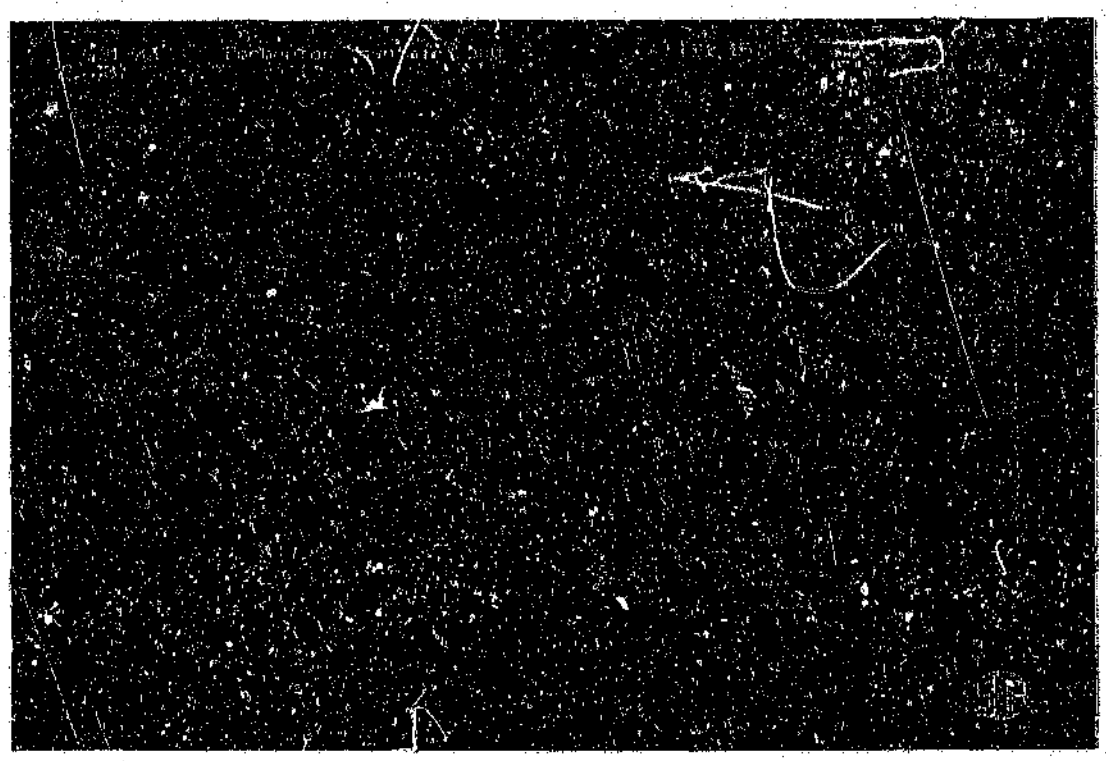

Photo 7.18 Directed Principal Components using Normalized Vegetation Index

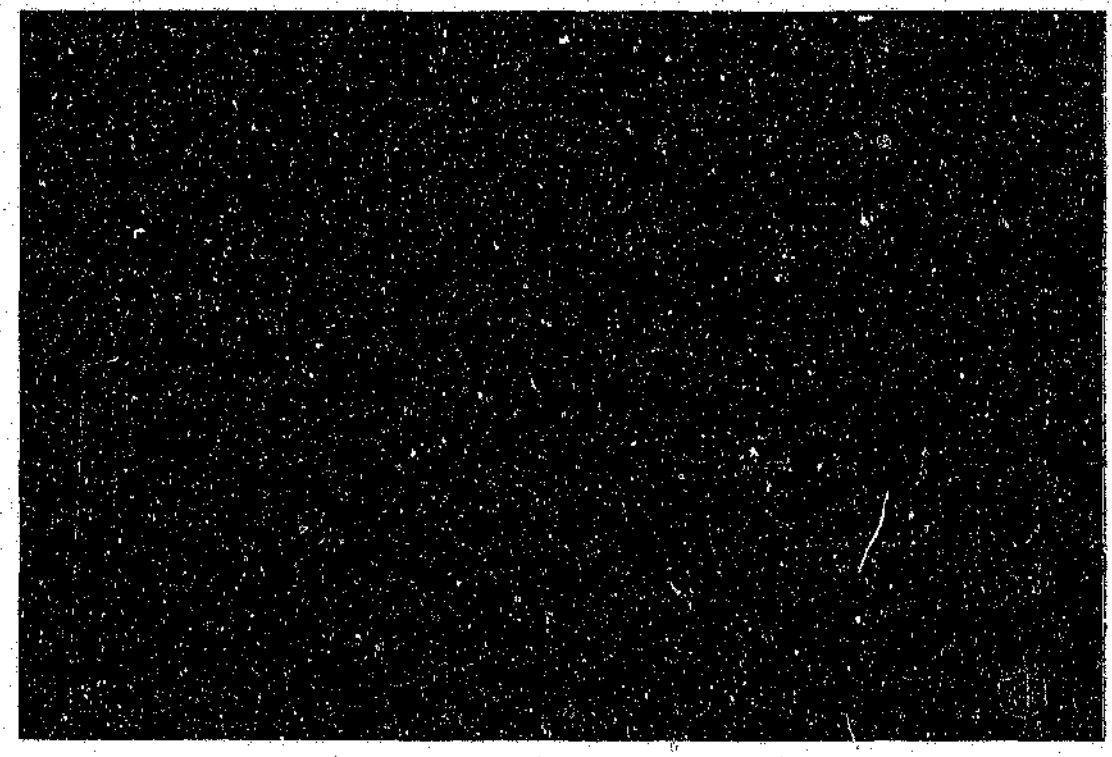

Photo 7.19 Multiplicative technique applied to Defoliated view

7.4.4 Further Processing

Processing does not have to stop after principal component transformation. Where the transformation is used as a data compression technique, it is considered to be part of the pre-processing stage and therefore most of the processing for content is still to follow. It this case principal components transformation was not used for data compression, although enhancing and combining the various components of features present in the various bands into only a few bands is what data compression is all about. The aim was to redistribute information throughout the six bands in such a way that false colour combinations may reveal features thus far hidden (See Photo 7.10).

Using Photo 7.6 (Section 7.3.2) as input dataset, (a step 1), a three band principal components transformation resulted in Photo 7.20. As with the

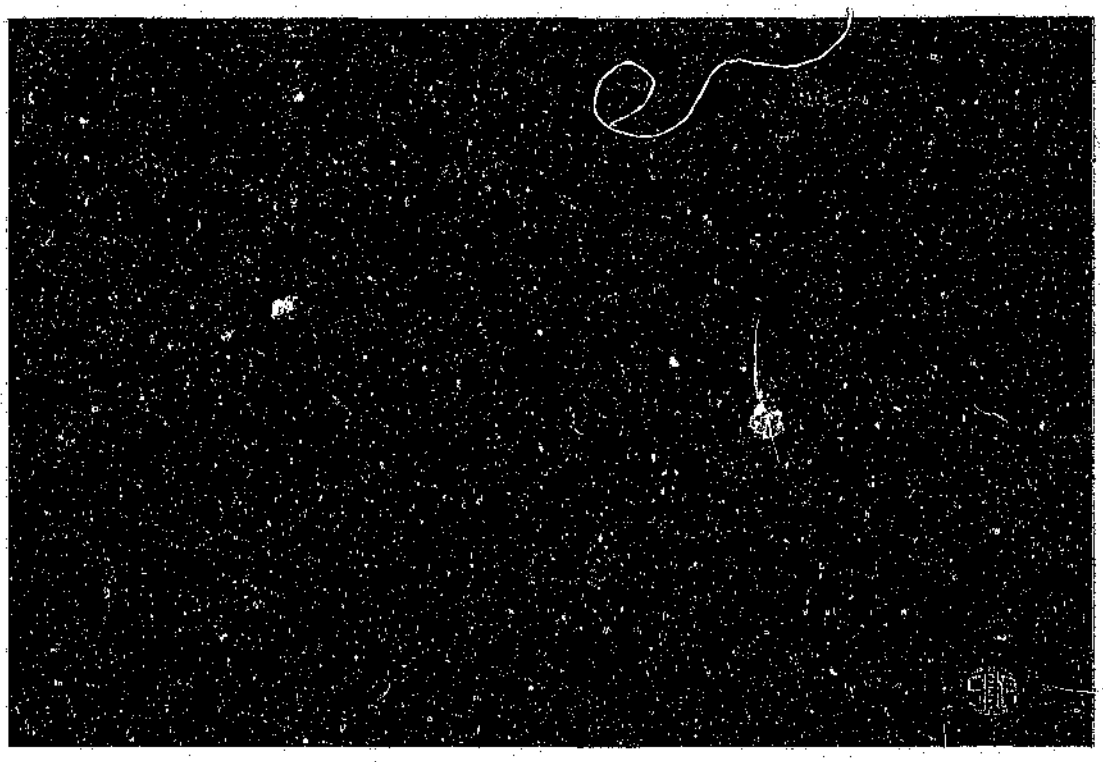

Photo 7.20 Step 2: PC-123 from pair-wise TM bands with Auto Linear stretch

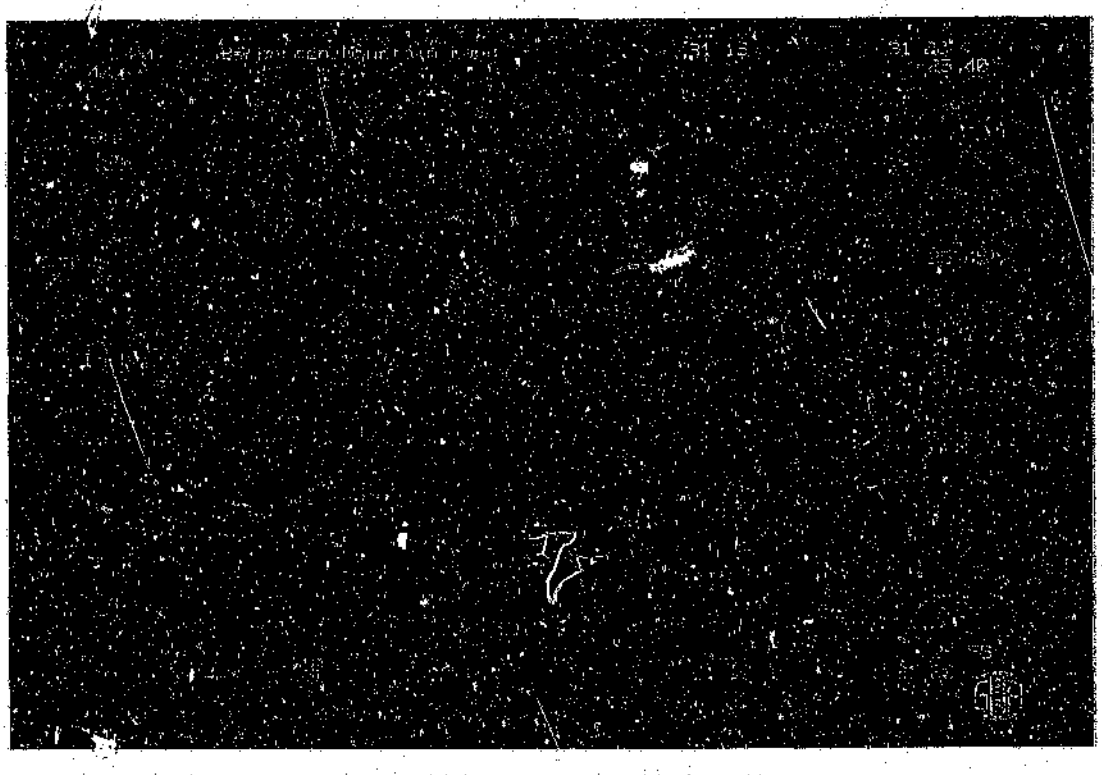

Photo 7.21 Step 3: Inverse PCT with DN128 grey as PC1 with Auto Linear stretch

principal components combinations PC-234 (Photo 7.10) and PC-534 (Photo 7.11), the iron bearing units can be traced, even on this scale. It is quite possible that an enlargement of this view to, say, 1:100 000 will show more information than either of the two PC combinations on the same scale. Again, the slight smoothing of information over the forested areas is to be expected. For step 2 (Photo 7.21) the inverse transformation was effected with PC1 being replaced by a 128 DN grey image. Using this as input for a HLS colour transformation again resulted in a colour flooded view, as can be seen on Photo 7.22. As no stretch was used for this view, an Auto-2-Linear stretch was applied to see if contrast stretching could soften the harsh colours somewhat.

The rather surprising result, Photo 7.23, displays quite a bit of detail over the forested areas, if one consider that neither of these steps have been submitted to the defoliation routine used previously (Section 7.4.3). Transforming the Auto-2-Linear stretched HLS colour space back into RGB colour space lessened the information over the forested areas, but greatly enhanced the amount of geological information visible, as can be seen on Photo 7.24. Note that no stretch was applied for this view.

Changing the order of processing routines utilized also varies the output markedly. Starting with the same Photo 7.6, a similar principal components-colour transformation set of routines resulted in Photo 7.25, a slightly less bright but possibly more usable view. The set and sequence of routines applied to the starter set consisted of:

1) Principal components transformation of the three input bands, displayed without any contrast stretch;
2) RGB to IHS colour space transformation, again without a stretch;

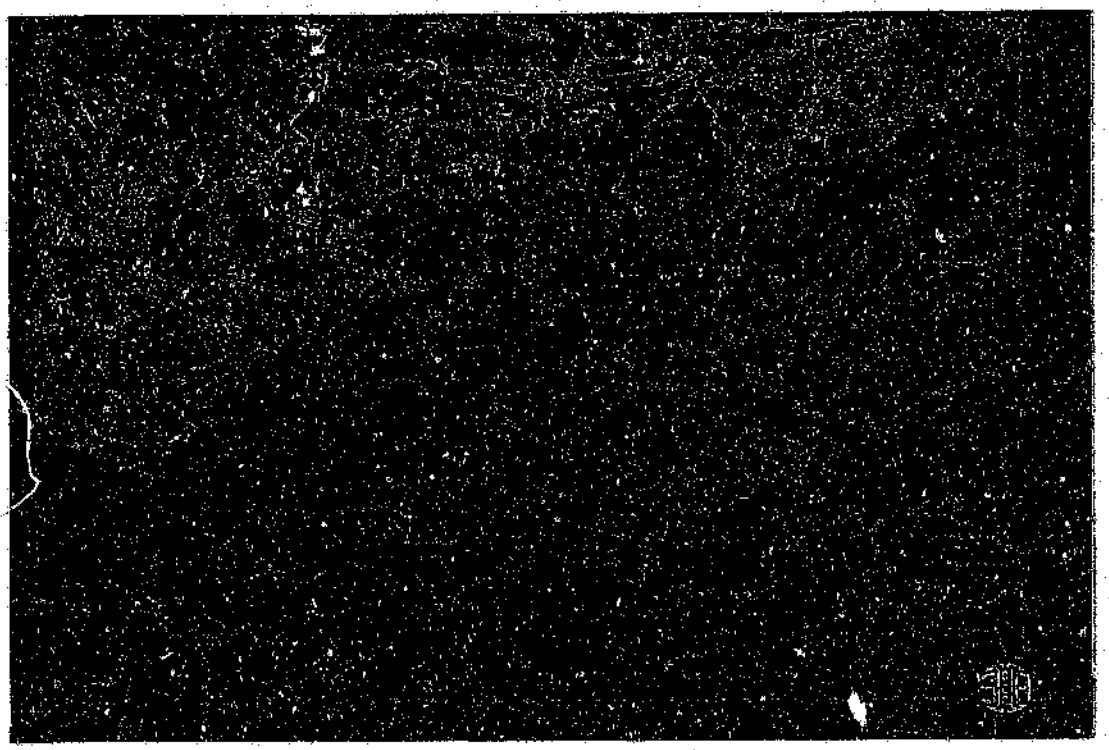

Photo 7.22 Step 4: HLS transformation viewed without stretch

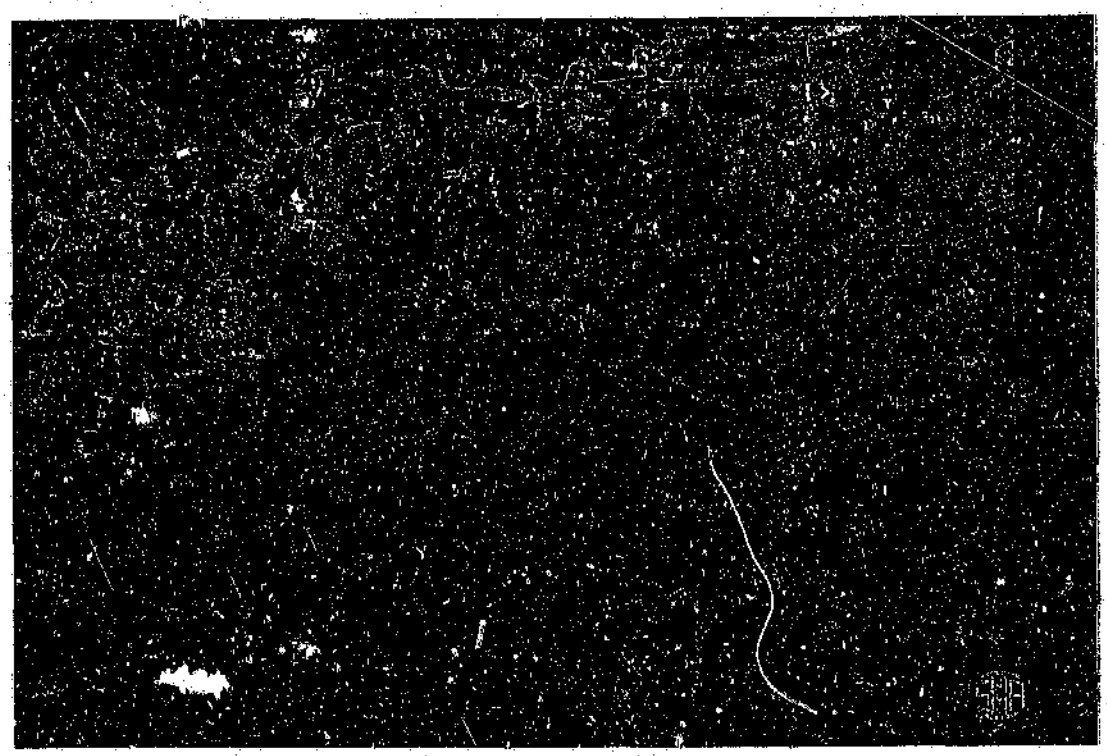

Photo 7.23 Step 4: HLS transformation viewed through an Auto-2-Linear stretch

Photo 7.24 Step 5: HLS to RGB transformation viewed without stretch

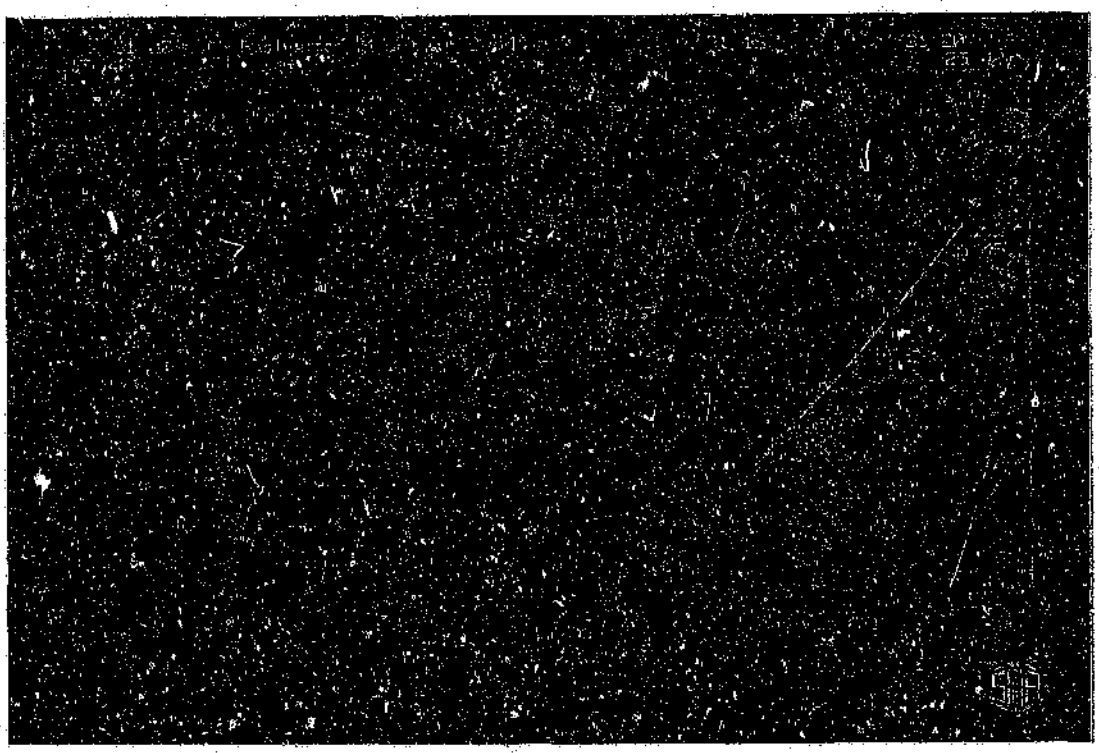

Photo 7.25 Inverse PCT on IHS transformation of three PC combinations

3) An inverse colour transformation, IHS to RGB, but with the intensity component replaced with a 128 DN grey image and no stretch, and

4) An inverse principal components transformation using the transformed RGB colour space as input.

The results were viewed through an Auto Gaussian stretch. On this view the ferruginous formations is displayed as dark bands.

8. Conclusions

Scanning through the photographs contained in this report, one is struck by the diversity of the views (photographs) present. It is clear that even simple operations like contrast stretching and edge enhancement cause a marked improvement in the visual result, as can be seen from Photo 5.12 and Photo 5.13, as well as the accompanying histograms (Photo 5.14), among others. Techniques like supervised and unsupervised classification does not always live up to expectations, as can be seen in Photo 5.19.

Although the use of the word beautify in the same breath as image processing techniques (Section 5) may be construed as being insulting to the remote sensing community at large, it should be pointed out that the more pleasing the picture presented, the more likely the use thereof by laymen. Having said that, the author must immediately concede that it is often not these pretty pictures that supply the good solid information which further scientific knowledge. In actual fact, quite a bit of additional information gathered during the course of this study had very little to do with the beauty rating of the views.

Enhancing for structural features proved relatively easy. Edge enhancement using a 5 x 5 kernel produce good results without overprocessing the data (Photo 5.1). Viewing different band combinations also enhanced features differently, but there is only so much information that can be extracted without removing the inherent correlation between the bands. Applying principal components transformation, either as a data compression technique, or as a processing

technique in it's own right, the results are still qualitative and worth very little unless interpreted by someone. Comparing the C-stretched image, combination 145 as viewed through an Auto-2-Linear stretch (Photo 8.1) to Photo 5.13, it is clear that each of these views has something to contribute to the bigger picture. Photo 5.13 shows less lineament information than Photo 8.1, but it does show the ferruginous lithologies associated with the Barbrook fault and Joe's Luck Formation.

Since plantations covered areas critical for identification of lithological boundaries, a concerted effort was made to find, deduct or develop techniques which would enable one to at least minimize the contribution of the vegetation component to the pixels being investigated. Utilizing various techniques, ranging from masking operations followed by differential contrast enhancement to the directed principal components approach, and leading to some quite drastically

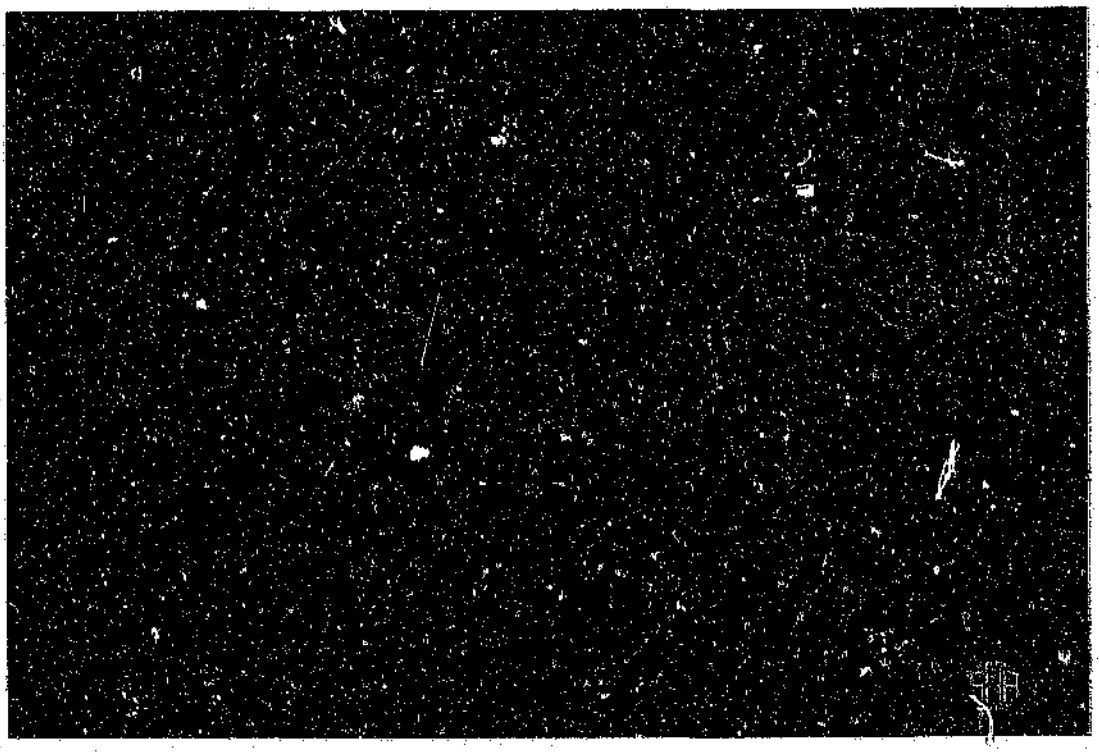

Photo 8.1 C-stretch Combination 145 viewed through an Auto-2-Linear stretch

different results, it was possible to enhance and isolate areas covered by dense vegetation, including both plantation and riverine forests (refer Photo 5.7, Photo 7.1 and Photo 7.15).

As was to be expected, the production of one single view which would enable near complete visual interpretation turned out to be pretty much impossible. The best single view result came from the addition of two of the directed principal component second combination bands (Photo 8.2). Again, this is only a better base for visual interpretation.

As the pixel size of LANDSAT TM is 30 m, enlarging these photographs to a scale of 1:50 000 produce[illegible] ixelated image. Resampling the dataset down to a 15 or 10 m pix[illegible] ev[illegible] dramatically, but it also implies an accuracy which th[illegible] ave.

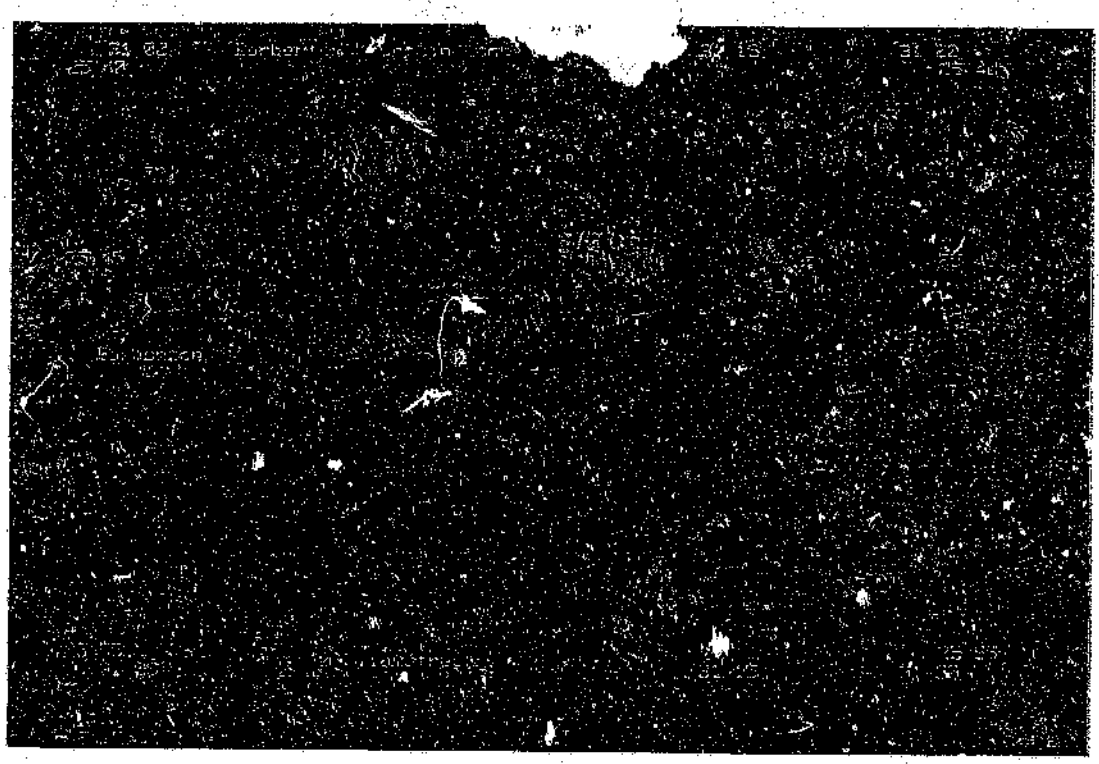

Photo 8.2 Two Directed Principal Component second combination added together

Deciding which of the procedures tested during this study resulted in enhancements which could be justified with regards to computational expense, the foremost enhancement came from the directed principal components transformation (Photo 7.16). Multiplying the square roots of PC's produced acceptable results, but this was also partly attainable through band selection of principal component combinations. Similarly D-stretch (Photo 7.12) and C-stretch (Photo 7.13, Photo 8.1) algorithms resulted in usable views.

Relating the views to the geology show a definite increase in information when compared to the existing published maps (Photo 3.1). Lineaments with a northwest-southeast strike dominate the processed views, with quite a number of northeast-southwest trending lineaments also visible.

After comparing these views with the geological map, it is clear that some of the linear features are not represented to their fullest extent on the map. Most of these features seem to be somewhat larger than indicated. Some of the shorter northwest-southeast trending dykes seem to be just parts of the same dyke, for example the dykes to the southeast of the town, stretching over a greater distance than indicated, that is, from the Mountain Land right through into the Kaap Valley Pluton (Photo 5.3, Section 5.2.2.1.2 and Photo 7.20, Section 7.4.4).

Some of the northwesterly trending valleys to the southeast of the Saddleback fault show distinct evidence of structural control (Photo 7.16, Section 7.4.3), however, none are indicated on the geological map.

Since a large part of the Saddleback syncline and the associated faults are covered by commercial forests, these features turned out to be less easy to trace

through. In this case the illumination angle also played a part, as the northwest trending features are quite visible, regardless of their size.

The outlines of both the Eureka and Saddleback synclines can be traced on more than one view (Photo 7.6, Section 7.3.2 and Photo 5.12, Section 5.3.2.1), but the more complex Makonjwa and Emlembe synclinoriums are not visible. Some lithological delineations can be made, but any interpretation of this nature must be verified with fieldwork.

Enhancing for iron content utilizing the ratio TM5/1 produced disappointing results, however, ferruginous shale and ironstone formations were highlighted through the use of PCT. Viewing the PCT-534 combination, (Photo 7.11), the yellowish tinge highlighting the Joe's Luck Formation, as well as the Barbrook fault (associated banded ironstone) is quite clear. The same colour shading in other areas is probably also due to iron content, but this has to be verified with fieldwork.

Taking all the results, excluding the computationally unjustifiable results, into account, is the only way that most of the information contained in the datasets can be extracted. Utilizing a big enough subset of these procedures will ensure informed decision making within a reasonable timeframe, and often at a fraction of the cost of a regular exploration budget.

9. Reference List

Anhaeusser, C.R. (1986) - Archaean Gold Mineralization in the Barberton Mountain Land. IN: Anhaeusser, C.R., and Maske, S., Eds., Mineral Deposits of Southern Africa, Vol I, 1020p. Geological Society of South Africa. V1, 113-154

Bailey, G.B., Dwyer, J.L., Francica, J.R., Feng, M.S., Wang, W.Y, Song, J.G., Zhang, J., Fan, C.W. and Wang, T.X. (1982) - Evaluation of image processing of Landsat data for geologic interpretation of the Qaidan Basin, China. Proc 2nd Them Conf: Rem Sens of Environment, Ft Worth. V2, 555-557

Bierwirth, P.N. (1990) - Mineral mapping and vegetation via data-calibrated pixel unmixing, using multispectral images. International Journal of Remote Sensing V11(11), 1999-2017

Brooks, R.R. (1972) - Geobotany and Biogeochemistry in Mineral Exploration. Harper and Row. 290p

Chang, S.H., Collins, W. (1983) - Confirmation of the airborne biogeophysical mineral exploration technique using laboratory methods. Economic Geology. V78(4), 723-736

Crippen, R.E. (1988) - Image Display of four-dimensional spectral data. Proc 6th Them Conf: Rem Sens for Explor Geol, Houston. V2, 677-678

Crippen, R.E. (1989) - Selection of Landsat TM band and band-ratio combinations to maximize lithologic information in colour composite displays. Proc 7th Them Conf: Rem Sens for Explor Geol, Calgary. V2, 917-922

Crosta, A.P., Moore, J.McM. (1989) - Enhancement of Landsat Thematic Mapper imagery for residual soil mapping in SW Minas Gerais State, Brazil: A prospecting case history in Greenstone Belt Terrain. Proc 7th Them Conf: Rem Sens for Explor Geol, Calgary. V2, 1173-1188

Curran, P.J. (1985) - Principles of Remote Sensing. Longman Scientific & Technical. 282p

Elvidge, C.D., Lyon, R.J.P. (1984) - Mapping clay alteration in Virginia Range, Comstock Lode, Nevada with airborne thematic mapper imagery. Proc 3rd Them Conf: Rem Sens of Environment, Col Sprngs V1, 161-170

Fraser, S.J., Green, A.A. (1987) - A Software defoliant for geological analysis of band ratios. International Journal of Remote Sensing V8(3), 525-532

Goetz, A.F.H., Rowan, L.C. (1981) - Geologic Remote Sensing. Science. V211(4484), 781-791

Heller, R.C., Ulliman, J.J., (Eds). (1983) - Forest Resource Assessments. IN: Colwell, R.N., Ed., Manual of Remote Sensing, Vol II. Chap. 34. American Society of Photogrammetry. V2, 2229-2324

Jensen, J.R. (1986) - Introductory Digital Image Processing: A Remote Sensing Perspective. Prentice-Hall. 379p

Lamb, A.D. (1984) - A rationale for the use of principal component analysis (PCA) in geological image processing of remotely sensed images. Report, NPRL CSIR. VFIS (328), 15p

Liu, J.G., Moore, J.McM. (1989) - Colour enhancement and shadow suppression techniques for TM images. Proc 7th Them Conf: Rem Sens for Explor Geol. Calgary. V2, 901-916

Longshaw, T.G. (1983) - Edge-enhancement of Landsat imagery for geological applications. Proc EDIS Symposium. 16p

Moik, J.G. (1980) - Digital Processing of Remotely Sensed Images. NASA Special Publication. (431)

Podwysocki, M.H., Segal, D.B. and Abrams, M.J. (1983) - Use of multispectral scanner images for assessment of hydrothermal alteration in the Marysvale, Utah Mining Area. Economic Geology. V78(4), 675-687

Raines, G.L., Canney, F.C. (1980) - Vegetation and Geology. IN: Siegal, B.R. and Gillespie, A.R., Eds., Remote Sensing in Geology. 702p. Chap. 12. John Wiley and Sons, Inc. 366-380

Rothery, D.A. (1987) - Decorrelation stretching as an aid to image interpretation. International Journal of Remote Sensing. V8(9), 1253-1254

Rothery, D.A., Francis, P.W. (1987) - Synoenergistic use of MOMS-01 and LANDSAT TM data. International Journal of Remote Sensing V8(3), 501-508

Salisbury, J.W., Milton, N.M. and Walsh, P.A. (1987) - Significance of non-isotropic scattering from vegetation for geobotanical remote sensing. International Journal of Remote Sensing. V8(7), 997-1009

Short, N.M. (1982) - The Landsat Tutorial Workbook: Basics of Satellite Remote Sensing. NASA Reference Publication. (1078), 553p

Simpson, C.J. (1990) - Deep weathering, vegetation and fireburn: Significant obstacles for geoscience remote sensing in Australia. International Journal of Remote Sensing V11(11), 2019-2034

Singh, A., Harrison, A. (1985) - Standardized principal components. International Journal of Remote Sensing. V6, 883-896

South African Committee for, Stratigraphy (SACS). (1980) - Stratigraphy of South Africa. Part 1 (Comp. L.E.Kent). Lithostratigraphy of the Republic of South Africa, South West Africa/Namibia and the Republics of Bophuthatswana, Transkei and Venda. Handbook of the Geological Survey of South Africa. (8), 690p

Visser, D.J.L. (Compiler). (1956) - The Geology of the Barberton area. (Explanation for the 1:50 000 geological map). Special Publication Geological Survey of South Africa. (15), 253p

Voges, F.D. (1986) - The New Consort Gold Mine, Barberton Greenstone Belt. IN: Anhaeusser, C.R. and Maske, S., Eds., Mineral Deposits of Southern Africa, Vol I, 1020p. Geological Society of South Africa. V1, 163-168

Wiggett, B.S.A., Brink, W.C.J. and Vorster, M.A. (1986) - The Fairview Gold Mine, Barberton Greenstone Belt. IN: Anhaeusser, C.R. and Maske, S. Eds., Mineral Deposits of Southern Africa, Vol I, 1020p. Geological Society of South Africa. V1, 169-180

10. Select Bibliography

Abrams, M.J., Ashley, R.P., Rowan, L.C., Goetz, A.F.H. and Kahle, A.B. (1977) - Mapping of Hydrothermal alteration in the Cuprite Mining District, Nevada, using aircraft scanner images for the spectral region 0.46 to 2.36 μm. Geology V5, 713-718

Abrams, M.J., Brown, D., Lepley, L. and Sadowski, R. (1983) - Remote Sensing for Porphyry Copper deposits in Southern Arizona. Economic Geology. V78(4), 591-604

Ager, C.M., Milton, N.M., Eiswerth, B.A., Power, M.S. and Hauck, S.A. (1989) - Spectral response of vegetation to metallic elements in Northeastern Minnesota. Proc 7th Them Conf: Rem Sens for Explor Geol, Calgary. V1, 173-178

Amos, B.J., Greenbaum, D. (1989) - Alteration detection using TM Imagery: The effects of supergene weathering in an arid climate. International Journal of Remote Sensing V10(3), 515-527

Anhaeusser, C.R. (1986) - The Lily Gold Mine, Barberton Greenstone Belt: Geology, Mineralogy, and Supergene Gold Enrichment IN: Anhaeusser, C.R. and Maske, S., Eds., Mineral Deposits of Southern Africa, Vol I, 1020p. Geological Society of South Africa. V1, 187-196

Anhaeusser, C.R., Robb, L.J. and Viljoen, M.J. (1983) - Notes on the Provisional Geological Map of the Barberton Greenstone Belt and surrounding Granitic Terrane, Eastern Transvaal and Swaziland. (1:250 000 Colour Map) IN: C.R.Anhaeusser (ed) - Contributions to the Geology of the Barberton Mountain Land. Special Publication Geological Society of South Africa. (9), 221-223

Anhaeusser, C.R., Viljoen, M.J. (1986) - Archaean Metallogeny of Southern Africa. IN: Anhaeusser, C.R. and Maske, S., Eds., Mineral Deposits of Southern Africa, Vol I, 1020p. Geological Society of South Africa. V1, 155-161

Ballard, D.H., Brown, C.M. (1982) - Computer Vision. Prentice-Hall. 523p

Bodechtel, J., Frei, M. (1992) - Geoscientific achievements. International Journal of Remote Sensing. V13(6&7), 1305-1318

Buckingham, W.F., Sommer, S.E. (1983) - Mineralogical Characterization of Rock Surfaces formed by Hydrothermal alteration and weathering: Application to Remote Sensing. Economic Geology. V78(4), 664-674

Carrere, V. (1989) - Mapping alteration in the Goldfield Mining district, Nevada, with airborne visible/infrared imaging spectrometer (AVIRIS). Proc 7th Them Conf: Rem Sens for Explor Geol, Calgary. V2, 365-378

Colwell, R.N. (Ed). (1983) - Manual of Remote Sensing, 2nd Edition, Vols I & II. American Society of Photogrammetry. 2724p

Conese, C., Maracchi, F., Miglietta, F., Maselli, F. and Sacci, V.M. (1988) - Forest classification by principal component analyses of TM data. International Journal of Remote Sensing V9(10), 1597-1612

Conradsen, K., Nielsen, A.A., et.al., Coupez, Y., et.al., Ortega, E., et.al. (1987) - The Application of Remote Sensing and Data Integration as an aid to Mineral Exploration in the Almaden Region. Volumes 1 & 2. Sponsored by CEC. 1-354

Crosta, A.P., Moore, J.McM. (1989) - Geological mapping using Landsat Thematic Mapper imagery in Almeria Province, south-east Spain. International Journal of Remote Sensing V10(3), 505-514

Davis, J.C. (1973) - Statistics and Data Analysis in Geology. John Wiley and Sons, Inc. 550p

Drury, S.A. (1987) - Image Interpretation in Geology. Allen & Unwin. 243p

Drury, S.A., Hunt, G.A. (1989) - Geological uses of remotely-sensed reflected and emitted data of late Archean terrain in Western Australia. International Journal of Remote Sensing V10(3), 475-497

Elvidge, C.D., Lyon, R.J.P. (1985) - Estimation of the vegetation contribution to the 1.65/2.22 μm ratio in airborne thematic-mapper imagery of the Virginia Range, Nevada. International Journal of Remote Sensing, V6(1), 75-78

Ferrari, M C. (1992) - Improved decorrelation stretching of TM data for Geological applications: first results in Northern Somalia. International Journal of Remote Sensing, V13(5), 841-851

Ferreira, C.A.M., Lamb, A.D. (1990) - A geological comparison between Daedalus AADS-1268 and Landsat Thematic Mapper data over the Transvaal dolomites. Proc Symp: Daedalus Airborne Scanner Data in S.A., CSIR 35-40

Ford, J.P., Dokka, R.K. and Blom, R.G. (1990) - Undocumented faults revealed in multisensor image analysis, Mojave Desert, California, U.S.A. IN: Remote Sensing: an operational technology for the mining and petroleum industries. Institution of Mining and Metallurgy. 27-33

Fraser, S.J. (1991) - Discrimination and identification of ferric oxides using satellite Thematic Mapper data: A Newman case study. International Journal of Remote Sensing V12(3), 635-641

Geological Survey of South Afr. (1986) - 2530 Barberton, 1:250 000 Geological Series. Geological Survey of South Africa. Map

Ghosh, T.K., Viswanatham, S. (1991) - Neotectonic analysis of Mendha river Basin, Rajasthan, India. International Journal of Remote Sensing. V12(12), 2585-2595

Goetz, A.F.H., Rock, N.B. and Rowan, L.C. (1983) - Remote Sensing for Exploration: An Overview. Economic Geology. V78(4), 573-590

Gupta, R.P. (1991) - Remote Sensing Geology. Springer-Verlag

Hammerbeck, E.C.I. (1976) - Gold outside the Witwatersrand Triad. Handbook of the Geological Survey of South Africa. (7), 75-92

Hamming, R.W. (1977) - Digital Filters. Prentice-Hall. 226p

Hord, R.M. (1986) - Remote Sensing: Methods and Applications. John Wiley and Sons, Inc. 334p

Jaskolla, F., Henkel, J. (1989) - A new concept of digital processing of multispectral remote sensing data for Geological Applications. Proc 7th Them Conf: Rem Sens for Explor Geol, Calgary. V2, 877-890

Kaufmann, H. (1988) - Mineral exploration along the Aqaba-Levant Structure by use of TM data: Concepts, processing and results. International Journal of Remote Sensing V9(10), 1639-1658

Kawakami, T., Shibata, Y., Yamakawa, T. and Takiziwa, H. (1990) - Rock Identification by advanced data processing methods. IN: Remote Sensing: an operational technology for the mining and petroleum industries. Institution of Mining and Metallurgy. 43-48

Kowalczyk, P., Logan, K. (1989) - TM Processing for routine use in Mineral Exploration. Proc 7th Them Conf: Rem Sens for Explor Geol, Calgary. V1, 323-330

Kruse, F.A. (1989) - Spectral mapping with Landsat Thematic Mapper and imaging spectroscopy for precious metals exploration. Proc 7th Them Conf: Rem Sens for Explor Geol, Calgary. V1, 17-28

Lamb, A.D., Pendock, N. (1989) - Band prediction techniques for the mapping of hydrothermal alteration. Proc 7th Them Conf: Rem Sens for Explor Geol, Calgary. V2,

1317-1329

Lamb, A.D., Pendock, N. (1990) - Processing techniques for geological applications of airborne multispectral scanner data - an example using Daedalus AADS-1268 imagery. Proc Symp: Daedalus Airborne Scanner Data in S.A., CSIR 22-35

Lo, C.P. (1986) - Applied Remote Sensing. Longman Scientific & Technical. 393p

Loughlin, W.P. (1991) - Principal Component Analysis for Alteration Mapping. Proc 8th Them Conf: Rem Sens for Explor Geol, Denver. V1, 293-306

Marsh, S.E., Townsend, T.E., Podwysocki, M.H., Goetz, A.F.H, Vane, G. and Slater, P.N. (1983) - Imaging Systems for the Delineation of Spectral Properties of Geologic Materials in the Visible and Near-Infrared. IN: Henderson, F.B. & Rock, B.N. (eds) - Frontiers for Geological Remote Sensing from Space. Rep. of 4th Geosat Workshop, Flagstaff, Arizona. American Society of Photogrammetry. 13-20

Miller, N.L., Elvidge, C.D. (1985) - The Iron Absorption Index: a comparison of ratio based and baseline-based techniques for the mapping of iron oxides. Proc 4th Them Conf: Rem Sens of Environment, San Fran. V2, 405-415

Miller, R.L., Kahn, J.S. (1962) - Statistical Analysis in the Geological Sciences. John Wiley and Sons, Inc. 483p

Moore, J.McM., Liu, J.G. (1990) - Image enhancement of epithermal gold deposit alteration zones in southeast Spain. IN: Remote Sensing: an operational technology for the mining and petroleum industries. Institution of Mining and Metallurgy. 49-58

Mouat, D.A., Arp, G.K., Collins, W., Elvidge, C., Labovitz, M.L., Lyon, R.J.P., Milton, N.M., Parrish, J. and Rock, B.N. (1983) - The Importance of Geobotany in Geological Remote Sensing Applications. IN: Henderson, F.B. & Rock, B.N. (eds) - Frontiers for Geological Remote Sensing from Space. Rep of 4th Geosat Workshop, Flagstaff, Arizona. American Society of Photogrammetry. 57-64

Newton, A.R. (1990) - Geological Remote Sensing in Southern Africa - a literature review. South African Journal of Geology. V93(5/6), 795-802

Numan, N.M.S., Bakos, G.Y.B. (1987) - Detection of subsurface geologic structures in the Tharthar area of central Iraq using Landsat images. I.T.C. Journal (2), 145-152

Ormsby, J.P., Choudhury, B.J. and Owe, M. (1987) - Vegetation spatial variability and its effect in vegetation indeces. International Journal of Remote Sensing. V8(9), 1301-1306

Pendock, N. (1990) - Gold Exploration in greenstone belts by use of Landsat TM. IN: Remote

1317-1329

Lamb, A.D., Pendock, N. (1990) - Processing techniques for geological applications of airborne multispectral scanner data - an example using Daedalus AADS-1268 imagery. Proc Symp: Daedalus Airborne Scanner Data in S.A., CSIR 22-35

Lo, C.P. (1986) - Applied Remote Sensing. Longman Scientific & Technical. 393p

Loughlin, W.P. (1991) - Principal Component Analysis for Alteration Mapping. Proc 8th Them Conf: Rem Sens for Explor Geol, Denver. V1, 293-306

Marsh, S.E., Townsend, T.E., Podwysocki, M.H., Goetz, A.F.H, Vane, G. and Slater, P.N. (1983) - Imaging Systems for the Delineation of Spectral Properties of Geologic Materials in the Visible and Near-Infrared. IN: Henderson, F.B. & Rock, B.N. (eds) - Frontiers for Geological Remote Sensing from Space. Rep. of 4th Geosat Workshop, Flagstaff, Arizona. American Society of Photogrammetry. 13-20

Miller, N.L., Elvidge, C.D. (1985) - The Iron Absorption Index: a comparison of ratio based and baseline-based techniques for the mapping of iron oxides. Proc 4th Them Conf: Rem Sens of Environment, San Fran. V2, 405-415

Miller, R.L., Kahn J.S. (1962) - Statistical Analysis in the Geological Sciences. John Wiley and Sons, Inc. 483p

Moore, J.McM., Liu, J.G. (1990) - Image enhancement of epithermal gold deposit alteration zones in southeast Spain. IN: Remote Sensing: an operational technology for the mining and petroleum industries. Institution of Mining and Metallurgy. 49-58

Mouat, D.A., Arp, G.K., Collins, W., Elvidge, C., Labovitz, M.L., Lyon, R.J.P., Milton, N.M., Parrish, J. and Rock, B.N. (1983) - The Importance of Geobotany in Geological Remote Sensing Applications. IN: Henderson, F.B. & Rock, B.N. (eds) - Frontiers for Geological Remote Sensing from Space. Rep of 4th Geosat Workshop, Flagstaff, Arizona. American Society of Photogrammetry. 57-64

Newton, A.R. (1990) - Geological Remote Sensing in Southern Africa - a literature review. South African Journal of Geology. V93(5/6), 795-802

Numan, N.M.S., Bakos, G.Y.B. (1987) - Detection of subsurface geologic structures in the Tharthar area of central Iraq using Landsat images. I.T.C. Journal (2), 145-152

Ormsby, J.P., Choudhury, B.J. and Owe, M. (1987) - Vegetation spatial variability and its effect in vegetation indeces. International Journal of Remote Sensing. V8(9), 1301-1306

Pendock, N. (1990) - Gold Exploration in greenstone belts by use of Landsat TM. IN: Remote

Sensing: an operational technology for the mining and petroleum industries. Institution of Mining and Metallurgy. 243-247

Rockwell, B.W. (1989) - Hydrothermal alteration mapping in spectral ratio feature space using TM reflectance data: Aurora Mining District, Mineral County, Nevada. Proc 7th Them Conf: Rem Sens for Explor Geol, Calgary. V2, 1189-1204

Rosenfeld, A., Kak, A.C. (1982a) - Digital Picture Processing. Second Edition, Volume 1. Academic Press, Inc. 435p

Rosenfeld, A., Kak, A.C. (1982b) - Digital Picture Processing. Second Edition, Volume 2. Academic Press, Inc. 349p

Rothery, D.A. (1983) - Supervised maximum-likelihood classification and post classification filtering using MSS imagery for lithological mapping in the Oman ophiolite. Proc 2nd Them Conf: Rem Sens of Environment, Ft Worth. V2, 417-426

Rothery, D.A. (1984) - Reflectances of ophiolite rocks in the Landsat MSS bands: relevance to lithological mapping by remote sensing. Journal of the Geological Society of London. V141, 933-939

Sabins, F.F., Jr. (1978) - Remote Sensing: Principles and Interpretation. W.H. Freeman and Company. 426p

Schowengerdt, R.A. (1983) - Techniques for Image Processing and Classification in Remote Sensing. Academic Press, Inc. 249p

Segal, D.S. (1983) - Use of Landsat Multispectral Scanner Data for the Definition of Limonitic Exposures in Heavily Vegetated Areas. Economic Geology. V78(4), 711-722

Settle, M., Chavez, P., Everett, J.R., Kahle, A.B., Kieffer, H.H., Kitcho, C.A., Milton, N.M. & Mouat, D.A. (1983) - Thematic Mapper Data Analysis. IN: Henderson, F.B. & Rock, B.N. (eds) - Frontiers for Geological Remote Sensing from Space. Rep. of 4th Geosat Workshop, Flagstaff, Arizona. American Society of Photogrammetry. 26-26

Siegal, B.R., Gillespie, A.R., Eds. (1980) - Remote Sensing in Geology. John Wiley and Sons, Inc. 702p

Tankard, A.J., Jackson, M.P.A., Eriksson, K.A., Hobday, D.K., Hunter, D.R. and Minter, W.E.L. (1982) - Crustal evolution of Southern Africa. Springer-Verlag 523p

Tibaldi, A., Ferrari, L. (1991) - Multisource remotely sensed data, field checks and seismicity for the definition of active tectonics in Ecuadorian Andes. International Journal of

Remote Sensing. V12(11), 2343-2358

Viljoen, M.J., Viljoen, R.P. (1969) - An introduction to the geology of the Barberton granite-greenstone terrane. IN: Upper Mantle Project. Special Publication Geological Society of South Africa. (2), 2-28

Visser, D.J.L. (Compiler). (1989) - Toeligting: Geologise Kaart (1:1 000 000) Die Geologie van die Republieke van Suid-Afrika, Transkei, Bophuthatswana, Venda, Ciskei en die Koninkryke van Lesotho en Swaziland. Geologie Opname 494p

Wadge, G., Quarmby, N. (1988) - Geological remote sensing of rocky coasts. Geological Magazine V125(5), 495-505

Wagener, J.H.F. (1986) - The Agnes Gold Mine, Barberton Greenstone Belt. IN: Anhaeusser, C.R. and Maske, S., Eds., Mineral Deposits of Southern Africa, Vol I, 1020p. Geological Society of South Africa. V1, 181-186

Wagener, J.H.F., Wiegand, J. (1986) - The Sheba Gold Mine, Barberton Greenstone Belt. IN: Anhaeusser, C.R. and Maske, S., Eds., Mineral Deposits of Southern Africa, Vol I, 1020p. Geological Society of South Africa. V1, 155-162

Williams, R.S., Jr. (Ed). (1983) - Geological Applications. IN: Colwell, R.N., Ed., Manual of Remote Sensing, II. Chap. 31. American Society of Photogrammetry. V2, 1667-1953